TAMPEREEN TEKNILLINEN YLIOPISTO
TAMPERE UNIVERSITY OF TECHNOLOGY

Tiina Salmi

Optimization of Quench Protection Heater Performance in High-Field Accelerator Magnets Through Computational and Experimental Analysis

Julkaisu 1311 • Publication 1311

Tampere 2015

Tampereen teknillinen yliopisto. Julkaisu 1311
Tampere University of Technology. Publication 1311

Tiina Salmi

Optimization of Quench Protection Heater Performance in High-Field Accelerator Magnets Through Computational and Experimental Analysis

Thesis for the degree of Doctor of Science in Technology to be presented with due permission for public examination and criticism in Rakennustalo Building, Auditorium RG202, at Tampere University of Technology, on the 28th of August 2015, at 12 noon.

Tampereen teknillinen yliopisto - Tampere University of Technology
Tampere 2015

ISBN 978-952-15-3554-3 (printed)
ISBN 978-952-15-3570-3 (PDF)
ISSN 1459-2045

Abstract

Superconducting accelerator magnets with increasingly high magnetic fields are being designed to improve the performance of the Large Hadron Collider (LHC) at CERN. One of the technical challenges is the magnet quench protection, i.e., preventing damage in the case of an unexpected loss of superconductivity and the heat generation related to that. Traditionally this is done by disconnecting the magnet current supply and using so-called protection heaters. The heaters suppress the superconducting state across a large fraction of the winding thus leading to a uniform dissipation of the stored energy. Preliminary studies suggested that the high-field Nb_3Sn magnets under development for the LHC luminosity upgrade (HiLumi) could not be reliably protected using the existing heaters. In this thesis work I analyzed in detail the present state-of-the-art protection heater technology, aiming to optimize its performance and evaluate the prospects in high-field magnet protection.

The heater efficiency analyses focused on the time delays from heater activation to normal zone initiation in the coils. I developed a numerical simulation tool CoHDA (Code for Heater Delay Analysis) to model the heat transfer from the heater to the cables and estimate the delay based on the superconductor critical surface. All the important parameters relative to the heater, the cable, and the magnet operation conditions were included. The simulation results were validated experimentally using measured data from several R&D Nb_3Sn quadrupoles and dipoles. Then, a method based on parametric sweeps was utilized to optimize the heater layouts. The goal was to minimize the delay to quench the entire coil, taking into account the different field regions. New heater designs were proposed for the Nb_3Sn R&D prototype LHQ and the HiLumi quadrupole QXF. Finally, I simulated the heaters in high temperature superconductor magnets, which are being considered for the LHC energy upgrade. Consequently, I proposed technology improvements to increase the heater energy in order to meet the requirements also in these very high-field magnets.

Preface

This doctoral thesis is completed at Tampere University of Technology (TUT), within the Electromagnetics group in the Electrical Engineering department. The topic of this work was a natural continuation to my M.Sc. thesis, which was related to accelerator magnet quench protection and done at CERN. The first three years of this research were done at Lawrence Berkeley National Laboratory (LBNL) at Berkeley, USA, with the University of Twente, the Netherlands, as the academic connection. After three years I moved to Finland and joined Tampere University of Technology to carry out the rest of the work.

I feel very grateful for this exceptionally versatile experience I have had during these five years of PhD training, both professionally and personally. Certainly the best thing professionally was the opportunity to work in different places which are among the best in the world either in Nb_3Sn magnet technology development or in mathematical quench modelling. The large international collaborations of LARP and EuCARD-2 further expanded my networks and allowed me to get well connected with the people of our field. Personally, apart from the interesting work topics, I appreciate that I got to know different places, cultures, and people. I learned more about the world and about myself that I could have ever imagined. One of the best parts of completing this thesis is to have the opportunity to formally thank the people who have made this experience that what it was.

First, I thank Antti Stenvall, my supervisor at TUT, for his guidance and trust. I look forward to working with him within my post-doc project too, knowing that I can trust in his professionalism, expertize, and word. For the Berkeley years, I thank Helene Felice, for the guidance in the early stages of the work. It was her who knew that quench protection will be an important topic for the future magnets. I also thank Shlomo Caspi for his interest to my work and for sharing his insights to quench modeling. I thank Herman ten Kate for the academic supervision during the first two years. I thank all the collaborators world-wide for the opportunities to work and connect with them, and for all the expertise shared. Especially Guram Chlachidze and

Giorgio Ambrosio from Fermilab, USA, GianLuca Sabbi, Maxim Marchevsky, and Diego Arbelaez from LBNL, Hugo Bajas and Ezio Todesco from CERN, Switzerland, and all the other members of the research teams, engineers and technical staff who have enabled the experimental work. They have taught me about the details in magnet fabrication that I'd never have learned from a text book. To Ezio Todesco I am also indebted for his expert advice regarding certain publications, and for the encouraging conversations. For "spiritual support" big thanks also go to the two colleagues at LBNL, Matthijs Mentink and Franck Borgnolutti. Both of them helped occasionally at the work, but much more importantly, they became good friends. I make a common thanks to all other friendly colleagues both at LBNL and TUT – You were important. I also gratefully acknowledge the wonderful work of the administrative personnel both at TUT and LBNL. I practically never had to worry about the practical organizations or bureaucratic matters. Finally, I want to thank my friends and family in Finland for the interest and support, even when I was far and bad at keeping in touch. They never tied their love to me to the success or failure of what I do in live, like I myself did at times. That's why I love them so much.

I also thank the pre-examiners of this thesis, Cesar Luongo (Jefferson National Accelerator Facility, USA) and Dariusz Bocian (Institute of Nuclear Physics PAN, Poland) for taking the time to evaluate this thesis and for their useful comments and encouraging words. I also thank Dariusz Bocian and Juho Rysti (CERN) for agreeing to act as opponents for the public defense.

The work during the Berkeley years was financially supported by the Director, Office of Science, High Energy Physics, U.S. D.o.E. under Contract DE-AC02-05CH11231. At Tampere, the work was supported by Stability Analysis of Superconducting Hybrid Magnets (Academy of Finland, #250652) and by EuCARD-2, which is co-funded by the partners and the European Commission under Capacities 7th Framework Programme, Grant Agreement 312453.

In Tampere, 20 August, 2015

Tiina Salmi

List of publications and author's contribution

Publication 1

Salmi T, Ambrosio G, Caspi S, Chlachidze G, Dhallé M, Felice H, Marchevsky M, Sabbi GL and ten Kate H H J 2012
AIP Conf. Proc. **1434** 656
"Quench protection challenges in long Nb_3Sn accelerator magnets"
doi:10.1063/1.4706976

Publication 2

Salmi T, Caspi S, Chlachidze G, Felice H, Prestemon S and ten Kate H H J 2013
CERN Yellow Report 2013-006, Proc. Workshop on Accelerator Magnet, Superconductor, Design and Optimization 30
"Modeling heat transfer from quench protection heaters to superconducting cables in Nb_3Sn magnets"
doi:10.5170/CERN-2013-006

Publication 3

Salmi T, Arbelaez D, Caspi S, Chlachidze G, Felice H, Marchevsky M, Prestemon S and ten Kate H H J 2014
IEEE Trans. Appl. Supercond. **24** 4701305
"Protection heater delay time optimization for high-field Nb_3Sn accelerator magnets"
doi:10.1109/TASC.2013.2287634

Publication 4

Salmi T, Arbelaez D, Caspi S, Felice H, Mentink M G T, Prestemon S, Stenvall A and ten Kate H H J 2014
IEEE Trans. Appl. Supercond. **24** 4701810
"A novel computer code for modeling quench protection heaters in high-field

Nb_3Sn accelerator magnets"
doi:10.1109/TASC.2014.2311402

Publication 5

Salmi T, Chlachidze G, Marchevsky M, Bajas H, Felice H and Stenvall A 2015
IEEE Trans. Appl. Supercond. **25** 4004212
"Analysis of uncertainties in protection heater delay time measurements and simulations in Nb_3Sn high-field accelerator magnets"
doi:10.1109/TASC.2015.2437332

Publication 6

Salmi T and Stenvall A 2015
IEEE Trans. Appl. Supercond. **25** 0500205
"Modeling quench protection heater delays in an HTS coil"
doi:10.1109/TASC.2014.2363523

Author's contribution

I have written all the text in the publications, guided by suggestions and revisions from the co-authors as will be specified below. The simulation model development and all the simulations were performed by myself. The experiments were performed as a part of the magnet tests by LARP (HQ01b-e, HQM01, HQ02a-b) or LBNL (HD3b). I wrote the test plans for the heater studies, iterated the plans based on the discussions at the test planning meetings, and participated actively in the heater testing. The physical electrical work, data acquisition system set-up, and magnet operation was performed by the other group members and the technical staff. I did not have a part in the tests of LQ and 11 T dipoles, but I got to use the measurement data. The work related to **Publications 1-4**, and part of **Publication 5** were done while working at Berkeley, with guidance from Helene Felice, and in close ties with the LARP project. The work for **Publication 6** and part of **Publication 5** was done at Tampere and supervised by Antti Stenvall. I presented work related to **Publications 1-5** several times before the publications and received feedback and suggestions. It is not possible to identify each individual contribution to all the ideas. However, the final conclusions were always made by myself – sometimes stubbornly. I can just say, that even if I consider having done most of the work by myself, with most of the ideas originated from myself (with the exceptions detailed below), the direction and ideas have profited greatly from meetings and discussions with several persons. In particular, Helene Felice and Antti Stenvall have been important in guiding the work.

Detailed author's contribution for each publication

When in the following I discuss about analysis and simulations without a reference to anything specific, I mean the heater delay simulations of the then investigated magnet and heaters with the computational tool that I implemented in Fortran 90. This includes collecting all the simulation parameters, which is not a negligible task in such a multidisciplinary project where the responsibilities are shared between institutes located in different continents.

Publication 1: I designed and wrote the test plans for the experiments in HQ01 and HQM01 magnets, taking into account the comments and feedback from Helene Felice and the LARP collaboration. The HQ01 measurements were done at Berkeley, and I participated in the test preparations, testing, and did the data analysis. The HQM01 measurements were performed at Fermilab by Guram Chladhidze. I and Helene Felice were connected with him via Skype during the measurements. In particular, during the MIITs studies each following test step was adjusted based on the earlier results. The progression of the MIITs test was impacted also by other collaboration members, in particular GianLuca Sabbi. The LQ heater delay measurements were taken from the LQ test report and the information on heater designs was provided by Helene Felice. I did the comparison of delays from different tests. The simulations with QuenchPro were run be Helene Felice based on the cases I asked her to consider. I did the analysis of the results. The text was written by myself, profiting greatly from the suggestions and revisions by Helene Felice. Also the other co-authors and the reviewers helped to revise the text.

Publication 2: The simulation model was developed by myself, and the simulations were done by myself. Helene Felice and Shlomo Caspi provided several suggestions. Diego Arbelaez helped greatly with the numerical modeling techniques during the early phases of the model development. I designed the test plan for HQ01e, again within the LARP collaboration. The HQ01e measurements were done at CERN by Hugo Bajas and Jerome Feuvrier. I was in daily correspondence by email and Skype, ensuring reciprocal understanding of the test procedure and results. I analyzed the voltage signals to determine the delays and analyzed the data. The 11 T measurements were done by others, and I got the detailed measurement data for my comparisons from Guram Chlachidze. The HQ01 magnetic field map needed in the simulations was provided by Helene Felice. Guram Chlachidze and Bernhard Auchmann were helpful in determining the simulation parameters for 11 T. The analysis of the results was done myself. The text was written by myself, considering the important feedback and revision help from Helene Felice and Ezio Todesco.

Publication 3: The simulations were done by myself, I devised the heater design routine and programmed it. The measurements in HQ02a1 were designed by myself (always with several iterations in the test plan meetings within the LARP collaboration). The measurements were performed at Fermilab, and I traveled there to participate on the spot. Guram Chaldhidze operated the magnet, and physically performed the measurement set-ups according to the plan. The measurement data for LQ and HQ01e is the same as presented in **Publication 1** and **Publication 2**. For the simulations, the LQ critical surface parameters were provided by Arno Godeke and the QXF field map was provided by Franck Borgnolutti. The text was written by myself, with revision help from Helene Felice and Ezio Todesco.

Publication 4: The entire computational tool was designed and programmed by myself. Helene Felice and Shlomo Caspi provided several suggestions and Diego Arbelaez was an important support on the numerical modeling side. The idea how to analyze the simulations sensitivity sparked from Matthijs Mentink in a conversation about the topic. The simulation and analysis was done by myself. The text was written by myself with feedback from Helene Felice, Antti Stenvall, Ezio Todesco and Matthijs Mentink.

Publication 5: The analysis was designed by myself, taking into account the suggestions from Antti Stenvall. All the simulations were done by myself. The HD3 experiments were designed by myself together with the LBNL group, and performed at LBNL together with Helene Felice and Maxim Marchevsky (and the magnet operation team). The 11 T (second model) measurement data was provided by Guram Chlachidze. The measurements in HQ02a2 and HQ02b were performed in Fermilab and CERN, respectively. I wrote again the test plans and stayed in correspondence by email as the tests proceeded. The data from HQ01e and 11 T (first model) is as described for **Publication 2**. The text was written by myself and revised by Antti Stenvall.

Publication 6: The analysis is designed by myself and the simulations are performed by myself. Antti Stenvall provided suggestions. Erkki Härö and Glyn Kirby helped in finding the cable parameters. The text was written by myself and revised by Antti Stenvall.

Contents

Lists of symbols and abbreviations

A_{cable}	Cross-sectional area of a cable
A_{Cu}	Cross-sectional area of a copper
B	Magnetic flux density
B_{c1}	Lower critical magnetic flux density
B_{c2}	Upper critical magnetic flux density
B_{HS}	Magnetic field under heating station
B_{max}	Maximum magnetic field within a cable (coil turn)
B_{prof}	The profile of magnetic field across a cable (coil turn)
C	Capacitance
c_{p}	Specific heat
cos-θ	Sector dipole
cos-2θ	Sector quadrupole
d_{ss}	Thickness of stainless steel
E_{dump}	Energy dissipated in the dump resistor
E_{margin}	Cable energy (enthalpy) margin to quench
E_{PH}	Energy dissipated in the heater
E_z	Electric field in z-direction
e	Elementary charge
f_{gen}	Volumetric heat generation
H	Height of the stimulation domain in y-direction
I	Current
I_{c}	Critical current
I_{Cu}	Current flowing in copper
I_{mag}	Magnet operation current
$I_{\text{mag,max}}$	Maximum magnet operation current
I_{PH}	Heater current
$ierfc$	integral error function
J	Current density
J_{c}	Critical current density
J_{Cu}	Current density in copper

J_{ss}	Current density in stainless steel
K	Thermal conductance
k	Thermal conductivity
L	Inductance
L_{HS}	Length of the heating stations in one heater period (along the coil axis)
$L_{HS,path}$	Length of the current path within the heating stations in one heater period
L_{period}	Length of a heater period
L_{strip}	Length of a heater strip (along the coil axis)
l	Length
l_{PH}	Length of a heater segment
N_y	Number of elements in y-direction
N_z	Number of elements in z-direction
n	Unit normal
P_{PH}	Heater power
Q	Heat flow
q_0	Steady state heat flux
R	Resistance
R_{dump}	Resistance of dump resistor
R_{HS}	Resistance of the heating stations within one heater period
R_{strip}	Resistance of the heater strip
R_{wide}	Resistance of the wide segment within one heater period
T	Temperature
T_{A}	Temperature using analytical calculation
T_{bath}	Temperature of the helium bath
T_{c}	Critical temperature
T_{cs}	Current sharing temperature
T_{max}	Maximum temperature
T_{N}	Temperature using numerical calculation
T_{op}	Operation temperature
$T_{\mathrm{PH,max}}$	Maximum temperature of heater
t	Time
t_{delay}	Delay time between quench start and protection activation
V	Electric potential
V_{dump}	Voltage across the dump resistor
V_{mag}	Voltage across the magnet terminals
$V_{\mathrm{mag,max}}$	Maximum voltage across the magnet terminals
V_{PH}	Voltage across the protection heater
$V_{\mathrm{PH,max}}$	Maximum voltage across the heater
V_{th}	Voltage threshold for quench detection
w_{HS}	Width of heating station
w_{wide}	Width of the wide segment

w_{tape}	Width of the HTS tape
α	Thermal diffusivity
γ	Mass density
Δt	Time step
Δt_{PH}	Heater delay
Δt_{PH}^{QP}	Time of quench propagation between heating stations
Δt_{PH}^{tot}	Heater delay + time of quench propagation between heating stations
$\Delta t_{PH}^{tot,max}$	The largest Δt_{PH}^{tot} of all the turns covered by heater
Δx	Length of unit cell in x-direction
Δy	Length of unit cell in y-direction
Δz	Length of unit cell in z-direction
ϵ	Relative error
λ	Time-step scaling factor
λ_{Cu}	Cable copper fraction
ρ	Resistivity
ρ_{Cu}	Resistivity of copper
ρ_{ss}	Resistivity of stainless steel
τ	Heater RC circuit time constant

11 T	Dipole magnet developed in collaboration with Fermilab and CERN
AC	Alternating current
ANSYS	A FEM based simulation software
B01	Heater ID for LHQ outer layer heater with LQ-style layout
B02	Heater ID for LHQ outer layer heater with Pulse-wave layout
Bi-2212	Bismuth based high temperature superconductor
BNL	Brookhaven National Laboratory in Upton, New York, US
BSCCO	Bismuth based high temperature superconductors
CAD	Computer-aided design
CERN	European Organization for Nuclear Research in Geneva, Switzerland
CLIQ	Coupling-Loss-Induced Quench System
CoHDA	Code for Heater Delay Analysis
CORC	Conductor on Round Core cable configuration
COMSOL	A FEM based simulation software
cr	Current redistribution
CS	Closing switch
cs	Current sharing
DC	Constant current (direct current)
EuCARD	European Coordination for Accelerator R&D
EuCARD-2	Enhanced European Coordination for Accelerator Research & Development

Exp.	Experimental data
FEM	Finite element method
Fermilab	Fermi National Accelerator Laboratory in Batavia, Illinois, US
FM0	Feater-M0 YBCO dipole magnet being designed by EuCARD-2
FM2	Feater-M2 YBCO dipole magnet being designed by EuCARD-2
FRESCA-2	A high-field dipole designed for the CERN cable test facility by EuCARD
HD	High-field Dipole magnet developed at LBNL
HFU	Heater Firing Unit
HiLumi	LHC luminosity upgrade program
HiPot	Dielectric withstand voltage test
HE-LHC	LHC energy upgrade program
HF	High-field
HL-LHC	LHC luminosity upgrade program
HTS	High temperature superconductor
HD	High-field Dipole magnet developed at LBNL
HQ	High-gradient Quadrupole magnet developed with LARP
HQM	HQ coil tested individually in the mirror structure
HS	Heating station
IL	Inner coil layer
IR	Interaction-region in LHC
KEK	High energy accelerator research organization in Tsukuba, Japan
L1	Layer 1
L2	Layer 2
LARP	LHC Accelerator Research Program consisting of four US laboratories
L.A.S.A.	Laboratorio Acceleratori e Superconduttivita Applicata in Milan, Italy
LBNL	Lawrence Berkeley National Laboratory in Berkeley, California, US
LF	Low-field
LHC	Large Hadron Collider
LHQ	Long HQ
LTS	Low temperature superconductor
LQ	Long Quadrupole magnet developed with LARP
LR	Long Racetrack dipole magnet developed with LARP
MB	LHC main dipole Nb-Ti magnet
MBHSP01	First 11 T dipole model (2 m long)
MBHSP02	Second 11 T dipole model (1 m long)
MIITs	Current decay integral
MQ	LHC main quadrupole Nb-Ti magnet
MQXA	LHC IR quadrupole Nb-Ti magnet
MQXB	LHC IR quadrupole Nb-Ti magnet
Nb_3Sn	Niobium-tin based low temperature superconductor
Nb-Ti	Niobium-titanium based low temperature superconductor

NZPV	Normal Zone Propagation Velocity
OL	Outer coil layer
OS	Opening switch
PH-1L	MBHSP01 heaters with 1 layer of Kapton insulation
PH-2L	MBHSP01 heaters with 2 layers of Kapton insulation
PIT	Powder-in-tube based fabrication process for superconducting wires
QLASA	A quench simulation software
QUENCH	A quench simulation software
QuenchPro	A quench simulation software
QXF, MQXF	LHC IR upgrade quadrupole Nb_3Sn magnet under development
R&D	Research and development
RF	Radio frequency
ROXIE	A magnet design software
RRR	Residual resistivity ratio
SC	Superconducting
Sim.	Simulation result
SPQR	A quench simulation software
SQ	Subscale Quadrupole magnet developed with LARP
SQXF	Short QXF
ss	Stainless steel
SSL	Cable current short sample limit
THEA	A quench simulation software
TQ	Technology Quadrupole magnet developed with LARP
US	United States
WS	Wide segment
YBCO	Ytrium based high temperature superconductor

Chapter 1

Introduction

The discovery of superconductivity by Heike Kamerlingh Onnes in 1911 raised hopes of quickly seeing no-loss electrical transmission and strong electromagnets to improve various applications. Quite soon it was discovered, that although a superconductor is able to carry large currents without a loss, building practical magnets is challenging. The unstable nature of a superconductor makes it irreversibly lose the superconductivity, i.e. to quench, from the smallest disturbance. Today, after over 100 years of advancement both in the theoretical understanding and in the fabrication methods, large superconducting magnets have become established technology in applications of medical imaging, particle accelerators and detector magnets. It is also being applied to fusion reactors and radiotherapy with hadrons or ions.

This thesis focuses on the superconducting magnets for particle accelerators, although the concepts and findings are useful for other environments too. Accelerator magnets are challenging to built because they have very small mechanical and thermal tolerances. One of the most important aspects in their design is the protection in a case of a quench. The aim of the quench protection is to safely discharge the magnet's energy, avoiding serious overheating due to localized resistive losses. The quench protection schemes in accelerators such as the Large Hadron Collider (LHC) at CERN (the European Organization for Nuclear Research) and Tevatron at Fermilab (Fermi National Accelerator Laboratory) have been based on electric quench protection heaters. The idea is that the heaters suppress the superconducting state over a large fraction of winding allowing for faster and more uniform dissipation of the stored energy. The heater efficiency is characterized by how fast they deposit sufficient energy to the coils in order to increase their temperature above the critical value and cause a quench. The needed efficiency depends on the stored energy density

of the magnet and cable's properties. Now, when more and more powerful magnets are being developed for the accelerator upgrades, the efficiency of the heaters must be improved. The heater power cannot simply be increased due to voltage limitations, and consequently new approaches must be developed. The research contained in this thesis analyses the present status, future possibilities, and eventual limitations of heater based protection. The central research questions were:

- How to computationally simulate the efficiency of the state-of-the-art heater technology in Nb_3Sn based accelerator magnets and benchmark the results experimentally?

- How to optimize the heater design for the future magnets using the existing technology?

- Can the HTS-based magnets be protected using heaters? What are the limits that are faced in the heater based quench protection?

1.1 Scope of the thesis

To approach the above presented research questions, a central topic in this thesis work was to evaluate the efficiency of various quench protection heaters in different conditions. The important parameters are the time delay to normal zone initiation in the coil after the heater activation, i.e. the heater delay, and the amount of coil quenched by the heater. Ultimately, the efficiency is characterized by the produced current decay integral after the heater activation. However, the physics of the current decay are rather complex due to the presence of also AC-losses and therefore strongly depending on the cable and magnet design. Therefore, this thesis focused only on the heater delays. A computational tool was developed for heater simulation taking into account all the relevant parameters. Experiments were performed in order to validate the simulated delays. Parametric studies of the impact of various design parameters were used to propose new heater layouts with improved performance.

The research focused on the Nb_3Sn quadrupoles that are being developed for the LHC luminosity upgrade by the US LARP (LHC Accelerator Research Program) collaboration.

1.2 Structure of the thesis

Chapter 2 gives the background needed to appreciate the research presented later in the thesis and in the appended publications. It starts with the basics of superconducting accelerator magnets and their protection, including an overview of the existing quench protection simulation tools. Then, the heater technologies that have been used in the LHC and Tevatron or tested in R&D magnets are reviewed. This literature survey is aimed to work as a reference for the heater based protection technology development, since up to now this information has been spread over the literature and conference proceedings. It becomes clear that the heater design for the protection of the next generation accelerator magnets faces new challenges. This motivates the development of a novel heater analysis tool for the heater design optimization.

The development of the novel heater simulation tool is presented in Chapter 3. The rationale for using a relatively simple 2-D heat conduction model is explained, and the mathematical background of the implemented modeling tool is presented. The challenges in the heater modeling, such as the short time scales in the transient problems and what this means for the time stepping, are discussed. The correct implementation of the computational tool was verified by comparing the simulation results with ones given by an analytical solution in a simplified case and a commercial finite element method (FEM) based software in an actual heater simulation.

The simulation tool was applied to several high-field Nb_3Sn magnets. The feasibility of the approach was studied by comparing the computed delays with experimental data from dedicated measurements. The model sensitivity and uncertainties were also analyzed, since an understanding of the required design safety margin is important. These studies are presented in Chapter 4.

The 5th Chapter presents the simulation-based protection heater design studies for two Nb_3Sn magnets under development. One of these heaters was tested, and the test results as well as comparison with a traditional heater layout are presented.

In Chapter 6, the suitability of the modeling approach to HTS based magnets is discussed as well as the suitability of these heaters for protecting such magnets. This chapter looks for still unproven possibilities of quench heater technology and their modeling with the tool developed in this thesis.

Chapter 7 presents the final conclusions of this thesis work. It summarizes the main findings and their impact on the design and development of future high-field accelerator magnets and academic research in the area.

Chapter 2

Superconducting accelerator magnets and their protection

Particle accelerators are instruments into which electrically charged particles are injected and subsequently accelerated to a higher velocity thus increasing their kinetic energy. In circular machines, superconducting magnets are needed to produce the strong magnetic fields with very high quality to control the particle trajectories during their orbital motion. The ultimate framework for the magnet design and construction is given by the critical surface of the chosen superconductor material, i.e. the temperature, current density and magnetic field that limit the superconducting state. However, the possibility of an irreversible sudden loss of superconductivity, i.e., a quench, can never be fully excluded. In addition to disturbing the accelerator operation, a quench can lead to violent heat and voltage generation in the magnet windings and a pressure rise in the cryostat. In the worst case this can destroy the machine. Therefore, magnet protection in case of a quench must be included in the magnet development.

This chapter gives first an overview of the general features of superconducting accelerator magnets and their design and fabrication. The focus is on aspects, which are relevant for the magnet quench protection. The principles of quench protection design and heater based protection are then discussed in detail.

This thesis work focused on circular particle accelerators used in high energy physics research, in particular the LHC and the planned upgrades. Other uses for accelerators include isotope creation for medical imaging, radiotherapy for cancer treatment, and basic material and chemistry research [TIARA2015].

2.1 Superconducting accelerator magnets

2.1.1 Particle accelerators in high energy physics

In high-energy physics research particle accelerators are used as colliders. Particles are first accelerated to velocities near the speed of light and to energies in the GeV or TeV range. Then they are are made to collide against each other at the experiments [CERN2015b]. From the high energy densely localized in the collision, new particles emerge. The goal is to learn how matter, and ultimately our universe, was formed. The maximum energy, or the mass, of the new particles depends on the sum of the energies in the colliding particles. The quest for search of new higher and higher energy particles is the reason for the continuing pursuit to build higher and higher energy accelerators. In addition to the beam energy, an important parameter in the statistical analysis of the events is the luminosity, i.e., the number of collisions per cm^2 and per second.

The acceleration itself is obtained by oscillations of electric field in the RF-cavities [CERN2015a]. The field oscillations are timed with great precision so that the particle traveling in the beam vacuum pipe feels the attraction by the cavity it is approaching, and repulsion by the cavity that it has just passed. In the circular machine the particle travels several turns before the collision, gaining momentum at each turn. The control of the particles closed orbit is obtained by guiding them using magnetic fields: dipole fields bend them and quadrupole fields keep the particle bunches focused. The magnetic field strength must be increased synchronously with the beam energy increase, therefore this accelerator type is called a synchrotron.

2.1.2 General features of accelerator magnets

The dipoles and quadrupoles in accelerators are characterized by long length (several meters), high-field (several Tesla) with high-quality (inaccuracies limited to the order of 10^{-4}), high-current densities and high stored energies (on the order of MJ/m). In addition, the magnets must have good mass production quality. Limitations to the design space are also set by the high radiation environment. To obtain the high field with high accuracy is more challenging in dipole and quadrupole magnets than in solenoids for two reasons. First, because the management of large forces during the operation, and second, because the design of magnetic field profile is more complex.

In a circular accelerator the maximum energy (or momentum) of the particle is proportional to the dipole magnetic field that is available to exert a

bending force on it [Wie2007, p. 39]. Therefore, in order to build machines for higher energy particles, one needs to build dipoles with higher fields. An other option would be to build a circle with larger radius. In quadrupoles the important parameter is the field gradient which prevents the beam from enlarging. Special strong interaction region (IR) quadrupoles are used to minimize the beam size and increase the collision rate just before the interaction of the counter-circulating beams. Higher order multipole magnets are also used to further trim the beam and compensate for the predictable field errors.

Helium cooled superconducting electromagnets are used in accelerators because they enable magnetic fields above 1-2 T in a cost-effective and compact way compared to water-cooled copper magnets.

2.1.3 Superconducting materials

Superconductivity is characterized by two unique properties. First, the complete lack of electrical resistance. Second, the perfect diamagnetism known as the Meissner effect. In the 100 years following the discovery of superconductivity in 1911 over a hundred materials have been found to superconduct in conditions below certain temperature (T), current density (J) and magnetic field (B) (and stress) conditions. The critical values of those parameters are interdependent and together form a so-called critical surface specific to each superconducting material. Usually materials working below 30 K are referred as Low Temperature Superconductors (LTS), in contrast to the emerging High Temperature Superconductors (HTS), which can have critical temperatures up to 138 K [Dai1995]. However, only few of the materials are considered practical for accelerator magnet applications. All the practical materials are compounds and so called Type II hard superconductors. This means that they do not have abrupt transition from superconducting to normal state, but it happens gradually between two critical fields: B_{c1} and B_{c2}. Between these lower and upper critical field values, the external field partially penetrates the conductor as resistive flux vortices. The quantum mechanic theory of the superconductivity in LTS is generally accepted and described for example in [Bar1957]. The superconducting mechanism in HTS is not yet as well understood, but the theory development is active. One recently developed theory is presented in [Dav2013].

Presently, the most used material is the alloy niobium-titanium (Nb-Ti). It's popularity stems from its ductile structure, affordability and well established manufacturing processes [Car2003, p.609]. In practice, the use of Nb-Ti is limited below 10 T [Bot2000b]. At the moment the intermetallic compound

Nb_3Sn seems to be the only practical choice to replace Nb-Ti in large scale accelerator magnets and enabling fields up to about 15-20 T [Cas2005]. It was found in 1954 [Mat1954], 6 years earlier than Nb-Ti. It has a significant disadvantage of degradation of the superconducting properties when about 0.2% mechanical stress is present. This makes coil and magnet fabrication more difficult.

The HTS materials are often ceramics or rare earth cuprates, and were first discovered by Bednorz and Müller in 1986 [Bed1986]. They could be also called high-field materials, because when operated at low temperature, they offer a potential for a very high magnetic field. Their adoption in magnet applications has been slow due to technical difficulties related to their sensitivity to external magnetic field orientation, the slow transition to normal state making the quench protection difficult and, perhaps the most fundamentally, to the high cost of the conductor fabrication [Gur2011] and the limitations of conductor shape. However, several international projects are presently considering their use for future accelerators. The most promising materials presently are yttrium barium copper oxide (YBCO) and bismuth strontium calcium copper oxide (BSCCO).

2.1.4 Practical conductors

For the magnet winding, the superconductor must be available in wires and cables that are stable, i.e., which will remain superconductive during the operation. This requires complex fabrication methods.

Stabilization

The stabilization in LTS wires (also called strands) is obtained by embedding the superconducting material as thin filaments into a stabilizer matrix (usually copper) [Wil1983, p. 135]. Figure 2.1 a) and b) show cross-sections of Nb-Ti and Nb_3Sn wires. The stabilizer mitigates temperature excursions by increasing the wire heat capacity and improving the thermal conductivity. It also has a crucial role in magnet protection as it provides a low resistance path for the operation current in case the superconductor undergoes an unexpected transition to the normal state. This is discussed in detail in section 2.3. A typical wire diameter is in the order of 1 mm. The filaments must be thin (diameters less than 50 μm) to improve the stability, and reduce field errors due to persistent magnetization currents. The filaments are twisted to suppress the coupling of filaments through the resistive matrix during the mag-

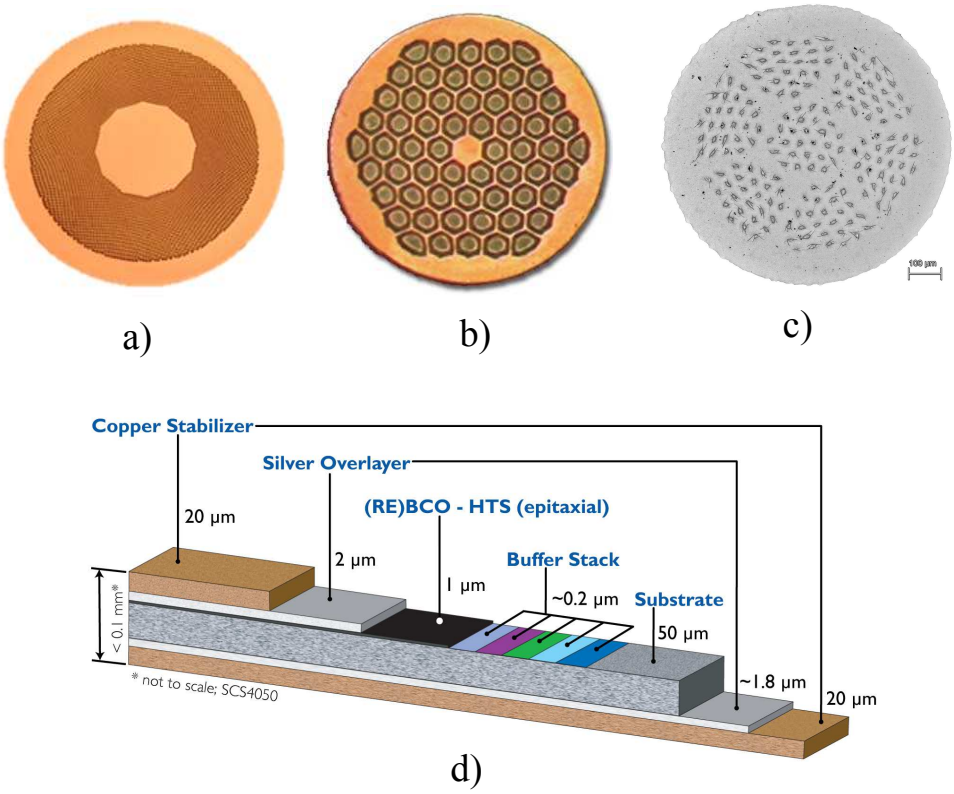

Figure 2.1: Cross-sections of a) Nb-Ti [LUVATA2015], b) Nb_3Sn [OST2015], and c) Bi-2212 [ASC2015] wires. d) Structure of a YBCO tape [SUPERPOWER2015].

netic field change [Lyl2013]. The heat generation by the flux flow movement is further limited by introducing so-called pinning sites where the flux vortices can adhere [tim2007].

Nb_3Sn wire fabrication

Nb_3Sn wires can be made in different techniques such as internal tin, powder-in-tube (PIT) and bronze process [Mat2002, p. 44], [God2005, p. 20]. Initially the wire components (Cu, Nb, Sn or Nb_2Sn) are separate and stacked in 5-30 cm diameter billets. Multi-step hot extrusion and drawing processes are used to draw the wire to the final length. Nb and Sn need several days of heat treatment in temperatures of about 650-700°C to react together to form the superconducting material Nb_3Sn. The Nb_3Sn phase is brittle, and sensitive to bending, so usually the cables are made from unreacted wire. The final coil can then be made with either reacted cable, or unreacted. If the coil is wound from unreacted cable then the whole coil must go in to the reaction oven. The

wind-and-react method is more common in accelerator-type magnets which require small bending radius. This is different to Nb-Ti fabrication because in Nb-Ti the superconducting phase is not brittle [Gre1992, Lau1998].

HTS conductor fabrication

On the HTS side, the BSCCO compound $Bi_2Sr_2CaCu_2O_{8+x}$, commonly referred as Bi-2212, can be made in round wires using the PIT and re-stacking processes and silver as the matrix metal [Mia2005, Mia2012]. A wire cross-section is shown in figure 2.1 c). However, the fabrication is more challenging than for Nb_3Sn due to the needed heat treatment at nearly 900°C and at 100 bar, where the temperature uniformity must be controlled within 1°C.

YBCO instead is commercially fabricated as a rectangular tape, so-called coated conductor, in which the superconducting layer is about 1 or 2 μm thick [SUPERPOWER2015] (1-2% of cross-section), see figure 2.1 d). It is a serious disadvantage to YBCO that the rectangular shape is like a large monofilament and it is difficult to twist for stabilization purposes. The advantage of YBCO over Bi-2212 and the LTS materials is the larger critical current density at low temperature, as shown in figure 2.2.

Cables

The most popular cable configuration in accelerator magnets is a flat multi-strand two-layer Rutherford cable. It provides the transposition that is needed to limit the interstrand coupling, as well as high packing factor, good stacking possibilities and good mechanical stability [Wil2009]. Because round strands are needed, Nb-Ti, Nb_3Sn and Bi-2212 can all be made as Rutherford cable, but YBCO cannot.

To provide twisting in the YBCO tape, cable configurations such as Roebel [Lon2010], Conductor on Round Core (CORC) [Van2009, Van2013] and twisted stacked-tape cable [Bar2015] have been proposed. Of these options, Roebel has the most similar properties to Rutherford and is considered presently the most promising for accelerator magnet purposes, see figure 2.3.

2.1.5 Coils and magnet assembly

The dipole magnets consist of two coils, and quadrupoles of four coils, which are arranged around the beam pipe. An important parameter is the magnet

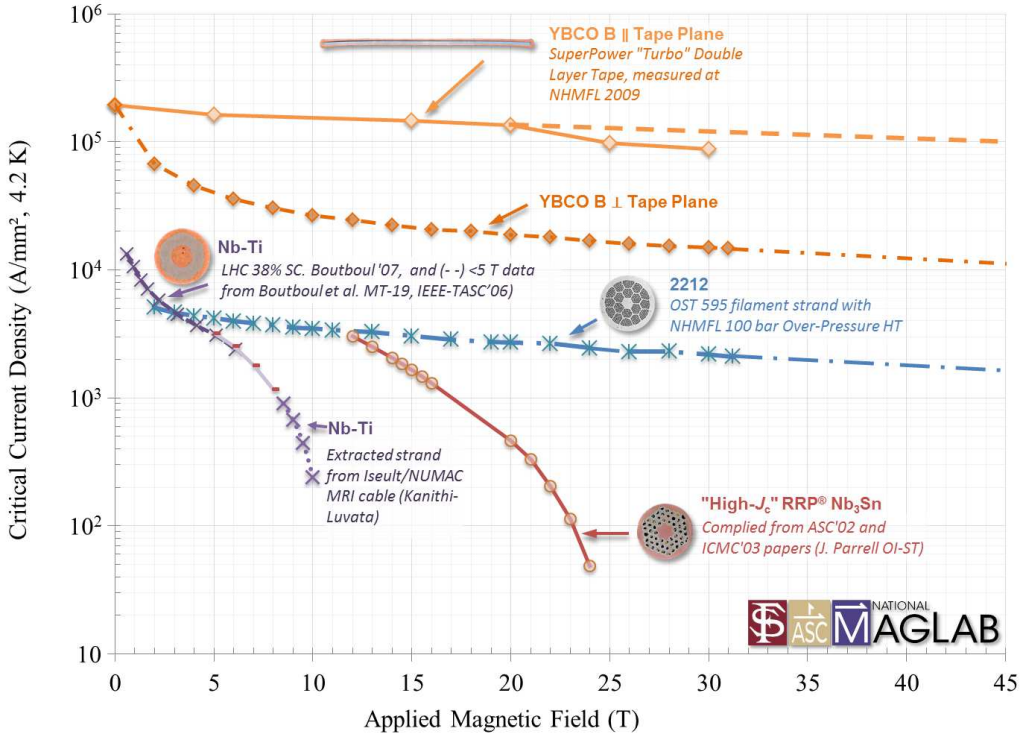

Figure 2.2: Critical current density vs. applied magnetic field in Nb-Ti, Nb_3Sn, Bi-2212 and YBCO at 4.2 K [Lee2014].

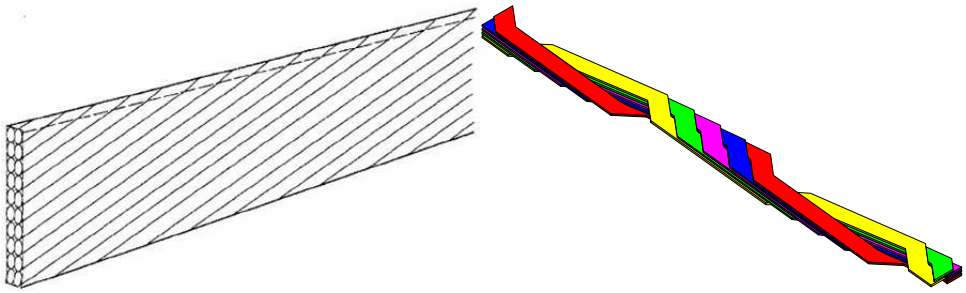

(a) Rutherford [Dev2004] *(b) Roebel [Bar2012]*

Figure 2.3: Cable configurations.

aperture, or the bore size, which is defined by the coil inner diameter. In existing accelerator magnets the apertures are within 50 and 90 mm [Per1996].

To get the dipole or quadrupole field in the aperture, the goal is often to obtain a cos-θ current density distribution around the bore for a dipole field, and cos-2θ for quadrupole field. Figure 2.4 shows the field profiles in

ideal dipoles and quadrupoles where the coil is a uniformly thick cylinder. However, with rectangular cable it is more practical to approximate this current density distribution by using sector coils with wedges between cable blocks. The Rutherford cables are keystoned (pressed to a trapezoidal shape) in order to better fit them in sector geometries. Figure 2.5 shows the cross-sections of the LHC main dipole and quadrupole coils. The two layers of the coils are wound around central pole pieces. Other coil configurations include a block dipole [Sab2015], Canted-Cosine-Theta magnet [Cas2014] and common coil [Amb2001]. The magnetic field design and optimization is discussed in detail for example in [Ros2006, Ros2007, Rus2006].

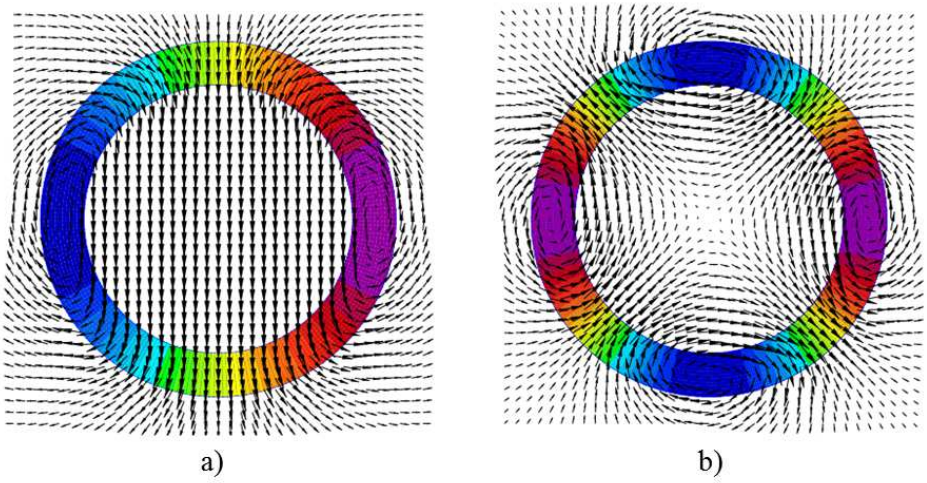

Figure 2.4: A cylindrical coil with a) cos-θ and b) cos-2θ distribution of current density to create perfect dipole and quadrupole fields, respectively [Rus2006].

The so-called short sample limit (SSL) is the highest possible current that the magnet can be exited to. It is based on measuring the critical current of a short sample of the cable (often using one extracted strand). This current is not always reached in the magnet, probably because some degradation occurs during the winding and assembly processes. The present Nb_3Sn accelerator magnets are designed to operate at 80% of SSL.

The cables are insulated before winding to electrically separate the turns. Nb-Ti coils are usually insulated with Kapton, but this cannot be used in the wind-and-react Nb_3Sn coils because Kapton cannot withstand the high heat treatment temperature. Materials such as pre-impregnated glass, e-glass, s-glass and ceramic insulation have been considered [Imb2003]. Typical insulation thickness is in the order of 0.1 mm.

The coils are assembled together, and clamped inside so-called collars of

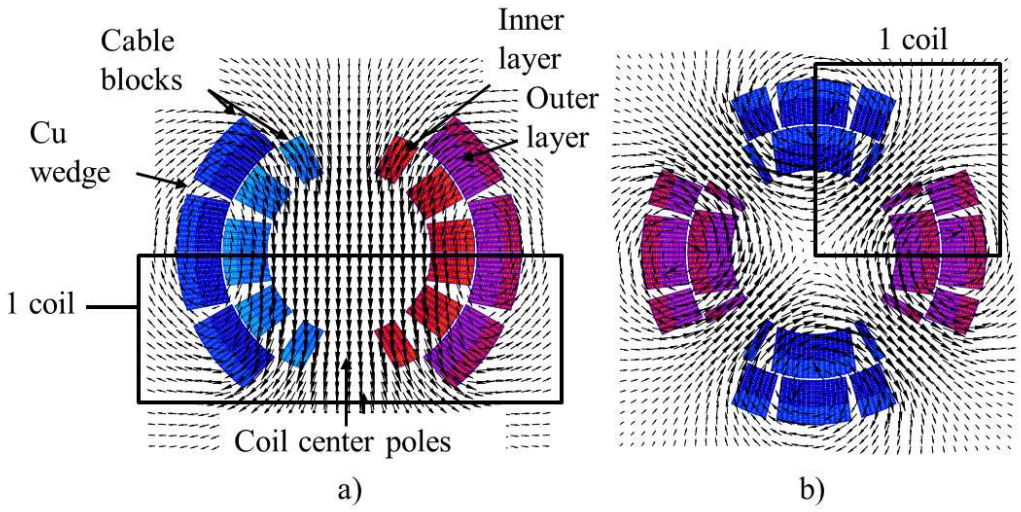

Figure 2.5: LHC a) dipole and b) quadrupole coils with two-layer sector coils made with keystoned Rutherford cable. The LHC dipole has a different cable on inner and outer layer. Modified from [Rus2006].

non-magnetic material (usually austentic stainless steel or aluminum) to hold them in place. The collared coils are surrounded by iron yoke which enhances the field and limits the stray field around the magnet. This assembly is usually inserted into a cylindrical shell. The mechanical structure must be strong enough to withstand the large Lorenz forces during operation. Finally, the magnet is inserted into a cryostat. The Nb_3Sn coils are usually epoxy impregnated before the assembly.

The space inside the cryostat is expensive due to the very low temperature. This limits the instrumentation wires to the minimum. Further limitation to the impregnation, insulation, electronics and all materials come because they must survive the high radiation dose, especially near the interaction regions.

2.2 The Large Hadron Collider

The LHC at CERN is a 27 km long synchrotron collider, installed in a tunnel having diameter of 4 m about 90 m underground [Brü2004, Brü2007]. Two proton beams circulate in opposite directions and are made to collide at four experiments [CERN2015b] with maximum collision energy of 14 TeV. The LHC can be also used with lead ion beams [ALICE2008]. The first collisions started in 2009 [CERN2009] and 2012 one of the main goals, experimental

observation of the particle called Higgs boson, was announced [CERN2015c]. In 2013 theoretical physicists Englert and Higgs were awarded the Nobel Prize in Physics for the theory of the Higg's mechanism "that contributes to our understanding of the origin of mass of subatomic particles" [NOBEL2013].

The LHC design value for luminosity is 10^{34} $cm^{-2}s^{-1}$. The near-future plan for upgrading the machine includes the luminosity upgrade around 2020, which requires stronger quadrupoles for the interaction region. This requires replacing the present Nb-Ti technology with Nb_3Sn. The magnets in focus for this thesis are related to the LHC upgrade plan, particularly the interaction region upgrade.

2.2.1 Superconducting magnets

The LHC main dipoles (MB) and main quadrupoles (MQ) are used to guide the beam inside the ring. The interaction region quadrupoles MQXA and MQXB provide the final focusing before the beam-beam interaction (collision). Table 2.1 reviews the parameters of the LHC MB, MQ, MQXA and MQXB. The conductor parameters are summarized in table 2.2.

The LHC MB and MQ magnets have two apertures in a common collar and yoke to house the two beam pipes for the two counter-circulating particle beams. The cross-section of MB assembled in a cryostat is shown in figure 2.6. The coils in each aperture are arranged in two layers. In MB, different strand and cable are used for each coil layer to obtain higher current density in the outer layer, where the field is lower. This is called grading and it serves for saving in material costs and facilitates the quench protection. The main quadrupoles are made of the MB outer layer cable.

The IR quadrupoles MQXA and MQXB are single aperture magnets. MQXA was built at KEK, and MQXB at Fermilab. Four magnets are arranged in a sequence to form the so-called inner triplet [Brü2004]. The cross-section of MQXB is shown in figure 2.7.

2.2.2 Upgrades R&D program

Luminosity upgrade

The High Luminosity project (HiLumi or HL-LHC) has a goal to increase the LHC luminosity by a factor of 10 and exploit the full potential of the LHC. The upgrade includes replacing the inner triplet Nb-Ti quadrupoles with new

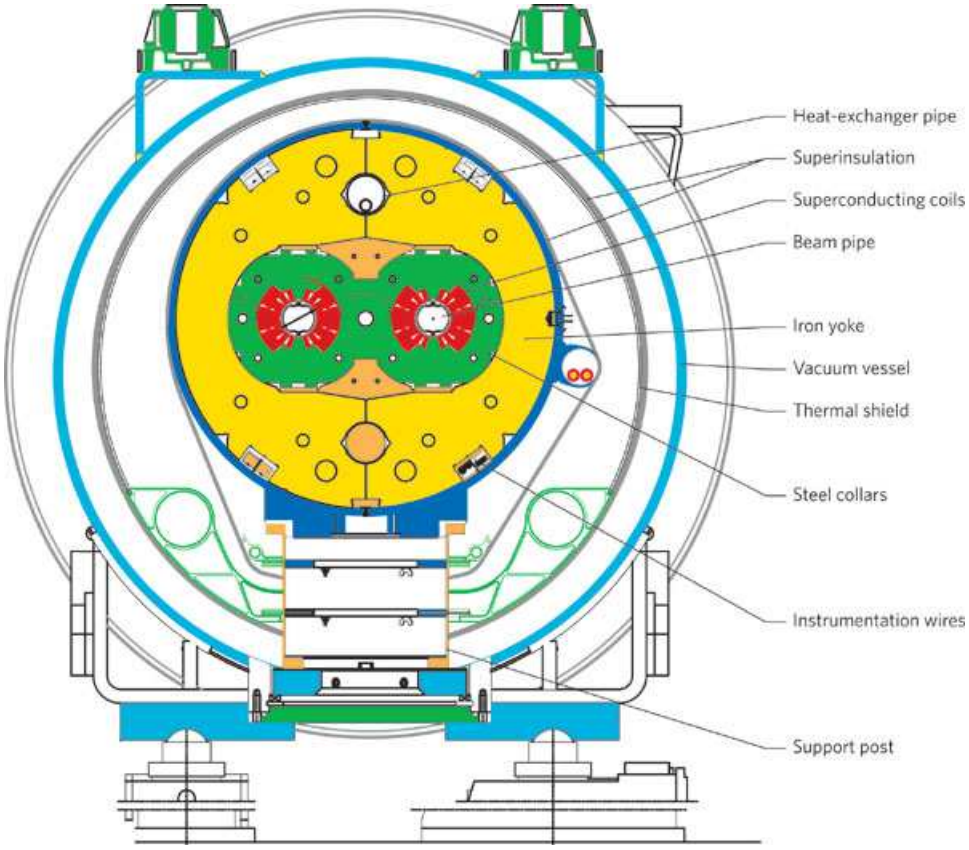

Figure 2.6: Cross-section of the LHC dipole in a cryostat, showing the two beam pipes, coils and collars surrounded and the iron yoke [Brü2007].

Table 2.1: LHC superconducting main dipoles (MB), quadrupoles (MQ) and the interaction region quadrupoles (MQXA and MQXB) in operation conditions. [Brü2004, Yam2005]

Magnet	MB	MQ	MQXA	MQXB
Number of magnets	1232	392	16	16
Magnetic length [m]	14.1	3.1	6.4	5.5
Aperture [mm]	56	56	70	70
Nominal current [A]	11900	11900	7200	11900
Peak field [T]	8.3	6.7	8.6	7.7
Field gradient [T/m]	N/A	223	215	215
Stored energy / aperture [MJ]	3.5	0.395	2.24	1.36

larger aperture Nb_3Sn magnets by 2023 [Fer2014]. The new quadrupoles are referred as QXF, or MQXF. Then, some of the dipoles are replaced with shorter

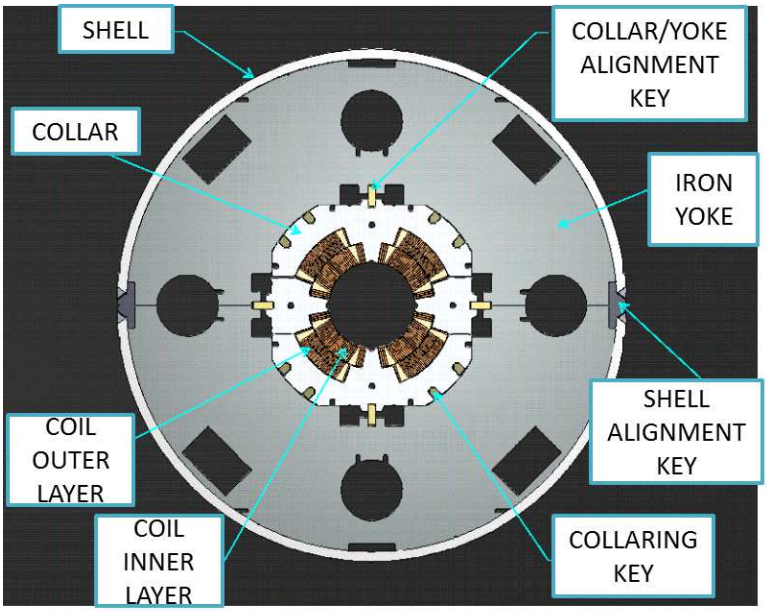

Figure 2.7: Cross-section of the LHC MQXB quadrupole, modified from [Zlo2005].

Table 2.2: Conductor parameters in LHC main dipoles (MB) and IR quadrupoles (MQXA and MQXB) on coil inner (IL) and outer layer (OL). The main quadrupole (MQ) used the MB OL cable. [Bos2003, Brü2004, Yam2005]

Magnet	MB	MQXA	MQXB
Strands in cable (IL/OL)	28/36	27/30	37/46
Strand Cu/Non-Cu (IL/OL)	1.65/1.95	1.2/1.9	1.3/1.8
Strand diameter (IL/OL)(mm)	1.065/0.825	0.815/0.735	0.808/0.65

dipoles having higher field and collimators to have the same bending effect and increased focusing. These new dipoles are called 11 T dipoles and built in collaboration with CERN and Fermilab. The HiLumi project is supported in part by funding from the Seventh Framework Programme of the European Commission.

The US is contributing to the project withing the LARP framework (LHC Accelerator Research Program) [LARP2015]. LARP is a collaboration of four US national laboratories: Lawrence Berkeley National Laboratory (LBNL), Fermilab, Brookhaven National Laboratory (BNL), and SLAC National Accelerator Laboratory. Since 2003 LBNL, BNL and Fermilab have been developing prototype quadrupoles using Nb_3Sn conductor. The studies within this thesis mostly considered the LARP R&D magnets, although data is used also from the 11 T dipoles.

The key parameters for QXF have evolved during the project, and presently are fixed at gradient of 140 T/m in 150 mm aperture. Two different lengths of the magnets will be built: 6.8 m and 4 m. In the case of the 4 m long magnets, two magnets are connected together in one cold mass [Fer2014]. The operation current will be about 17.5 kA and peak field about 12.1 T. The stored energy density (1.3 MJ/m of magnet) is several times larger than in the present Nb-Ti magnets.

The prototype development by LARP started from a Subscale Quadrupole magnet program (SQ) to study small, about 0.3 m long, Nb_3Sn racetrack coils, and proceeded to the Technology Quadrupole program (TQ) [Fel2009b] to study the SQ technology in 1-m long cos-2θ coils and the impact of different support structures. The Long Racetrack (LR) and Long Quadrupole (LQ) tested the application of these concepts to 3.6-m long racetrack and cos-2θ coils, respectively. The 1-m long High-gradient Quadrupole (HQ) series aims at producing the accelerator field quality in 1-m long 120-mm aperture quadrupoles. The HQ is the closest prototype up to date of the final IR quadrupole to be installed in the luminosity upgrade. The magnet cross-sections are shown in figure 2.8, and the most important parameters are summarized in table 2.3. Details of the HQ magnet are shown also in figure 2.9.

Table 2.3: Examples of the R&D Nb_3Sn magnets and their short sample (SSL) conditions built within the US LARP collaboration. QXF is in the design phase.

Magnet	TQ	LQ	HQ	QXF
Magnetic length [m]	0.9	3.6	0.9	2x4 or 6.8
Aperture [mm]	90	90	120	150
SSL @1.9 K [kA]	14-15	14.6	19.1	21.6
B_{peak} @SSL @1.9 K [T]	13-14	12.5	15	14.7
Gradient @SSL @1.9 K [T/m]	250-270	240	230	171
Stored energy @SSL @1.9 K [MJ/m]	0.5-0.6	0.5	1	1.9

Energy upgrade

Several projects are underway to explore the upgrade of the LHC to a higher energy (HE-LHC) [Ros2015, Tod2011]. One of the research topics is the use of HTS coils. Although this thesis mainly focuses on the quench protection of the HiLumi magnets, the final chapter presents the first analysis of heater based protection in the HTS magnets developed in preparation for the HE-LHC.

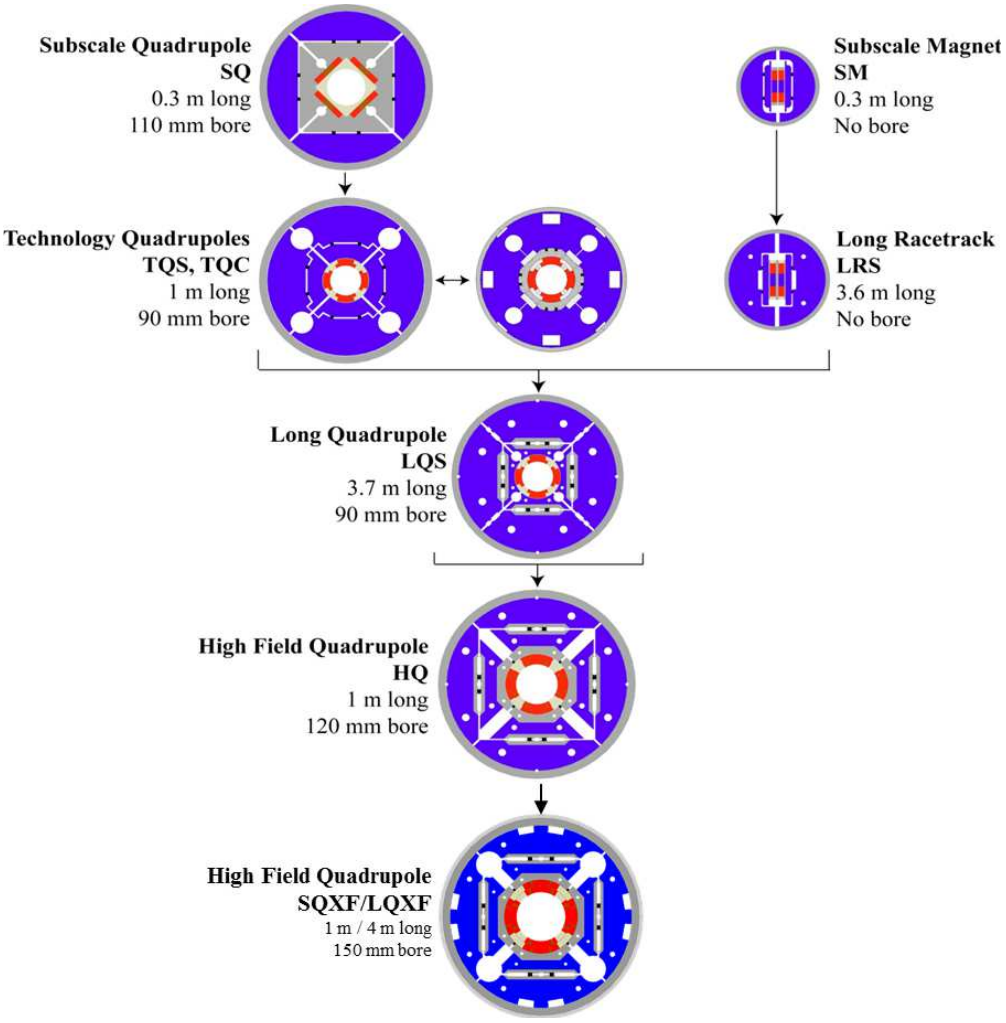

Figure 2.8: LARP magnet development flow-chart [Apo2014].

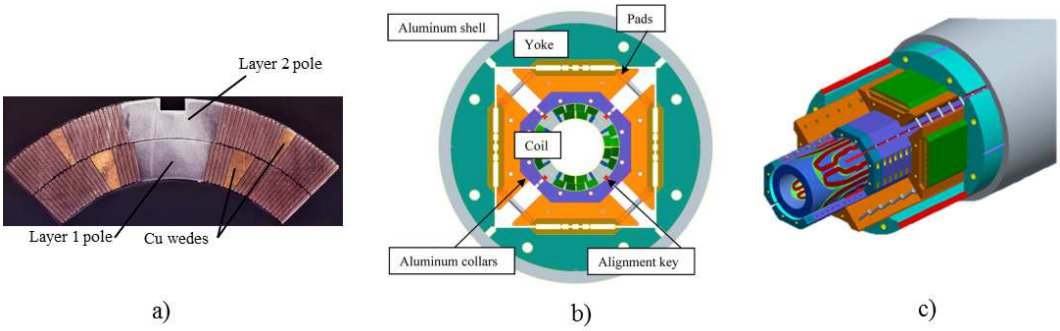

Figure 2.9: HQ01 a) coil cut, b) magnet cross-section, b) exploded view.

2.3 Quench protection of accelerator magnets

2.3.1 What is a quench?

In regular magnet operation the current flows in the superconducting fraction of the cables and causes no resistive losses. However, even small disturbances may lead to local temperature (or magnetic field) increase and consequently lower the cable critical current (I_c) below the magnet operation current (I_{mag}). Figure 2.10 shows the critical surface for Nb_3Sn and Nb-Ti demonstrating the material critical current density dependency on the temperature and field. When the critical surface is punctured, the excess current (the difference between I_{mag} and I_c) cannot be carried without resistance anymore and losses will occur. The stabilizer matrix of high-conductivity metal in parallel with the superconductor allows a lower resistance route to the excess current and increases the heat capacity to absorb the generated heat. The phase when both the superconductor and the matrix carry the current is called current sharing regime, and the conductor temperature at which it starts the current sharing temperature (T_{cs}). If the cooling is not sufficient to remove the generated heat, the temperature increases and the adjacent cable segments also heat up and transit to the resistive, or normal conducting, state. This cascade of events is known as a thermal runaway, a quench, and quench propagation. The region of resistive current flow is called a normal zone in the cable. The current densities in the copper matrix of Nb_3Sn magnets can be over 1 kA/mm^2, so temperature rises rapidly. If nothing is done, the damage may be lethal to the accelerator.

The initial energy to precipitate a quench can come internally from the magnet via for example AC-losses during the magnet ramp, magneto-thermal instabilities, or conductor movement under the large Lorenz forces. Also external disturbances such as beam losses or temperature rise of the coolant can cause a quench. Willering discussed in his PhD thesis [Wil2009] the impact of the different phenomena on the conductor stability in Rutherford cables.

The goal of quench protection is to safely dissipate the energy stored in the magnetic field after a quench and limit the magnet temperature and voltages to safe values. In practice the aim is to detect the quench as fast as possible and then switch off the current supply and obtain as fast as possible current decay. The magnet energy can be discharged either to an external dump resistor, or internally into the windings.

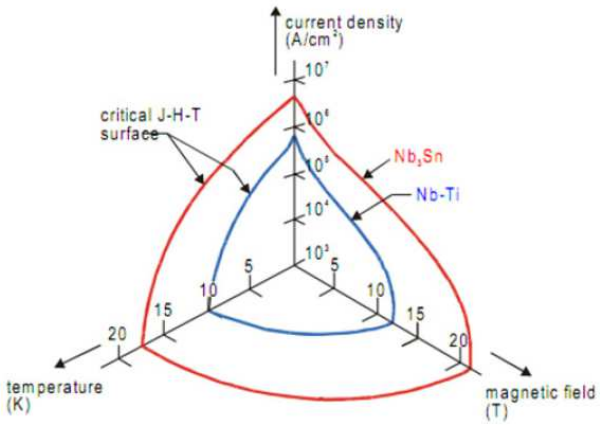

Figure 2.10: A schematic of the critical surface of Nb_3Sn and Nb-Ti. [Eva2009, p. 70].

2.3.2 Peak temperature estimation

The peak temperature is the most critical quench parameter. The heat generation in the quenched cable segment is predominantly caused by the operation current flowing in the resistive matrix metal. When the cable parameters are known, the so-called MIITs concept can be used to relate the current decay profile after a quench to the peak temperature [Tod2013a].

In the MIITs analysis, the heat generated in the cable cross-section is assumed adiabatically absorbed in the cable thermal mass. The temperature rise $\mathrm{d}T$ during time $\mathrm{d}t$ is

$$J(t)^2\rho(B,T)dt = \gamma c_p(T)\mathrm{d}T, \tag{2.1}$$

where J (in $\mathrm{A/m^2}$) is the current density in the cable cross-section, ρ (in Ωm) is the electrical resistivity, γ (in $\mathrm{kg/m^3}$) is the mass density of the cable absorbing the generated heat, and c_p (in J/kg/K) is its specific heat. The material properties are averaged over the participating cable components. Based on the studies of Imbasciati [Imb2003], the preference is to consider the cable and its insulation but exclude the helium.

If all the current flows in the copper, the average power density in the cable cross-section is

$$J(t)^2\rho(T) = J_{Cu}(t)^2\rho_{Cu}(T)\lambda_{Cu} = \frac{I_{mag}(t)^2}{\lambda_{Cu}^2 A_{cable}^2}\rho_{Cu}(B,T)\lambda_{Cu}, \tag{2.2}$$

where I_{mag} is the magnet current, and λ_{Cu} is the cable copper fraction. This is usually a valid assumption because the copper resistivity is about two orders

of magnitude lower than that of the Nb-Ti or Nb_3Sn in normal state. During the current sharing phase however, the losses in the superconductor should be considered too. Especially, in the case of HTS cables the current sharing phase cannot be neglected because it can take a considerably long time.

The squared current decay integral obtained by combining (2.1) and (2.2), and integrating after rearranging:

$$\int_0^\infty I_{mag}(t)^2 \mathrm{d}t = \int_{T_{cs}}^{T_{max}} \lambda_{Cu} A_{cable}^2 \frac{(\gamma c_p(T))_{cable}}{\rho_{Cu}(T)} \mathrm{d}T, \tag{2.3}$$

where T_{max} is the final temperature. The starting temperature in the integral is sometimes taken as the operation temperature, and it could be also taken as the T_c, i.e., when all the current has gone into the copper. However, because the relatively small heat capacities at temperatures below 10 K, the change in the result is negligible in LTS.

The left-hand side of (2.3) is also called the *quenchload*, and when it is scaled with 10^{-6}, the unit is called MIITs[1]. It is a useful parameter, because it relates the current decay profile after a quench (which is easy to measure) to the hotspot temperature (which is difficult to measure).

Figure 2.11 shows the calculated MIITs vs. temperature curve for a typical Nb_3Sn cable, approximating the LARP HQ cable. In the computation A_{cable} was 25.1 mm^2, epoxy and G10 fraction of the cable unit cell were both 0.15, representing the impregnation in the cable voids and the glass cable insulation. The copper to superconductor ratio was 1.23 resulting to λ_{Cu} of about 0.39. The copper RRR was 150. It is also shown how the MIITs value corresponding to 300 K varies as a function of magnetic field (through the magnetoresistance impact on ρ_{Cu}), linearly with λ_{Cu}, and quadratically with A_{cable}. The temperature and magnetic field dependent material properties are as described in section 3.1.4.

2.3.3 Quench detection

The first thing to do after the origin of a quench is to detect it as rapidly as possible with dedicated hardware. In practice, the quench detection in an accelerator magnet is based on measuring the voltage rise associated to the resistive zone in the cable. Detecting resistive voltages from some tens of mV to a few hundred of mV, requires compensation of the inductive voltages that are present during the magnet current ramps[2]. This is commonly done using a

[1] MIITs is an abbreviation of Mega*Current*Current*Time

[2] Magnet can quench at constant current or during a ramp.

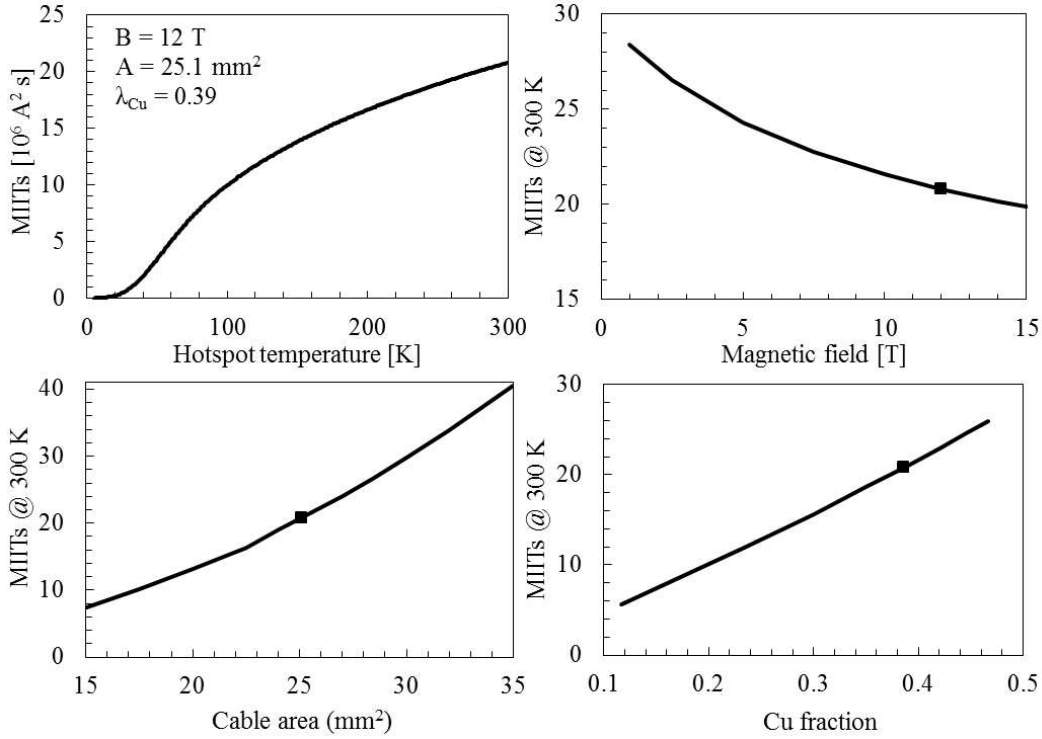

Figure 2.11: MIITs vs. temperature in a Nb_3Sn cable, and the MIITs budget for 300 K as a function magnetic field, cable copper fraction and cable area. Squares present the reference case (i.e. parameters from the top left hand corner).

balanced bridge circuit, which compares the voltage over at least two identical segments of the magnet. As the inductive voltages are assumed equal on both sides of the bridge, the imbalance is associated with a resistive voltage on either side. Additional logic may be implemented to catch symmetric quenches, i.e. when both sides of the bridge quench simultaneously.

When the resistive voltage exceeds a detection threshold, V_{th}, and stays above it for the so-called validation time, it triggers the quench protection system. The V_{th} must be as low as possible, however being above the system noise level to avoid false triggers.

In the LHC main dipoles and quadrupoles the threshold is 100 mV with a validation time of 10 ms [Den2006]. The analogical detection bridge compares continuously the voltages over the two magnet apertures [Den2011] in the dipoles, and over two coils in one quadrupole (the two apertures in MQ are powered separately). The single-aperture interaction region magnets, including the inner triplet quadrupoles, have a digital detection system [Den2006]. The voltage bridge includes voltage taps at the middle of the coil, and on the cold-

end of the current leads. The two coil-halves are compared in the bridge. The time delay from quench onset to reaching the threshold voltage is called detection time and it depends on the magnet operation conditions. During the LHC dipole commissioning, a detection time of about 20 ms was measured near the maximum operation current [Ver2008].

2.3.4 Current supply disconnection

Following the quench detection, the current supply is disconnected as fast as possible after the safe abort of the particle beam. The current then decays in the magnet circuit according to a time constant defined by the ratio of inductance and resistance of the circuit. [Sie2013]

It is typical that in accelerators several magnets are powered in series. For example, the main dipoles of the LHC are powered in circuits of 154 magnets, having inductance of 16 H and stored energy up to 1.3 GJ at the maximum current of 13 kA. When the current supply is disconnected, a 150 mΩ dump resistor is switched in series with the magnet chain and the quenched magnet is decoupled from the chain with cold diodes. In the quenching magnet protection heaters are activated to accelerate the normal zone propagation and the increased coil resistance will drive the current decay faster (in about 100 ms, as will be discussed later). Other circuits will stay superconducting, and decay with a longer time constant, 16 H / 150 mΩ = 107 s. [Dah2001]

2.3.5 Quench protection

External energy extraction

Although this is not the case in the dipoles of LHC, part of the stored energy of the quenching magnet could be deposited into an external dump resistor, which is switched in series with the magnet after the current supply disconnection. The advantages of the external resistor are its prompt availability, and that it limits the energy dumped in the helium thus reducing the cryostat pressure and fastening the recovery of the operation temperature again after the quench. In the tests of individual magnets dump resistors are commonly used.

The maximum size of the dump resistor ($R_{dump,max}$) is limited by the maximum voltage allowed across the magnet terminals ($V_{mag,max}$). In the case of one magnet with maximum current $I_{mag,max}$ and one dump resistor connected

in series:

$$|V_{mag}| = |V_{dump}| = R_{dump} I_{mag} \Rightarrow R_{dump,max} = |V_{mag,max}|/I_{mag,max}. \quad (2.4)$$

A typical maximum voltage is 1 kV, so the dump resistor value is between 100 and 50 mΩ for magnet currents between 10 and 20 kA. The energy that is dissipated in the resistor can be computed from the current decay integral:

$$E_{dump} = R_{dump} \int_0^\infty I_{mag}^2(t) \mathrm{d}t. \quad (2.5)$$

It is important to note, that the maximum dump resistor size depends only on the magnet current (for a given voltage limit), and not on magnet length. Therefore, in longer magnets, relatively smaller fraction of the energy can be extracted. For example in the HQ magnet, the current integral of about 20 MIITs corresponds to peak temperature of 300 K. The SSL at 1.9 K is 19 kA, so the maximum R_{dump} is 53 mΩ and the extracted energy is about 1 MJ. Note, that this is overly optimistic because it assumes that the dump resistor was active immediately at the quench onset. In this case the 1 m long magnet could be protected by the dump resistor, but from 4 m or 8 m long magnets only 25% or 12.5% of the energy, respectively, could be extracted.

Quench protection heaters

In long high-field magnets only a small fraction of the stored energy can be extracted from the magnet system. Most of the energy must be absorbed by the winding itself. In order to avoid over-heating of the relatively small volume associated with the initial quench, protection heaters are used to suppress the superconducting state over a large fraction of the winding. This provides a larger resistive volume that participates in the absorption of the stored energy. The decrease of hotspot temperature is also clear from the increased circuit resistance, which leads to faster current decay and lower MIITs.

The protection heaters are resistive strips in close contact to the cables. They are usually powered with a capacitor discharge. The heater surface power (P_{PH}) (in W/cm^2) is an important design parameter. It is computed adiabatically by dividing the heater power by the heating surface area [Fel2009a]. Electrical insulation between heater and coils is usually obtained by a thin layer of polyimide.

The heater efficiency is characterized by the heater delay, which is the time delay between heater activation and the heater induced normal zone development in the coil. It depends on the cable characteristics and its energy

margin to quench as well as heater characteristics in particular the heating power, heater layout and insulation scheme. Another important parameter is the fraction of the coil the heaters manage to quench. Usually it is not possible to cover the whole coil surface with heaters due to voltage limits and technical difficulties related on positioning heaters on coil inner surfaces. Different heater designs, including those used in the LHC magnets, are discussed in detail in the next section.

Redundancy is important because some heaters may not be functional due to a damage of the insulation, or a capacitor bank, which is used to fire the heaters, may have failure. The LHC guideline for redundancy is that the magnet should be protected even when half of the heaters are functional.

Quench back

The term quench back refers to the quenches induced by the AC-losses during the magnet current decay. After firing the heaters, the magnet current change rate $\mathrm{d}I/\mathrm{d}t$ can be several tens of kA/s, associated with a field change rate $\mathrm{d}B/\mathrm{d}t$ of several thousands of T/s. In LHC the $\mathrm{d}I/\mathrm{d}t$ can be up to 60 kA/s [Rod2000] corresponding to $\mathrm{d}B/\mathrm{d}t$ of 43 kT/s estimated using a linear $\mathrm{d}B/\mathrm{d}I$ dependence. The changing field induces eddy currents in the normal conducting components such as the copper wedges and in the loops formed by the cable strands and filaments. In the superconductor magnetization losses are generated. The heat generated by these losses may cause transition in the still superconducting parts of the magnets. In addition of spreading the quench, the AC-losses help because part of the stored energy is dissipated in the magnet support structure. It is also possible to design special resistive quench back cylinders or secondary coils that work as secondary circuits. They heat up during the current decay and cause quench back to the coil due to the thermal conduction [Gre1984].

Other methods

Quench protection methods based on coil subdivision or actively induced AC-losses have been proposed [Meß1998]. However, their suitability in an accelerator is limited. The magnet current ramps would cause unwanted heating in the secondary inductive elements, and the subdivision would increase the number of current leads from the cryostat and complicate the electric circuit.

The development is still ongoing because the heaters and dump resistors are believed to be at the limit when it comes to the high-energy Nb_3Sn mag-

nets. A recent innovation developed at CERN is to discarge a capacitor into the coils, which generates an oscillation leading to $\mathrm{d}B/\mathrm{d}t$ able to quench the cable [PATENT2013, Rav2014]. This Coupling-Loss-Induced Quench system (CLIQ) has been tested with promising results [Rav2015], and is considered as a back-up for heater based protection.

2.3.6 Quench protection simulation tools

Quench protection analysis and design heavily relies on simulation of magnet current decay and temperature evolution. Based on [Fel2013], the approaches can be classified in the different level of approximation they use. The most simple are adiabatic ones based on the MIITs concept. Complexity is added when the heat diffusion within the coil and cooling by heat exchange with helium are included. An array of different programs have been developed within the last 50 years. Here are the most important simulation tools used in the quench protection design of the LHC or of the recent R&D Nb_3Sn accelerator magnets.

Tools based on normal zone propagation velocities

The code QUENCH (Wilson 1968) is the father of several numerical quench analysis tools. It was developed for solenoidal coils, but later developments, such as QLASA [Mar2013, Ros2004] by L.A.S.A. (Laboratorio Acceleratori e Superconduttivita Applicata), Milan, Italy, have extended its use to accelerator type dipoles and quadrupoles. It is based on analytic computation of the normal zone expansion in both longitudinal and transverse direction within a coil. The normal zone volume increases at each time step by an isothermal layer. Each layer generates heat due to the current flowing in the normal conducting fraction of it. At each time step the layers temperatures and resistances are evaluated (taking into account the temperature dependent material properties), and the current decay and voltages are calculated based on the resistance development. QLASA allows adding a dump resistor and protection heaters. The heaters delay and the fraction of the coil they quench are given as input parameters. Although the discretization is in the coil level, several coils can be defined to represent the different layers in the accelerator coil, and they can be powered separately. QLASA has been used in the design and analysis of the Nb_3Sn magnets.

An other adiabatic model used in Nb_3Sn magnet design is QuenchPro [Bau2000, Bau2001a, Bau2001b, Ros2012], implemented in a MathCad spread-

sheet at Fermilab. The quench propagation velocities are given in the input. The discretization is at the coil level like in QLASA, and up to 16 in series powered "sub-coils" can be defined. The computation occurs in two parts: First the temperature evolution and the corresponding resistance increase and current decay are computed. The second part computes the resistive and inductive voltages to ground and between turns based on an inductance matrix which is based on the coil coordinates. Dump resistor and protection heaters can be introduced. The heater delay and the fraction of the coil they cover are again input parameters.

Tools based on solving the heat diffusion equation

The program SPQR (Simulation Program for Quench Research) was developed at CERN and widely used in the LHC protection design. The program includes various cases that can be considered: The quench propagation in 1-D, 2-D or 3-D, heat diffusion from protection heaters, and quench back [Son2001a, Son2001c, Ver1995]. It can be coupled with the quench protection package QUABER [Hag1992], which is based on the commercial network solver SABER [SABER]. It computes the magnet current decay based on the coil resistances and estimates the temperature distribution based on the MIITs curve. The magnetic field distribution and its decay as a function of current decay are inputs provided by the CERN -developed magnet optimization suite ROXIE [Rus2010].

In SPQR, the quench propagation and temperature evolution is computed by solving the joule heat generation and the heat balance equation using the finite difference method. The transverse cooling with helium is taken into account as a cooling term in the equation. The two and three dimensional models compute also the heat transfer through different turns. To decrease the computational complexity, the temperature profiles between the coil turns and the cable and helium are assumed linear. A so-called matrix model is also included for a more detailed treatment of the heat flux through the insulation. The heater delays are computed by solving the heat diffusion from the heater to the cable taking into account the heat generation in the heater due to the heater current. [Son2001a, Son2001b]

ROXIE has its own quench module [Sch2008, Sch2009], too. The thermal propagation after a quench is computed in the entire coil, which is modeled at the cable level. It allows adding the heaters and dump resistor.

THEA [Bot1998, Bot2000a] and other SuperMagnet software allow good flexibility to model a quenching cable in the strand level and the helium cooling.

They are specially designed for the stability analysis of internally cooled cables.

Commercial FEM software

ANSYS has been used in quench simulations to understand the thermal stresses during a quench [Cas2003, Fer2004, Yam2003]. The advantage of such engineering software is the flexibility in geometry but on the other hand they can be slow to run and have never been used for the series of studies needed for quench protection design.

2.4 Review of heater designs

The quench heaters typically are made of stainless steel strips on close contact with the cables. Insulation, most commonly a polyimide foil, is used to isolate them electrically from the coil. This section reviews the details of heater designs adopted in accelerator magnets by the date, and the different designs that have been used in individual research magnets. The measured delays are also given, when available.

2.4.1 Heaters in the Tevatron

Tevatron in Fermilab was the first accelerator complex that had high-energy magnets protected with heaters. Tevatron was operational between years 1987 and 2011 providing proton-anti proton collisions at energies of about 2 TeV. It was the worlds highest energy particle collider before the LHC. This synchrotron had 774 superconducting dipoles and 240 quadrupoles distributed around a 6.4 km long ring [Sti1979]. The string of magnets was divided into quench protection units, each consisting of four dipoles and a quadrupole [Flo1979]. In case of a dump, the magnets in the quenching unit were shorted and stainless steel strip heaters were fired in all of the magnets. The heaters in the 7-m long [The1993] dipole were attached into the wide sides of the cables of the first turn of the coil outer layers [Koe1979]. They were 0.13 mm x 5.1 mm stainless steel strips separated from the turn by 0.254 mm of Kapton. The quench then propagated transversely between the coil turns. Stiegning [Sti1979] presented experimental results showing how the two heaters effectively reduced the quench load and peak temperature in the magnet protection. This heater location is different that was considered in LHC magnets.

2.4.2 Copper plated heaters in the LHC

In the LHC, there are about 2000 superconducting magnets which are protected with heaters. The heaters are 15 mm wide stainless steel strips on the coil outer surfaces, extending the entire coil length. Periodic copper plating is applied on the strip surface in order to reduce the strip resistance and ensure that sufficient heating power can be provided in the un-plated heating stations, while the total heater voltage does not exceed the insulation threshold. Quenches are assumed to initiate under the heating stations, and the entire coil layer is brought to the normal state by natural quench propagation between the heated segments. The 25 μm thick stainless steel heater strip is sandwiched between two 75 μm layers of polyimide. It is pressed on the coil surface by the collars. [Rod2000, Rod2001]

For the main dipoles the copper plating sequence was optimized using the programs SPQR and QUABER together with experimental data from model magnets. The quench propagation velocity was assumed to be 15-20 m/s at nominal operational current. The optimum plating pattern for the dipole was determined to be 120 mm unplated sections alternating with 320 mm copper plated sections. The design power was 70 W/cm^2 with the RC-circuit time constant 77 ms [Son2001c]. Because all the LHC heater circuits had to use the same kind of heater power supply (900 V), the plating of other heaters was adjusted to lead to a same heater current decay time constant [Rod2001]. The heater delay at nominal operation current was about 25 ms. Figure 2.12 shows the heater locations on coil outer surface and table 2.4 summarizes the heater parameters.

When Fermilab started developing the IR-quadrupole MQXB for the LHC, the first heater study program was carried out using a modified Tevatron low-beta quadrupole which had stainless steel heaters installed on the coil outer surfaces. The 0.025 mm thick and 12.5 mm wide stainless steel heater strips were placed in the middle of four layers of Kapton sheets. The total Kapton insulation between the heater and the cable was 0.05 mm + 0.075 mm of the cable insulation [Feh1998]. The measured delays at high magnet current (80% of SSL) were about 20-30 ms, and 40-60 ms at 60% of SSL. The heaters covered 24 out of the 47 coil turns [Lie1997].

The MQXB heater design continued in Fermilab with more experimental studies using 2-m long model magnets HGQ's during the years 1998-2000 [Bau2001c]. The optimized parameters were 1) heater location (outer or inter layer), 2) insulation thickness, 3) the distribution of low-resistance copper paths, and 4) heater width. From the short model tests, the heater power was

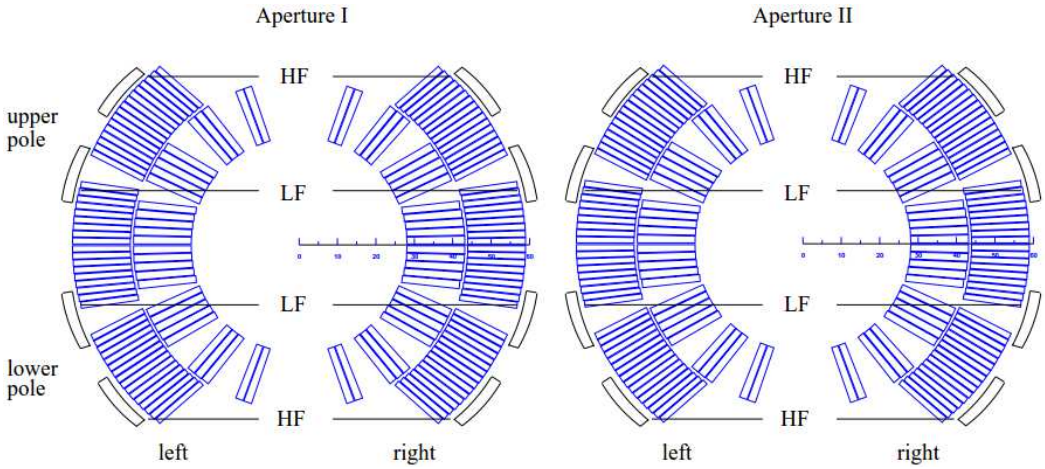

Figure 2.12: Location of heaters on the outer surfaces of the LHC main dipole coils. [Son2001c]

Table 2.4: Summary of the heater designs and delays in LHC. When the used references [Bos2002, Lam2004, Lam2006, Nak2002, Son2001c] had contradicting information, the values from the most recent were taken.

Magnet	MB	MQ	MQXA	MQXB
Heating station length [mm]	120	120	120	105
Heater period [mm]	540	440	240	315
Strip length [m]	14.4	3.1	6.5	5.7
Strip width [mm]	15.0	15.0	15.0	15.0
Coverage [# of coil turns]	26	-	24	24
# Turns in coil	80	-	114	60
Coverage [% of coil turns]	33	-	21	40
Strips in series	2	8	4	4
Heater power supplies	4	2	2	2
Powering voltage [V]		900 (+/- 450)		
Insulation thickness [mm]		0.075		
Delay at 80% of SSL [ms]	25	-	20	20

decided so, that the heaters will quench the magnet at I/Ic = 0.05 (800 A), which is the LHC injection current. Finally, tests were done for the full length prototype using a heater provided by CERN with 105 mm long segments without copper alternating with 210 mm copper segments. It was verified that the magnets were adequately protected [Lam2004, Lam2006].

2.4.3 Stainless steel strips in Nb_3Sn R&D Magnets

Several different stainless steel and copper plated heater options have been considered in the LARP Nb_3Sn R&D magnets. The heaters are insulated with polyimide, which cannot withstand the heat treatment of the coil. Thus, they are mounted on the coils after the heat treatment. Due to this consideration, the heaters cannot be placed between the coil layers, but must be placed either on the inner layer (IL) or the outer layer (OL). Experience with the inner layer heaters has shown that they are prone to detachment of the coil over time, presumably because they have no mechanical support on the bore side, and are in direct contact with superfluid helium [Amb2011]. The available technology is therefore most reliable when used in the coil OL. Heater between the layers have been studied too, either by using a ceramic insulation or a react-and-wind coils [Imb2003]. In Chapter 4 several heater designs are analyzed in detail.

The straight strip with and without copper plating

The simple straight heater strip with a constant width has been adopted in the TQ magnet series, LBNL High-field Dipole (HD)-series, and in the inner layer of HQ-series. Designs with and without copper plating have been tested in the TQ and HD magnets. In TQ it was observed that the in-house made copper plating did not have good contact with the stainless steel. This is the reason to develop different patterns using only stainless steel for the proceeding magnets.

Straight heaters were used also in the CERN-Fermilab 11 T dipoles. The novelty was that the heater on coil lower field region had higher power than the higher field heater. [Chl2013]

Un-plated stainless heaters with heating stations

In the LR and LQ magnets the low resistance path between the heating stations was provided by a wider strip between the narrow, high resistance regions, instead of the copper plating.

For the protection of the four meter long LQ, it was estimated that 100% of the coil should be resistive in 12 ms, after a detection delay of only 5 ms in order to keep the peak temperature below 380 K [Amb2007, Fel2009a]. In addition to the heaters, 60 mΩ dump resistor was accounted because the magnet was tested individually. The concern of how to protect even longer and higher energy magnets in an accelerator started to rise after this analysis.

Wider coil with wavy shape heater

On the HQ magnet outer layer the uniformly wide strip has a wavy shape, which provides partial coverage at several turns. The coils' inner layers had straight heater strips.

HQ coils have been tested with Kapton thickness of 25, 50 and 75 μm. Electrical problems frequently manifested in the coils with only 25 μm thick Kapton. The problems were detected using the Dielectric Withstand Voltage test (HiPot). It often showed breakdown or unacceptable leakage current before reaching the target potential, 1 kV between the heater and structural parts. Nominally the Kapton should hold 7700 V (60 Hz) [DUPONT]. Therefore, insulation degradation seems clear. The LHC standard requirement of dielectric strength was 2.5 kV between heater and coil.

Chapter 3

Protection heater delay simulation

The large high-field accelerator type magnets require active quench protection, which is usually based on protection heaters and possibly an external dump resistor. Designing a safe protection requires computation of the expected magnet current decay profile and the resulting coil temperatures and voltages. In long magnets the current decay is mainly due to the protection heater induced spread of normal zone within the windings.

The protection heater and quench protection design for the short Nb_3Sn research magnets were based on adiabatic thermal model. The utilized tools took the heater delay as an input, and typically used a uniform delay over a large block of the coil. As presented in Chapter 2, similar analysis will not suffice for long magnets because the heater design is not directly scalable to long magnets and experimental data is not available. Indeed, it is not clear if the present technology can protect longer magnets because these would require longer heater strips and consequently larger voltages if the strip is not redesigned. In order to optimize the design with present technology, the impact of the heater layout, power and insulation must be understood. Experimental investigation would be unacceptably expensive and time consuming. Therefore, more detailed simulations are required to guide the design process.

The simulation of the heater delay requires modeling the heater-coil thermal system all the way to the superconductor resistive transition. One needs to take into account the non-linear temperature dependence of material properties. The complexity of the problem calls for numerical computation. Commercial software exists, but a home-made code has the advantages of flexibility, transparency and efficiency. Eventually it can be interfaced with a full coil quench analysis tool.

In this chapter, I describe the development of a tool for computing the heater delay in impregnated Nb_3Sn magnets. The tool is called CoHDA: Code for Heater Delay Analysis, and it is described in detail in **Publication 4**. Then the correct implementation of the tool is verified using a comparison with analytical solution in a simplified case and finally with a commercial FEM software for a complete heater simulation.

3.1 Thermal model

The principle of the heater is to increase the coil temperature above the critical surface. Therefore, the heater delay modeling is done by modeling the heater powering and heat transfer from the heater to the superconducting coil and comparing the cable temperature with the cable critical surface in the given operational conditions. Figure 3.1 shows the magnet protection circuit and the heat transfer in focus.

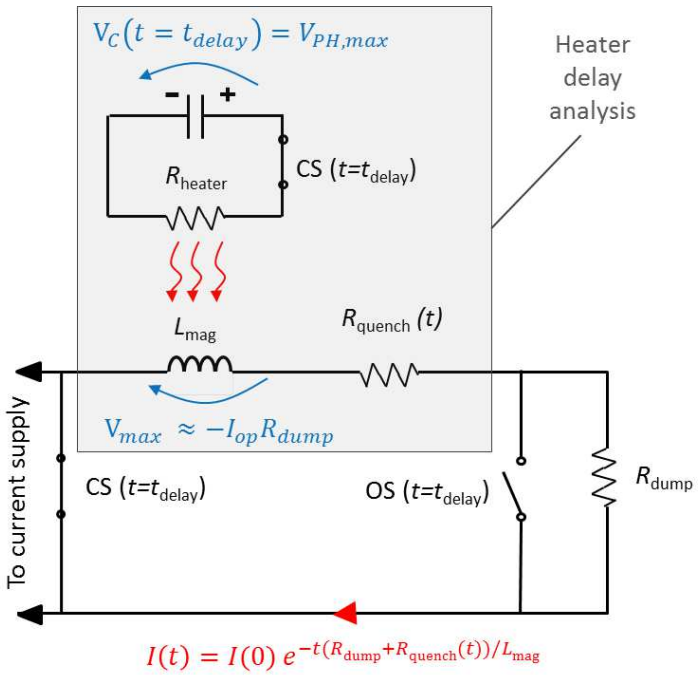

Figure 3.1: A schematic of the protection circuit showing the heater connection. The heater heats the coil and brings it to the normal state thus increasing its resistance. The t_{delay} is the time instant when the quench has been detected and the switches opened (OS) or closed (CS). The focus in this thesis is indicated by the shaded area. In particular, numerical modeling is used for the heat transfer computation.

Assuming that the helium cooling can be neglected in an impregnated winding simplifies the thermal problem to heat generation in the heater and heat diffusion to the cable. Figure 3.2 shows a schematic of the heater on the coil surface. However, the thermal system includes thin layers of materials with very different thermal conductivities which requires fine discretization of the domain for accurate numerical solution. It turns out that modeling the entire coil (several meters long) would become computationally too expensive. Fortunately, the symmetry of a periodical heater geometry allows to reduce the modeling domain to one period (L_{period}). If the period is symmetric at its center, the domain further reduces to a half of the period. Assuming that the adjacent turns are sufficiently uniformly heated, further allows to neglect the heat transfer between coil turns and each coil turn can be independently. The CoHDA modeling domain is shown in figure 3.3. Further simplifications include homogenizing the material properties in the bare cable (an assumption commonly made in quench simulation codes), which means that individual strands are not modeled. The thermal problem now reduces to two-dimensional heat balance equation for one coil turn:

$$\gamma c_p \frac{\partial T}{\partial t} = \frac{\partial}{\partial y}\left(k\frac{\partial T}{\partial y}\right) + \frac{\partial}{\partial z}\left(k\frac{\partial T}{\partial z}\right) + f_{gen}, \tag{3.1}$$

where $T = T(z, y, t)$ (in K) is space and time dependent temperature, $c_p = c_p(z, y, T, B)$ (in J/K/kg) is specific heat, $\gamma = \gamma(z, y)$ (in kg/m^3) is mass density, and $k = k(z, y, T, B)$ (in W/K/m) is thermal conductivity. The material properties space dependence is due to the presence of different materials in the modeling domain. The term $f_{gen} = f_{gen}(z, y, t, T)$ is an internal volumetric heat source in units of W/m^3. In all simulations heat is generated in the heater component to simulate heater powering. In later expansion of the tool to consider quench propagation, this term can represent also Joule heat generation in the cable.

The magnetic field and current distribution in the conductor cross-section are assumed uniform. The default quench onset criterion is to monitor the cable maximum temperature and compare it with the current sharing temperature. Attempts to improve this criterion as well as to take into account a more realistic magnetic field distribution will be discussed later.

Inputs to the computational tool are the geometric domain composed by the stacked layers of different materials. The user defines the number of layers in the domain (currently, max. 6), their thicknesses and materials. To compute the cable material properties and critical surface the user defines the cable parameters: Cu:Non-Cu ratio, filling factor (the fraction of bare cable cross-section occupied by the strands), RRR, the critical surface with fit parameters

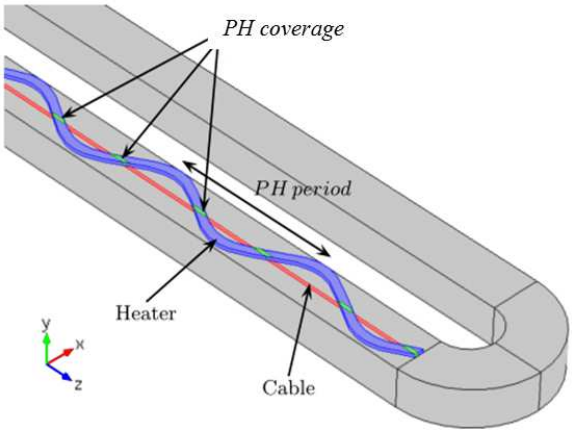

Figure 3.2: A schematic view showing how generic heater geometry can be expressed in terms of periodical heater coverage at different turns.

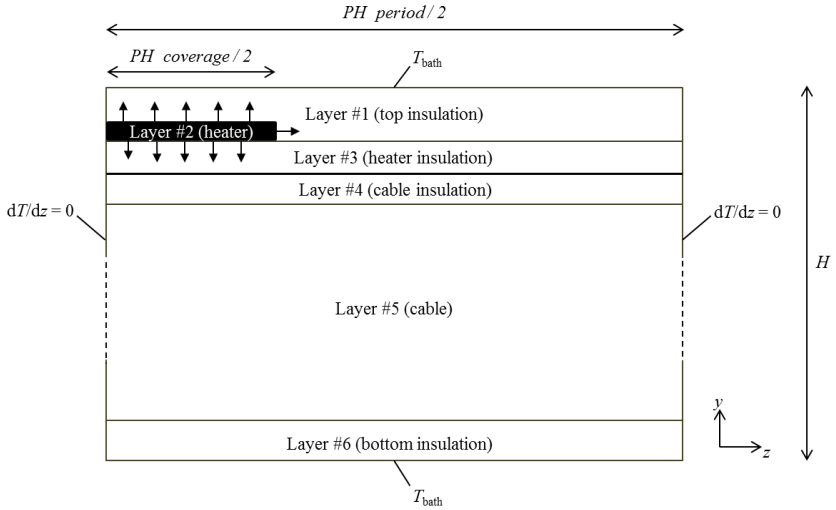

Figure 3.3: Thermal model for half period of the protection heater geometry. Not in scale.

as well as the magnet operation conditions. For the heater, one gives its coverage, period, and power. The heater power is defined either by giving the heater voltage (and length), current (and width), or peak power together with the heater voltage pulse shape (exponential with a decay time constant or a square). It is worth mentioning, that no specific scaling factors are used in the model. As an output, the program gives the temperature evolution in the modeling domain and the heater delay time.

3.1.1 Heater powering

The heater power distribution is assumed to be homogeneous in the heater covered cable segment and it is defined using

$$f_{gen}(t,T) = \rho_{ss}(T) J_{ss}^2(t), \tag{3.2}$$

where $J_{ss}(t)$ (in A/m^2) is the heater current density and $\rho_{ss}(T)$ (in Ωm) is the stainless steel electrical resistivity. For CoHDA, it can be given by specifying the heater current and the heater strip width and thickness.

Because also the voltage $V_{PH}(t)$ and the adiabatic surface power density are important parameters in heater design, the heater powering in CoHDA can be expressed also using these parameters. For a uniformly wide strip, with given $V_{PH}(t)$ (in V) and the length of the heater strip l_{PH} (in m) over which $V_{PH}(t)$ is given, f_{gen} becomes

$$f_{gen}(t,T) = \frac{V_{PH}^2(t)}{\rho_{ss}(T) l_{PH}^2}. \tag{3.3}$$

Consequently, it is assumed that heater has constant electric field, which leads to homogeneous current dissipation.

With $P_{PH}(t)$ (in W/m^2), f_{gen} becomes

$$f_{gen,ss}(t,T) = \frac{P_{PH}(t)}{d_{ss}}, \tag{3.4}$$

where d_{ss} (in m) is the thickness of the stainless steel strip. It is worth noting that generally $P_{PH}(t)$ is not the same as the heat flux from the heater to the cable.

3.1.2 Boundary conditions

Adiabatic boundary conditions are set on the symmetry boundaries; the heat flow in z-direction is zero at $z = 0$, and at $z = L_{period}/2$ (see figure 3.2), i.e.,

$$k \frac{\partial T}{\partial z}\bigg|_{z=0, z=\frac{L_{period}}{2}} = 0. \tag{3.5}$$

The temperatures at the top and bottom of the system, i.e. at $y = 0$, or at $y = H$, are fixed at T_{bath} by default, but also adiabatic conditions can be set.

Perfect thermal contact is assumed at the interfaces between the different materials. Therefore, the temperature is continuous and the equation to be solved is unchanged at the internal boundaries between materials. The reliable experimental characterization of the thermal contact resistances would require a large effort. Eventually, they could be used as fit parameters. The large pressure which is used to compress the coil is also expected to reduce these resistances, at least on the coil outer surfaces.

3.1.3 Numerical solution

The numerical solution of the heat balance equation was achieved by utilizing the thermal network method with explicit forwards finite difference discretization. The discretization is discussed for example in [Cen2003]. The equations implemented in CoHDA were adopted from [Blo1996]. The main difference is that we apply temperature dependence to the thermal conductivity and specific heat. Similar thermal network method has been used to study quench evolution in superconducting solenoids [Eys1995], and the beam induced heating in LHC dipoles [Boc2008, Boc2009] and in Nb_3Sn magnets [Boc2012].

The region is divided in z-, and y-direction into N_z and N_y elements indexed with i and j and size given by Δz_i and Δy_j respectively, see figure 3.4 a). Figure 3.4 b) shows the heat flows associated with cell (i, j).

The heat flow exiting cell (i-1,j) and entering cell (i, j) through their shared boundary Δy_j is denoted as $Q^n_{i-1/2,j}$ (in W/m), and given by:

$$Q^n_{i-1/2,j} = K^n_{i-1/2,j}\left(T^n_{i-1,j} - T^n_{i,j}\right), \tag{3.6}$$

where $T^n_{i-1,j}$ and $T^n_{i,j}$ are the temperatures at the cell centers, and $K^n_{i-1/2,j}$ is a thermal conductance between the cells. The superscript n denotes the time step. The conductance is given per unit length (perpendicular to the (z,y)-plane between the cells) in units of W/m/K, and calculated as

$$K^n_{i-1/2,j} = \frac{\Delta y_j}{\frac{\Delta z_{i-1}}{2k^n_{i-1,j}} + \frac{\Delta z_i}{2k^n_{i,j}}}, \tag{3.7}$$

where $k^n_{i-1,j}$ and $k^n_{i,j}$ (in W/m/K) are the material, temperature, and magnetic field dependent thermal conductivities that are evaluated in the corresponding cell centers. The heat flow in y-direction (between cells (i,j-1) and (i,j)) is computed in a similar manner.

The heat flows through the adiabatic boundaries are set to zero (relevant for the cells (1, j) and (N_z, j)). The surrounding temperature for the boundary

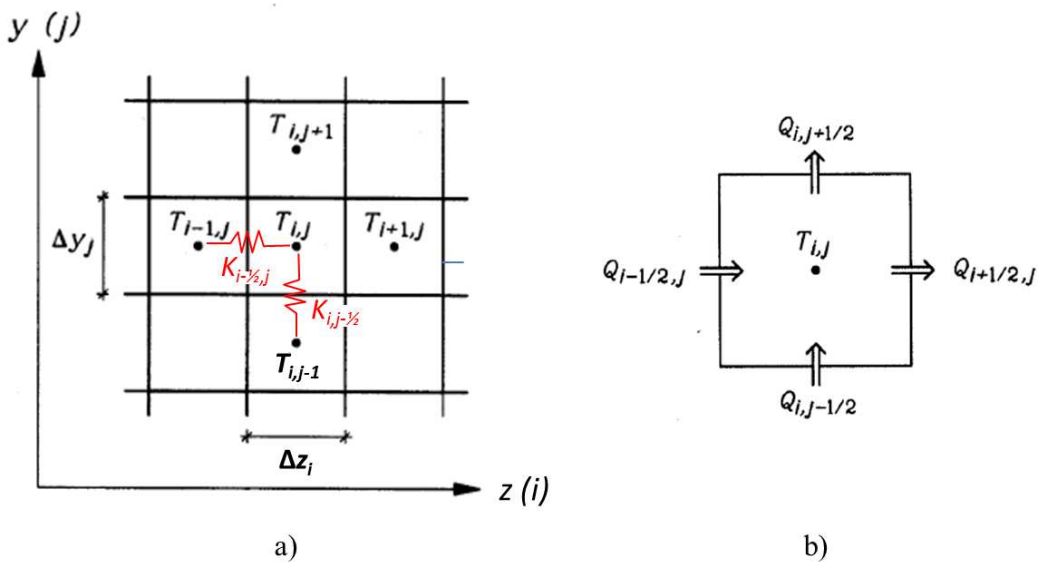

Figure 3.4: Numerical scheme. Modified from [Blo1996].

cells $(i,\ N_y)$ and $(i,\ 1)$, is fixed at T_{bath} – unless these boundaries are set to adiabatic as well. The new temperature $T_{i,j}^{n+1}$ after a time increment Δt^n is:

$$T_{i,j}^{n+1} = T_{i,j}^{n} + \frac{\Delta t^n}{\gamma_{i,j} c_{p,i,j}^{n} \Delta z_i \Delta y_j} \left(Q_{i-1/2,j}^{n} - Q_{i+1/2,j}^{n} + Q_{i,j-1/2}^{n} - Q_{i,j+1/2}^{n} + q_{i,j}^{n} \Delta z_i \Delta y_j \right), \quad (3.8)$$

where $\gamma_{i,j} c_{p,i,j}^{n}$ (in J/K/m^3) is the volumetric heat capacity and $q_{i,j}^{n} \Delta z_i \Delta y_j$ is the optional internal heating, corresponding to integral of f_{gen} over cell $(i,\ j)$.

The time increment Δt^n for each time step n is based on material properties and the spatial discretization [Blo1996]. The smallest time step obtained for all $(i,\ j)$ cells in the computational domain is used to guarantee stability:

$$\Delta t^n = \lambda \min \left(\frac{\gamma_{i,j} c_{p,i,j}^{n} \Delta z_i \Delta y_j}{K_{i-1/2,j}^{n} + K_{i+1/2,j}^{n} + K_{i,j-1/2}^{n} + K_{i,j+1/2}^{n}} \right). \quad (3.9)$$

A user-supplied scaling factor $\lambda < 1$ is adopted to scale the time increment. Smaller λ makes the calculation more accurate but also computationally more expensive. Without compromising the accuracy, the spatial discretization can be made coarser in the regions involving materials with higher thermal conductivity.

3.1.4 Material properties

The temperature and magnetic field dependency is considered for all material properties. The thermal properties of the uninsulated cable are averaged by its components volumetric fractions: Nb_3Sn, copper and epoxy (and/or G10), which fills the cable voids.

The copper properties are based on [CRYOCOMP], the Nb_3Sn specific heat is based on a fit proposed in [Man2011], and epoxy specific heat is based on [CRYOCOMP] (below 4.4 K a linear extrapolation is used with an assumption that epoxy specific heat is 0 J/K/kg at 0 K). The thermal conductivities of Nb_3Sn and epoxy are assumed to be negligible relative to the thermal conductivity of copper. The G10 properties are from [Mar2000]. The heater polyimide insulation is based on Kapton properties from [Mar2000] (with an extrapolation presented in [Man2011] for thermal conductivity below 4.3 K). The stainless steel specific heat and thermal conductivity are based on [Mar2000], with an extrapolation proposed in [Dav2011] for its specific heat below 5 K. The stainless steel resistivity is based on [Pre2011].

3.2 Comparison with an analytical solution

Analytical heat transfer solutions are available for solids with constant and uniform material properties. This kind of a solution was used to verify the correct implementation of the numerical solution. The analyzed case was one-dimensional heat conduction into a slab with its other side perfectly insulated and a steady heat flux (q_0)on the other side (starting at $t = 0$ s), see figure 3.5.

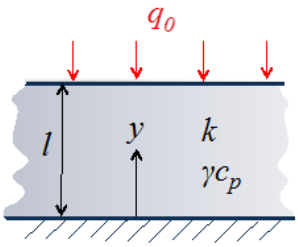

Figure 3.5: Insulated slab with constant surface heat flux.

The analytical solution for the temperature of the slab is [Car1959]:

$$T(y,t) = T(y,0) + \frac{2q_0\sqrt{\alpha t}}{k}\sum_{n=0}^{\infty}\left\{ierfc\frac{(2n+1)l-y}{2\sqrt{\alpha t}} + ierfc\frac{(2n+1)l+y}{2\sqrt{\alpha t}}\right\}. \quad (3.10)$$

where T_y (in K) is the temperature, t (in s) is time, k (in W/m-K) is the thermal conductivity, α (in m^2/s) is the thermal diffusivity, q_0 (in W/m^2) is the heat flux rate, and $ierfc$ is the integral error function. The initial temperature of the slab $T(y,0)$ is a constant.

In the example computation, the slab thickness was 11.11 mm, k was 1.0 W/m/K and volumetric specific heat γc_p was 1000.0 $J/m^3/K$, giving α of 0.001 m^2s. The heat flux q_0 was 1.0 W/cm^2, and initial temperature was 1.9 K.

In CoHDA the slab was presented with four layers. The layers had the same material properties and were in perfect thermal contact, but discretized using a different segment size. This allows assessing the thermal calculation in the bulk of the material and at the layers boundaries. The layers thicknesses were 0.01 mm, 0.1 mm, 1.0 mm and 10.0 mm, and the segment sizes (Δy) were 0.005 mm, 0.050 mm, 0.025 mm and 0.1 mm respectively. The time step was scaled using $\lambda = 0.2$ leading to a time step of 0.11 μs. The heat flux was set at the surface of the thinnest layer. The other boundary was set adiabatic.

Table 3.1 summarizes the temperatures given by CoHDA ($T_{N,y}$) and the analytical solution ($T_{A,y}$) at different time instants. The comparison is presented at the surface ($y = l$), and at the center of the domain ($y = l/2$). The relative percentage error ϵ_y at both locations was calculated as $|T_{N,y} - T_{A,y}|/T_{A,y}$. In the sampled locations the error was below 0.02%.

To check the numerical stability, the numerical computation was repeated using two times coarser spatial and temporal resolution. In that case, ϵ_y was at most 1.6%, which was larger (as expected) than with the denser mesh. The convergence towards analytical solution when the mesh is refined is a strong indication that the numerical solution was adequately implemented.

3.3 Comparison with commercial FEM software

In order to validate CoHDA in a real heater design case, including different domains with temperature dependent properties, the same simulation domain was built with COMSOL Multiphysics [COMSOL2013] and the results were

Table 3.1: Analytical solution compared to the numerical result.

t (ms)	$T_{N,l}$ (K)	$T_{A,l}$ (K)	ϵ_l (%)	$T_{N,l/2}$ (K)	$T_{A,l/2}$ (K)	$\epsilon_{l/2}$ (%)
2	17.861	17.858	0.018	1.933	1.933	0.007
10	37.585	37.583	0.007	6.491	6.491	0.004
20	52.378	52.377	0.002	15.264	15.263	0.003
50	83.526	83.525	0.002	42.251	42.251	0.000

compared. The COMSOL model was built by Juho Rysti, who adopted a similar method than used in CoHDA to simulate the heaters at CERN.

The parameters of the full scale heater simulation were based on the LARP HQ heater for one turn on the coil outer layer (see section 4.2). The layers materials and thicknesses as well as the heater properties are reported in tables 3.2 and 3.3.

Table 3.2: The thickness of various material layers in the analyzed case with COMSOL and CoHDA.

Layer #	Thickness (mm)	Material
1	0.3000	G10
2	0.0250	Stainless steel
3	0.0254	Kapton
4	0.0900	G10
5	15.000	Cu + Nb_3Sn + G10
6	0.7080	G10

Both programs used the same sources for the temperature-dependent material properties. The properties used in CoHDA were implemented in COMSOL. The only exception is copper, for which both codes used the NIST data (at 0 T and RRR 150) [Mar2000].

The simulated maximum temperature at the cable ($T_{max,cable}$) and at the heater ($T_{max,heater}$) were compared at 5, 10 and 50 ms, as well as the time to reach 14 K in the cable (heater delay). The simulated temperatures are shown in table 3.4. The difference between the simulated heater delays and temperatures is less than 2% in all cases, which can be considered an acceptable deviation.

In this case the CoHDA was discretized with element size of 20 μm, 6.25 μm, 6.35 μm, 18 μm, 200 μm and 19.67 μm vertically for the layers 1 through 6 respectively. In z-direction the element size was 200 μm. The simulation was repeated with approximately twice larger element side lengths and

Table 3.3: The cable and heater parameters.

Parameter (unit)	Value
RRR	150
Cu/Nb_3Sn (strand)	1.05
Voids (G10) fraction in bare cable	0.15
Number of strands	35
Magnetic field (T)	3.0
T_{cs} for quench definition (K)	14.0
Initial temperature (K)	4.5
Heater coverage (mm)	60.0
Heater period (mm)	120.0
Heater period (mm)	120.0
Heater peak power (W/cm2)	50.0
Heater circuit time constant, RC (ms)	40.0

Table 3.4: Results of comparing COMSOL and CoHDA. The percentile difference is computed with respect to the COMSOL result

Criterion	COMSOL	COHDA	Difference
Heater delay	38.33 ms	38.11 ms	-0.6%
$T_{max,cable}$ at 5 ms	7.24 K	7.23 K	-0.2%
$T_{max,heater}$ at 5 ms	71.09 K	71.55 K	0.7%
$T_{max,cable}$ at 10 ms	9.37 K	9.36 K	-0.1%
$T_{max,heater}$ at 10 ms	81.54 K	81.60 K	0.1%
$T_{max,cable}$ at 50 ms	14.64 K	14.67 K	0.2%
$T_{max,heater}$ at 50 ms	62.94 K	63.96 K	1.7%

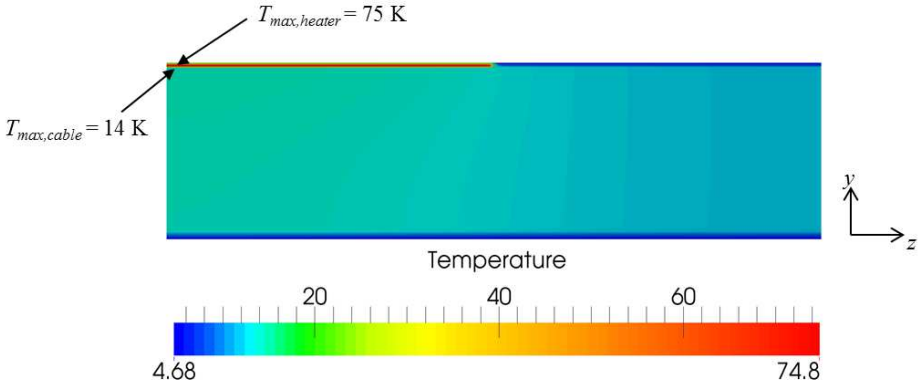

Figure 3.6: Temperature distribution in the CoDHA model at t = 38 ms.

the results varied less than 0.5% with respect to the finer case. The coarser one is the reference discretization in the heater simulations presented in the following chapters. The approximate element sizes are: 30-40 μm in G10, 13 μm in stainless steel, 13 μm in Kapton, and 400 μm in cable. In z-direction the cell width was 400 μm. The scaling constant λ for Δt was 0.5. This discretization leads to Δt of about 0.1 μs at the beginning of simulation and about 0.6 μs at 50 ms when the temperatures are higher.

Though CoHDA appeared to be considerably faster in simulations than COMSOL, rigorous comparison cannot be made because different computer hardware setups were used for the simulations.

3.4 Concluding remarks

This chapter described the development of a simulation tool CoHDA. The tool allows evaluating the heater delays as a function of large amount of parameters. It computes the heat diffusion from the heater to the cable in two dimensions and estimates the time it takes to bring the cable temperature above a given threshold, such as the current sharing temperature in the given operation conditions.

The correct functioning of the implemented simulation tool was verified with comparisons to analytical solutions in a simplified case and finally to a commercial FEM simulation software. In the next chapter the tool is applied to several R&D Nb_3Sn magnets and the simulated delays are compared to experimental data.

Chapter 4

Protection heater delay measurements and comparison with simulation results

In the magnet quench protection design, simulations and experiments complement each other and are both needed. The simulations are significantly faster and cheaper to run than experiments, and can estimate the impact of parameters which are not accessible experimentally. On the other hand, it is obvious that the simulations represent simplifications of the real world and their prediction power is limited. Experiments are therefore needed to validate the simulation results as well as to guide the future modeling. Clearly, also measurements of a complex system have uncertainties and perfect agreement between simulation and measurement is not a realistic expectation. Further, due to lack of 100% control of manufacturing process the intended prototype is not exactly produced. Therefore, the knowledge of the expected uncertainties is pivotal for the quench heater design.

This chapter presents measurement of heater delays in several high-field Nb_3Sn accelerator type magnets. The heater simulation tool was applied into each of these magnets and the simulated delays were compared with the measured ones. Finally, the uncertainties in both the measurements and simulations are analyzed.

The comparison of experimental and simulation data is presented in **Publications 2-5**. The heater tests are detailed in the magnet test articles: [Baj2013] (HQ01e), [Chl2014] (HQ02a), [Baj2015] (HQ02b), [Chl2011] (LQ), [Mar2014] (HD3b), and [Zlo2014, Zlo2013] (11 T). The parameters used in the simulations are detailed in Appendix A.

4.1 Experimental procedure

The goal of a heater delay measurement is to characterize the time delay between the heater activation and quench initiation in the coil under the heater. In the experiment, the magnet is operated at constant current, and one or more heaters are activated manually. The magnet current is kept constant until the heater provoked quench propagates and is detected by the regular quench detection circuit. The quench protection in such an experiment includes all its regular features (dump resistor and heaters) excluding the heater that is already fired. A dump resistor was used in the protection of all of the magnets discussed in this chapter.

In the experiments considered here, the heater delay was defined from the recorded voltage tap signals. The criterion for the quench onset was the time instant when the voltage signal from the coil rose above the noise level prior the heater activation, and kept rising. One can already here note that though the definition is precise, it uses vague terminology. For example, the noise level depends on the measurement system and different measurers may report different noise levels for the same measurement. Figure 4.1 shows an example from the HQ01e heater delay measurement at CERN.

The details of the test conditions are reported for each of the tested magnets in the following sections.

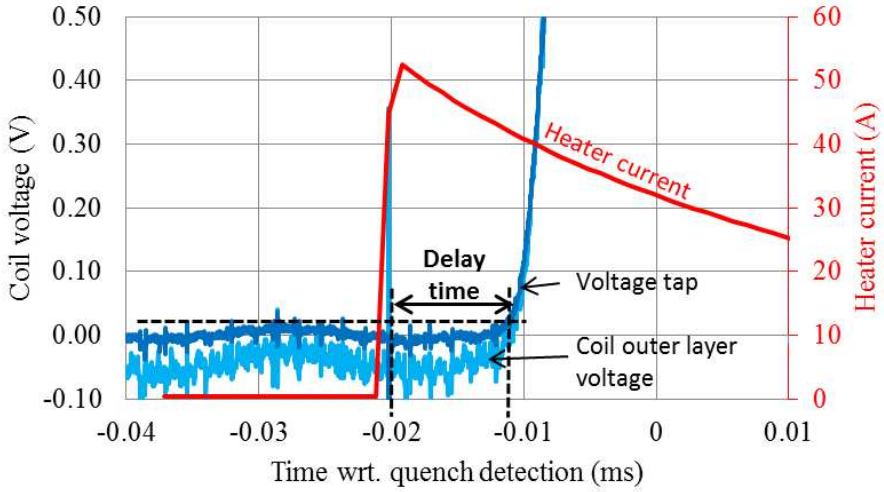

Figure 4.1: HQ01e outer layer heater delay measurement at 14 kA and 1.9 K (quench ID qh088). Shown are the voltage tap signal from the segment that quenched first (9B0405), the coil outer layer total voltage and the heater current.

4.2 Nb_3Sn High-gradient Quadrupole

The series of High-gradient Quadrupole (HQ) magnets are being developed within the LARP collaboration in preparation for the LHC IR-upgrade. They feature 1-m long, 120 mm aperture two-layer cos-2θ coils with maximum current of about 18-19 kA and peak field of 15 T. Five assemblies of the so-called HQ01 version (a-e) and two assemblies of the HQ02 version (a-b) were tested during the years 2010-2014.

4.2.1 Heater design

Each HQ coil has four heater strips impregnated on the surfaces; two on coil inner layer and two on coil outer layer. The inner layer heaters are straight stainless steel strips, running parallel to magnet axis. On the coil outer layer the heaters have a wavy shape providing partial coverage to several turns. Figure 4.2 shows photos of the heaters on HQ01 coil inner and outer surfaces.

The main difference for heaters between HQ01 and HQ02 is the increase of heater insulation polyimide from 25 to 75 μm. The outer layer heater design was also changed at the coil ends. This has an impact on the heater strip resistance, but is not expected to impact the heater delay in any other way.

We note here that there was a 13 μm thick layer of adhesive (Apical AVI) between the heater and polyimide. However, due to the lack of material properties, it was neglected in the simulations.

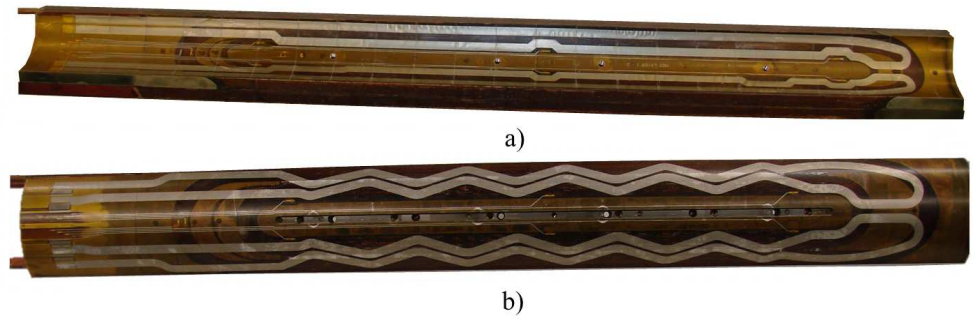

Figure 4.2: Layout of the HQ01 heater on the a) inner and b) outer coil.

4.2.2 Experiment

For regular quench protection the heater strips were connected in four circuits. Most of the circuits consisted of four heaters connected in parallel and powered by a capacitor bank, which is also called a Heater Firing Unit (HFU). In order to ensure coverage at each coil in case of an HFU failure, the goal was that each circuit included a strip at each coil. However, in HQ01 several times a compromised electrical integrity was revealed by the HiPot test. Depending on the level of degradation, these strips were either removed from the protection, or they were combined into a circuit which was powered with a lower voltage than the nominal. Consequently, in some cases the heater circuit had only three strips and a dummy resistor to keep the heater voltage decay time constant similar to the other circuits. Also, in some cases the circuit included two strips from the same coil.

The protection heater delay measurements were performed as a part of each magnet test. In magnets HQ01a-c measurements were done only at low magnet operation currents, and using an entire circuit with three or four strips to provoke the quench. In HQ01d for the first time one strip was connected to a separate capacitor. Using only one strip to provole a quench resulted to clearer signals and more reproducible delays. Figure 4.3 shows the measured delays in HQ01a-e at current levels 30, 60 and 80% of SSL at 4.4 K. The delays from the different tests and different coils show large spread, especially for the inner layer heater. The data quality improved in the tests of HQ01e and in later models because of a more rigorous definition of the test procedure. This included setting a 3-5 min holding time at constant current before heater activation, using only one heater strip for measurement, and choosing the location of that strip based on the electrical and quench performance of the coils. The single coils most extensively used for heater tests were coil 9 in HQ01(e) and coil 20 in HQ02(a and b). These coils were considered ”strong” because they passed the voltage tests and did not show premature quenching during the magnet tests (training). From the signals in these coils the quench onset was usually clear within 1 ms when tested close to the operation current, increasing at lower currents reaching about 5 ms uncertainty at 30% of SSL.

4.2.3 Simulation

Simulation parameters

The input parameters were collected from various design documents and measurements. Because this simulation aimed at predicting the first quenching

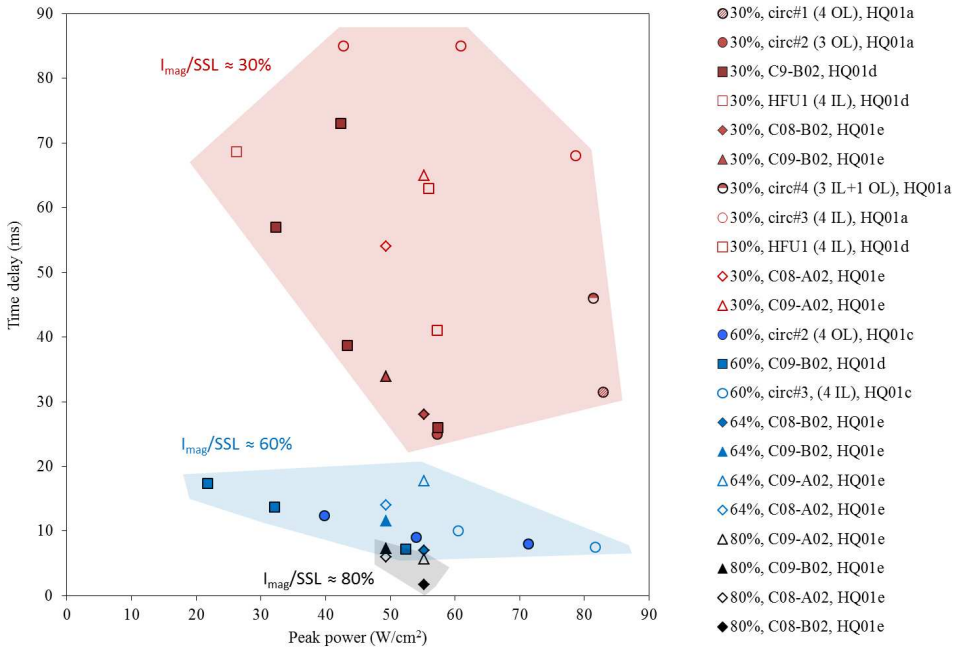

Figure 4.3: Measured delays as a function of heater peak power in HQ01 at 4.4 K. Heater circuit time constants were between 30 and 45 ms. The open markers represent heaters on coil inner layer (IL) and closed markers on the outer layer (OL). The legend shows the fraction of short sample limit and the fired heater strip or the circuit with the number of included strips and their location.

segment (among all the coil turns covered by the heater), the magnetic field and heater coverage were defined for the locations where the first quench was assumed.

The straight heater on the HQ inner layer was assumed to heat uniformly all the turns under it, provided that their entire width was covered. The location of the first quench was therefore assumed to be the third turn counted from the center pole piece, because it had the highest magnetic field, i.e., the smallest temperature margin. The longitudinal heat diffusion along the cable was neglected for the straight heater, and the simulations were reduced to effectively one dimension.

On the coil outer layer the location of the first quench was less obvious because the turn with the highest field had a shorter heater coverage longitudinally than some of the lower field turns. Figure 4.5 shows how the coverage increases in 1 cm steps from about 2 cm to 7 cm when moving from the 2nd turn to the 7th turn (from the pole). At the same time the magnetic field decreases. After the 7th turn the field keeps decreasing but the (continuous)

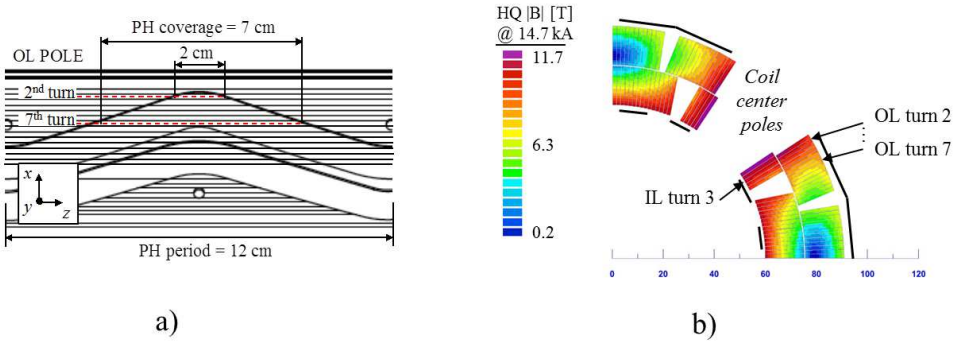

Figure 4.4: a) One period of the HQ outer layer heater geometry, showing the heater longitudinal coverage for the 2nd and 7th turn, b) Magnetic field in a quarter of the HQ01 cross-section, the heater locations, and the simulated turns on coil inner layer (IL) and outer layer (OL).

coverage does not increase. Both high field and long heater coverage were assumed to compete in decreasing the delay. Therefore, the first turn to quench was assumed to be one of these turns and they were all simulated.

The magnetic field strength for each turn was calculated at the coil inner or outer surface, i.e., at the locations closest to the protection heater. The computation was performed using Cobham Vector field Opera-2D [OPERA2015] and ROXIE [Rus2010]. The field at each turn was normalized to the magnet peak field. This allowed easy scaling of the field values at different currents when the field-current dependency was known for the magnet peak field. The normalized field was 0.9 in the inner layer, and in the outer layer turns from 2nd to 7th respectively 0.75, 0.74, 0.72, 0.70, 0.69 and 0.66. The calculated T_{cs} range was from about 14 K at 5 kA to about 10 K at 14 kA.

The heater power was computed from the measured current using (3.2) and (3.4) with ρ_{ss} at 4.5 K (0.5 $\mu\Omega$m). The resulting powers were 49 and 46 W/cm^2 in the HQ01e inner and outer layer respectively, and 55 W/cm^2 in HQ02.

Simulated delays at coil outer layer

Figure 4.5 shows the calculated heater delays for the fields associated with each simulated turn in HQ01e. The delays are shown as a function of heater coverage when the operation current was 14 kA and temperature 1.9 K. The delay time decreased with larger heater coverage and higher magnetic field, converg-

ing toward the 1-D case (infinite heater coverage) and magnet peak field. The impact of the coverage saturated around 20 mm in the high-field region, and around 50 mm in low-field region. The higher sensitivity to heater coverage in the low field regions can be understood in terms of larger T_{cs} margin because then more time was available for the longitudinal heat conduction. This suggests that when the heater coverage is only few centimeters, 2-D simulations are needed.

Figure 4.5 shows also the simulated delays in different coil turns versus normalized magnet current. These simulations took into account the heater coverage and field at each turn. The delays increased from about 5 to 40 ms when the magnet current was decreased from 80% of short sample limit to 20%. Above 60% of the short sample limit, the modeled turns quenched within 4 ms. At lower currents the variation between the delays was larger. For example, at 40% of short sample limit, the variation in delay time between the turns was over 20 ms. Also, the location of the first quench depended on the magnet current: At currents from 15.5 to 17 kA, the 3rd turn quenched first, from 13 to 14 kA, the 4th turn quenched first, from 8 to 11 kA, the 6th turn quenched first and below 7 kA, the 7th turn quenched first.

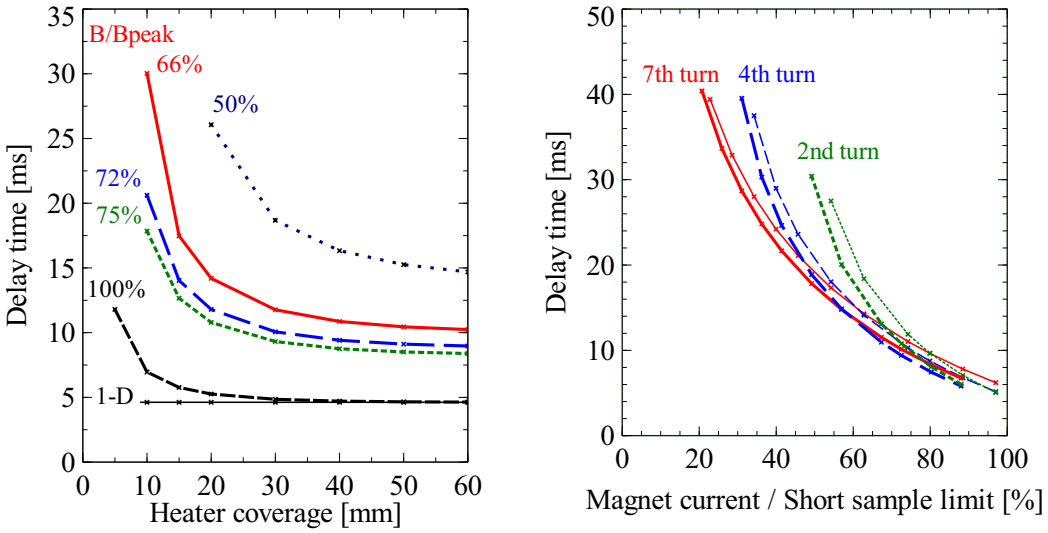

Figure 4.5: Left: Simulated HQ01 heater delays at 14 kA as a function of heater coverage. The magnetic fields values are related to the considered outer layer turns. The straight line is 1-D case at the peak field. Right: Simulated delays at several turns, taking into account the corresponding field and coverage. The thicker lines represent operation at 1.9 K and thinner lines at 4.4 K.

4.2.4 Simulation vs. experiment

Figure 4.6 shows a comparison of the simulated and measured delays in HQ01 coil 9. The delay simulation at outer layer represents the shortest delay among the modeled turns at each magnet current. The prediction on outer layer was very close to the experimental result: The average difference was 3 ms with standard deviation of 2 ms. The average difference percentage was 16% with standard deviation of 8%. On the inner layer, prediction was less successful: The simulated delays were up to 75% shorter than measured. One possible reason is that the heater contact with the coil was not good. The post-test observations of air bubbles under the inner layer heaters support this hypothesis.

The impact of the operation temperature to the delays was only a few percent in both the simulation and experiment. When the operation current is normalized at 1.9 and 4.4 K, the calculated heater delays were within 2 ms. At

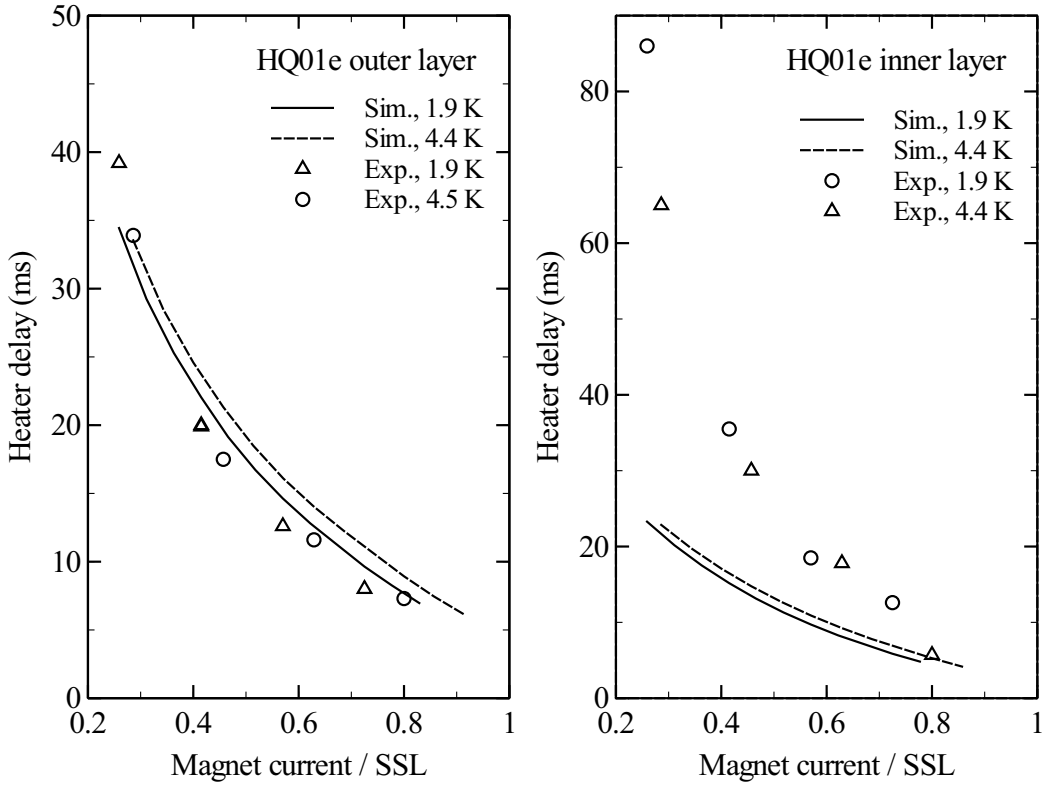

Figure 4.6: Simulated (Sim.) delays at HQ01 outer layer (left) and inner layer (right) versus normalized magnet current compared with experimental data (Exp.).

high currents their difference was approximately proportional to the difference in the energy margins (i.e., the change in enthalpy obtained by integration of the cable heat capacity from T_{bath} to T_{cs}). At lower currents the differences were slightly larger. This suggests that simply the time needed to heat up the coil explains the difference. The larger difference at low currents could be due to the overall larger fraction of the longitudinally diffused heat.

The simulation of HQ02 coil 20 captured the increase of the delays due to the thicker insulation, as shown in figure 4.7. The agreement with measurements at outer layer was within 5 ms (or 20%) above 40% of SSL. The average error for the entire investigated current range is 7 ms with standard deviation of 7 ms, or 18% with standard deviation of 7%. At inner layer, the simulations predicted the measured delay within 2 ms (or 16%) at magnet operation above 60% of SSL but are again too optimistic at low currents. One reason for the difficulty of inner layer heater simulation is the degradation of the contact between heater and coil inner surface which has been observed after several tests. It is interesting, that in HQ02 the inner layer heater consistently had shorter delays than outer layer, whereas in HQ01 the contrary was measured. Fortunately, the low current regime is less critical in the quench protection design because the available time budgets for heater efficiency are larger [Tod2013a].

4.3 Nb_3Sn Long Quadrupole

The LARP Long Quadrupole (LQ) is a 3.3 m long, 90 mm aperture Nb_3Sn cos-2θ quadrupole magnet. Like HQ, it was developed in view of the LHC IR-upgrade. The quench protection is based on external dump resistor and protection heaters which cover the entire coil surface.

4.3.1 Heater design

The outer and inner surface of the two-layer coils were each covered with two 25 μm thick stainless steel heater strips, which were electrically insulated from the coil by a 25 μm thick polyimide layer. To limit the heater voltage in the long coils, the heater design was based on so-called heating stations, see figure 4.8. The 9 mm wide heating stations (HS) were placed 110 mm apart and connected with a wider low-resistance segment (WS). The WS produced about 5 times less heating than the heating station. It was assumed that normal zones initiate under the heating stations and then propagate between the heating stations. Considering a typical normal zone velocity of 10 m/s,

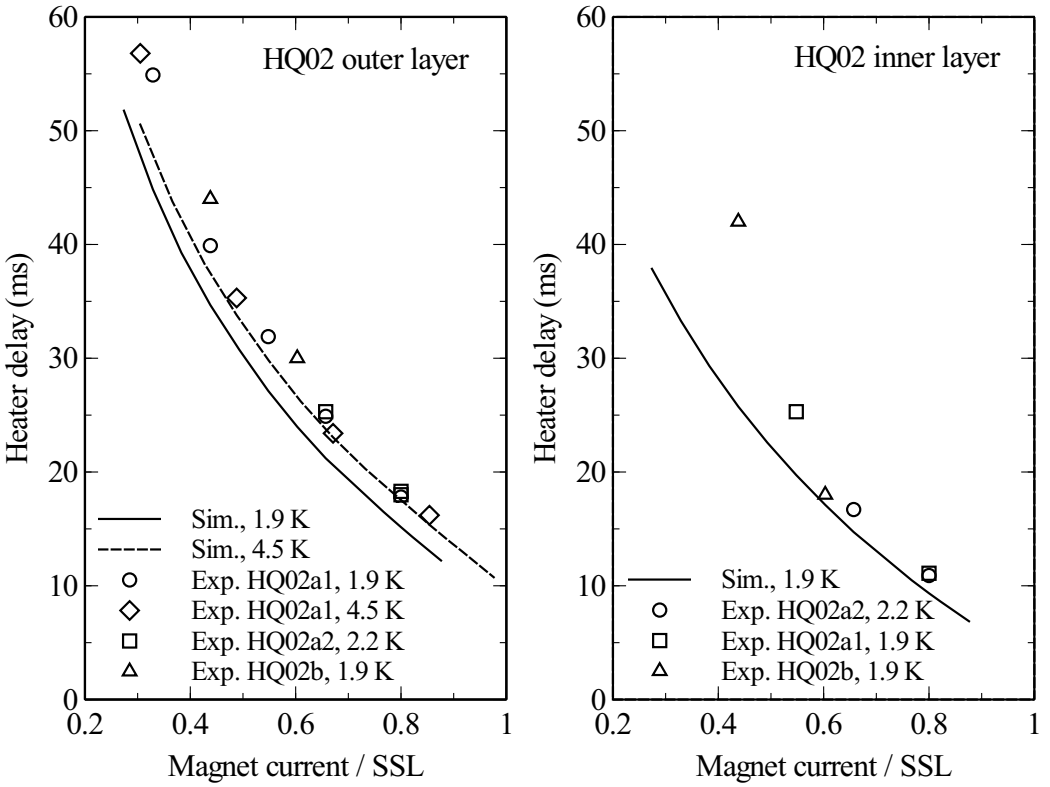

Figure 4.7: Simulated (Sim.) delays at HQ02 outer layer (left) and inner layer (right) versus normalized magnet current compared with experimental data (Exp.).

the 110 mm between two heating stations is transferred to the normal state within 6 ms. Figure 4.9 shows the cross-section of a coil half with the magnetic field map and the heater locations. Further details of the heater design can be found from [Fel2009a].

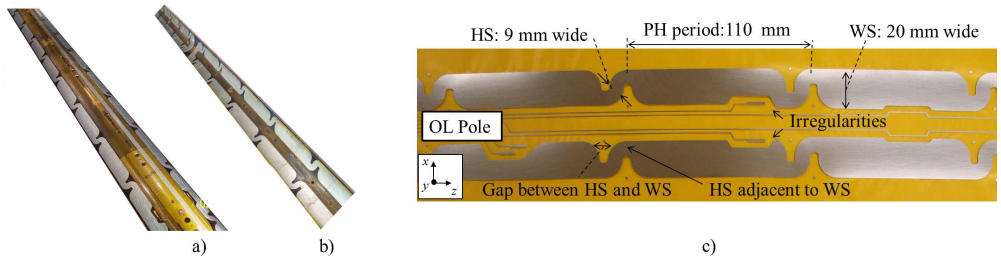

Figure 4.8: Layout of the LQS01 heater on the a) outer and b) inner coil surface, and c) a zoom-in to the outer layer heater features.

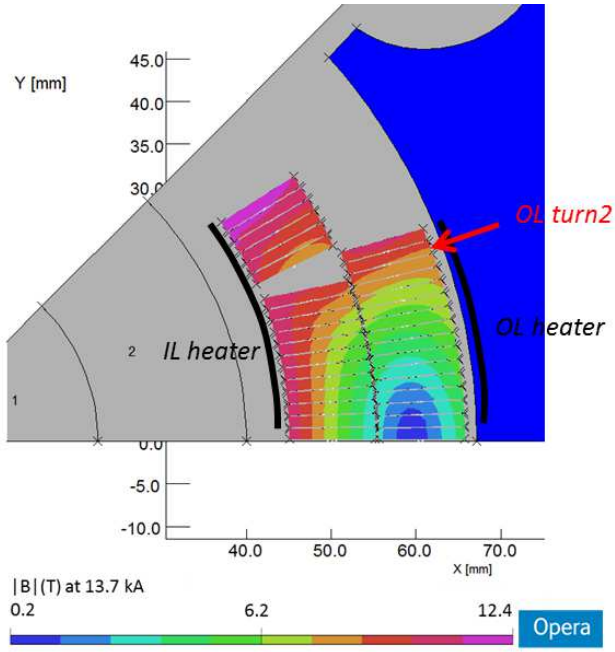

Figure 4.9: LQ magnetic field distribution and the heater locations and the simulated turn on the outer layer.

4.3.2 Experiment

The heater delays were measured at 4.5 K during the test of LQS01 assembly at Fermilab. The measurement was done by firing two heater circuits which included heaters either on coil inner or outer layer. Here were considered the tests of outer layer heaters as presented in the LQS01 test report [Chl2011].

Based on [Chl2011], the outer layer heater circuits were tested using HFU voltage of 250 V. All of the outer layer heater strips were not powered because they did not pass the electrical integrity test. Therefore, the circuits were modified by adding in parallel and series dummy resistors to fix the time constant in each circuit to be about 32 ms [Chl2011]. However, the details of these resistor connections are not reported in sufficient detail which makes the definition of the power at individual heater uncertain. Based on measurement in LQ coil 5, the resistance of 4 heater strips in parallel was 1.4 Ω [Chl2008]. Based on this, the heater current was 45 A, and power about 50 W/cm^2 in the heating station and 10 W/cm^2 in the wide segment immediately after launching the HFU. However, in the test report it is said, that the current in individual heaters varied from 45 to 52 A during the test, after referring to the nominal HFU firing voltage (300 or 350 V). Based on this, and to the fact that an additional

resistance in series was apparent to obtain the stated time constant, a 10% voltage drop was foreseen from the HFU to the heater strip circuit. This led to an estimation of 40 A, leading to about 40 W/cm^2 in narrow segment and 8 W/cm^2 in the wide segment.[1]

The test reports did not give an estimation of the measurement uncertainty.

4.3.3 Simulation

The simulation of the LQ heater geometry required considering also the wide segment between the heating stations. The simulation was performed for the heater covered turn closest to the pole piece, where the magnetic field was the highest. In that turn, the heating station directly attaches to the wide segment on its other side but on its other side there is a gap in between them. The code was limited to consider a heating segment at the center of the period and this asymmetrical case could not be simulated. I therefore considered the three symmetrical cases: (1) heating station alone, (2) heating station with 10 mm gap on both sides between heating station and the wide segment, and (3) no gap between heating station and wide segment on either side. The heating station was assumed to cover 9 mm of the cable length. The heater power was computed for both, heating station and wide segment based on the heater current density at both regions.

4.3.4 Simulation vs. experiment

A comparison between the simulated and experimental data for the LQ magnet is presented in figure 4.10. The model predicted conservative values: at 60% of SSL a delay of 21 ms was computed. Corresponding measured value was 16 ms. Reasons for this discrepancy could be high ramp rate to quench, non-uniform power distribution in the strongly curved heater shape, and a locally thinner insulation or a weak spot in the cable. Also, the homogenization of the cable internal structure may have had more impact when the heating station was short and touched only few of the strands. It is also possible, that the cable quenched under an "irregularity", such as the longer heating station due to the voltage tap position as shown in figure 4.8 c). Also, as seen in the case of HQ (figure 4.5), 1 mm difference in the heating station length has a strong impact in this range. It was not considered here, but actually the heater covered a

[1] After performing these simulations, it was confirmed that with the 4-strip circuit in coil 5 had a resistance of about 2 Ω when the HFU wiring was included [Chl2009]. This would lead to about 30 A and 30 W/cm^2 in the heater.

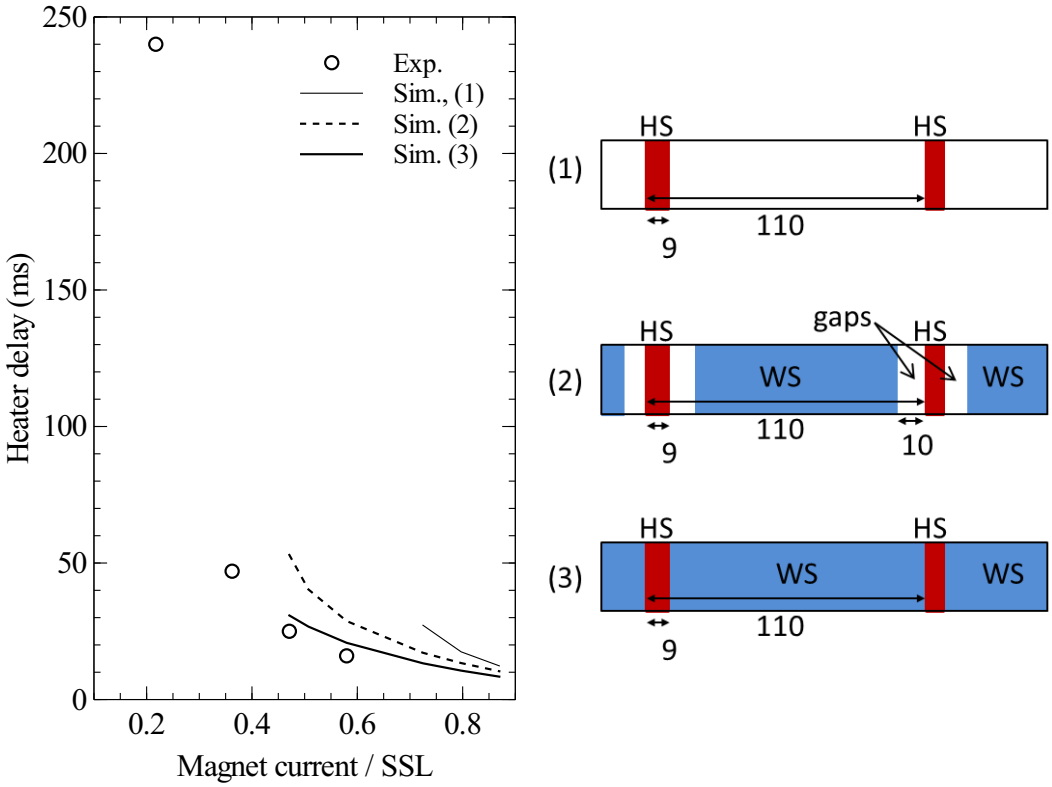

Figure 4.10: Simulated delays in LQ (Sim.) compared with experimental data (Exp.) versus normalized magnet current at 4.5 K. The heater geometry was simulated considering only the heating station (1), a 10 mm gap between heating station and wide segment (2), and a heating station directly attached to the wide segment (3).

couple of mm longer segment in the 3rd or 4th turn where the field was lower. Simulating a complex shape like this seems to call for a more detailed model which would take into account the current distribution and the irregularities of the detailed heater geometry, at least when a comparison with experiments is the simulation goal.

Another important finding from this simulation is that the wide segment has an important role in the simulated heat diffusion when the heating station is short. This should be taken into account in the future heater designs, as well as the heating station length optimization.

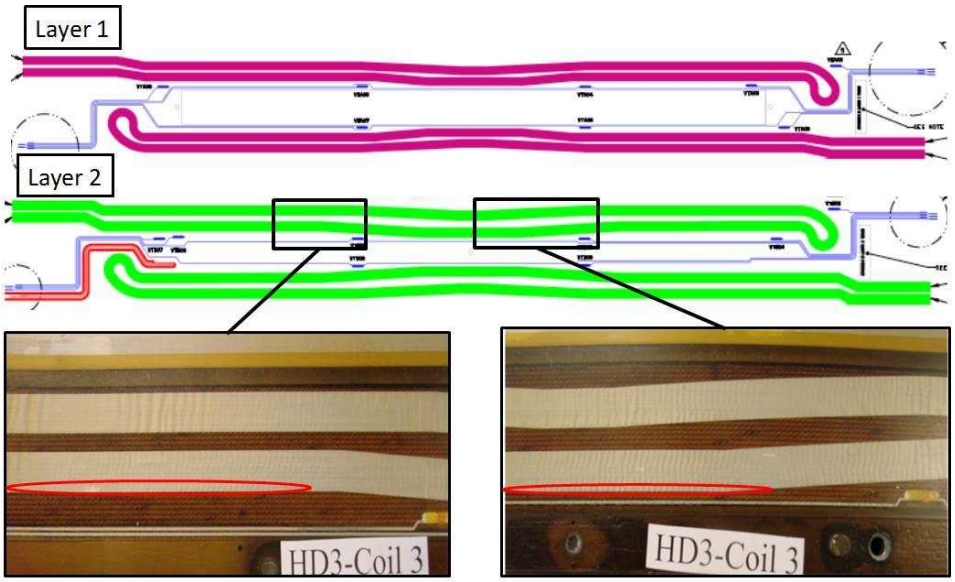

Figure 4.11: HD3 heater layout on coil layer 1 ("inner") and layer 2 ("outer"). Photos taken before the magnet test. The red circles point to the quench locations considered in the simulations.

4.4 Nb_3Sn High-field Dipole

The High-field Dipole HD3 was developed at LBNL. This block-type dipole features two-layer racetrack coils with flared ends [Che2013]. The experiments using the analyzed HD3b assembly are detailed in [Mar2014].

4.4.1 Heater design

The HD3 heaters are almost straight stainless steel strips parallel to the magnet axis, insulated from the coil surface with 25 μm thick polyimide. At the center of magnet straight section the heater is closer to the pole turn, while towards the ends the heater covers lower field regions, see figure 4.11. Figure 4.12 shows a quarter of the magnet cross-section with approximated heater locations.

4.4.2 Experiment

Each of the two HFU circuits consisted of a parallel connection of two heater strips in both coils at symmetric locations. The heater delay was measured

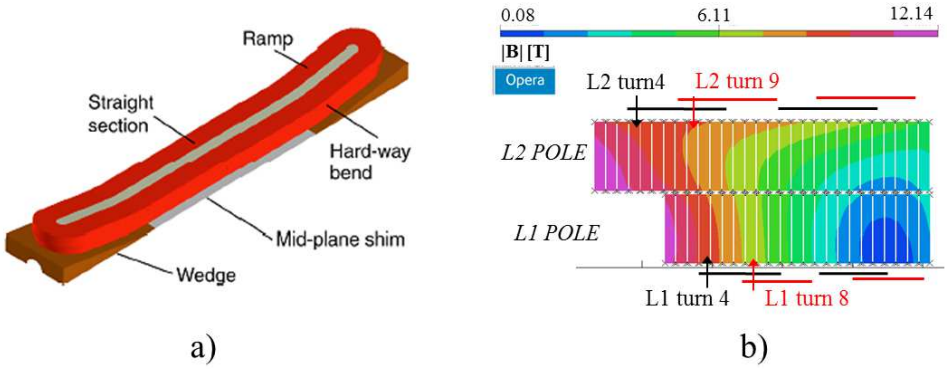

Figure 4.12: a) Shape of the HD3 coils. b) Magnetic field in a quarter of the magnet cross-section with the approximate heater locations at the center of the straight section (black) and near the coil ends (red). The arrows indicate the turns considered in the simulation.

after activating one such circuit. Two heater voltages were tested: 260 V, corresponding to 55-56 W/cm^2 (depending on the coil layer), and 225 V, corresponding to 42-43 W/cm^2. The definition of the quench onset from the test signals was sometimes difficult. One reason for the unclear signals is the coupling of the signals from the two coils quenching almost simultaneously. Also the short waiting time at plateau before heater activation obscured the signals. The plateau was kept short because of a suspected heat generation in one of the joints. An anomaly was indicated also by the quench location: The voltage tap and quench antenna data indicated, that on the outer layer the quench location was between the turns 5 and 29, i.e., not at the highest field under the heater, and that in several cases the quench location was shifted from the middle of the coil towards the coil ends.

4.4.3 Simulation

Because in HD3 experiment the layer 2 heater initiated the first quench in the lower field area, the delay was simulated at two locations. In layer 2 were simulated the 4th turn, which had the highest field, and the 9th turn, which was the first turn fully covered by the heater towards the coil end. The fields normalized to the magnet peak field were 0.75 and 0.70, respectively. In layer 1 were simulated the 4th and 8th turn, with respective normalized fields of 0.75 and 0.55.

The magnet consisted of two coils, identified as coil 1 and coil 3. These

coils had a cable with a different strand. Both coils were simulated to find out which one had the shorter delay. The simulated T_{cs} range was between 8.8 and 10.8 K at 16.5 kA and between 14.4 and 14.9 K at 4.5 kA.

4.4.4 Simulation vs. experiment

The simulated delays versus the magnet current together with the experimental results are shown in figure 4.13. The error bars in the experimental data represent the first activity observed in the coil (lower end of the bar) and the moment when the quench was clearly propagating (upper end of the error bar).

The lower field simulations (turn 9 on layer 2 and turn 8 on layer 1) gave about 2 ms longer delays in layer 2, and about 10 ms in layer 1, than the higher field simulations. The lower field simulations were in better agreement with the experiments. This, together with the photos shown in figure 4.14, supports the hypothesis of degraded heater contact at high-field region. Excluding the lowest currents in layer 1, the modeled heater delays differed about 2-25% from the experimental data, being within the experimental uncertainty. In simulation, and in 80% of experiments, coil 1 had shorter delay than coil 3.

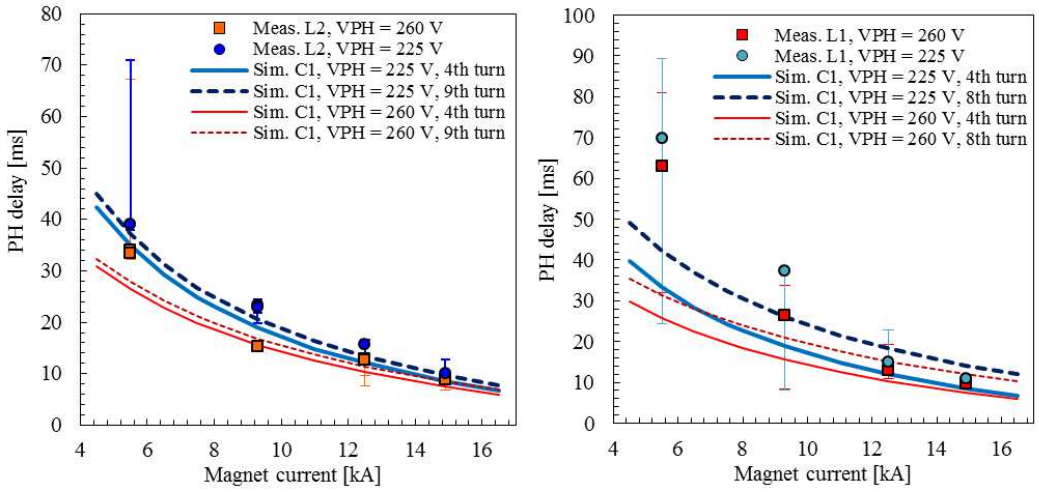

Figure 4.13: Simulated and measured delays in HD3 layer 2 (L2) (left) and layer 1 (L1) (right). The simulation results are from coil 1 (C1).

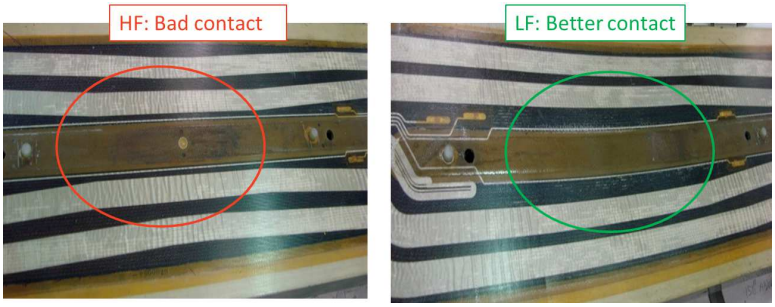

Figure 4.14: Photo of HD3 coil 1 taken between testing it in the HD3a and HD3b assemblies. One can see the compromised heater contact in the coil straight section (HF). The contact with the coil ends where the heater covers a lower field area seems better (LF).

4.5 Nb_3Sn 11 T dipole

The so-called 11 T dipole is a Nb_3Sn cos-θ dipole being developed by CERN and Fermilab for the LHC Luminosity-collimator upgrade. The protection heater delay measurements were analyzed from the two first single-aperture models which were tested at Fermilab: 2 m long MBHSP01 [Zlo2012], and 1 m long MBHSP02 [Zlo2013, Zlo2014, Bar2013].

4.5.1 Heater design

The 11 T dipoles had heaters only on their outer surface. In each coil side two straight heater strips were connected in series to form one U-shaped heater, as shown in figure 4.15. The strip closer to the central pole piece was 26 mm wide, and the strip closer to the magnetic mid-plane was 21 mm wide, giving higher power density to the lower field heater. The heaters in MBHSP01 were tested with one or two layers of polyimide insulation. The respective polyimide thicknesses were 76 μm (PH-1L) and 203 μm (PH-2L) [Chl2013]. Although nominally both layers were 127 μm thick, closer inspection showed that the 1st layer was 114 μm thick ($\pm$10%), and consisted of 76 μm of Kapton LT and 38 μm polyester adhesive [Nob2013]. Based on the long delays associated with the thicker insulation, for MBHSP02 only one layer of insulation was used (76 μm). The heaters in 11 T were not impregnated, in contrary to the HQ, LQ, and HD3 magnets.

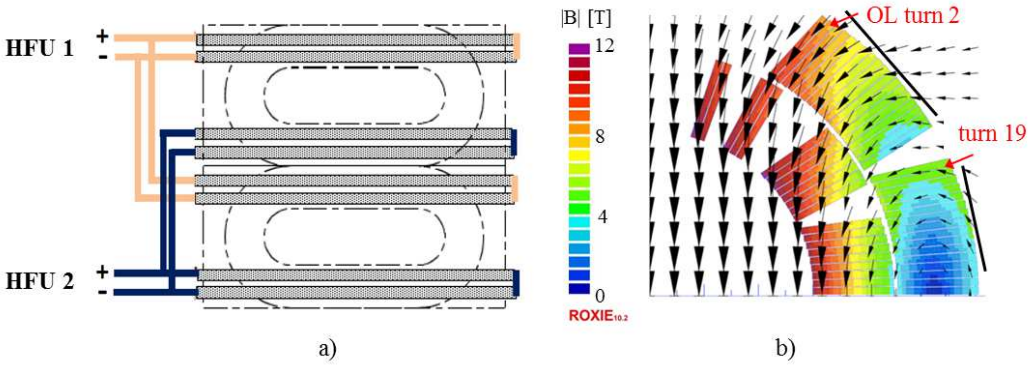

Figure 4.15: a) Heater layout in the 11 T dipole. In MBHSP01 the heaters connected to HFU1 had thicker polyimide insulation than heaters connected to HFU2. b) Magnetic field distribution with approximate heater location at coil outer surface. The simulated turn locations are shown with arrows. In MBHSP02 only the turn 2 was considered.

4.5.2 Experiment

Two U-shaped strips were connected in parallel in two HFUs (figure 4.15 a)). The heater delay was measured after firing both or only one of the heater circuits. In MBHSP01, measurements were performed between 40 and 60% of SSL using a relatively low heater power. In MBHSP02 also higher currents and higher heater powers and higher currents were considered.

The test performer gave an uncertainty of ±5 ms at 35% of SSL, ±1.5 ms at 63% and ±1 ms at 72% related to the coil quench signals interpretation.

4.5.3 Simulation

MBHSP01

In MBHSP01 it was investigated whether the ”high-field heater” with lower power, or the ”low-field heater” with higher power quenched the coil first. Therefore, the heater delays were simulated under both heaters, namely in the turns 2 and 19 from the outer layer pole because these turns had the highest magnetic field under the heaters (figure 4.15 b)).

It was not obvious which magnetic field to consider for the simulated turns. In the turn 2 the field on coil outer diameter was only 78% of the maximum field of that conductor, so the heater induced quench might start deeper in the cable, where the field was higher. We therefore considered three cases.

In Case 1, field was taken at the coil outer surface (65% of the magnet peak field). In Case 2, field was taken as the maximum field in the conductor (82% of the magnet peak field). And, in Case 3, the field profile varies across the conductor (1-D projection of the 2-D field map in the cable cross-section). In the turn 19, the field at the coil surface was the same as the cable's maximum field (42% of the magnet peak field), so simulations were done only for this field value. The variation of the field within the cables was assumed to have more impact in 11 T than for example in HQ, where the field at the coil outer diameter was 87-95% of the maximum field.

The heater power in simulations was 18.5 W/cm^2 in the high field and 29 W/cm^2 in the low field region. The adhesive layer between stainless steel heater and the coil was not included in the simulation.

MBHSP02

The MBHSP02 simulation was done only for the high-field heater turn 2, considering the maximum field in the conductor. This choice was based on the experience gained during the MBHSP01 simulation.

The simulated heater power was 40 W/cm^2, decaying according to the circuit time constant of 16 ms [Zlo2014].

4.5.4 Simulation vs. experiment

The simulation of MBHSP01 in general showed a good agreement with measurements, giving much longer delays for the thicker polyimide and the correct slope of delay increase at lower currents. The simulated delays at 1.9 K agreed the best with the experimental data for the high field heater when the utilized field was the maximum in the cable (Case 2). The agreement was within 20% for both insulation thicknesses when the considered operation currents were above 50% of SSL at 1.9 K. The delays using the realistic field profile (Case 3) were about 10-30% longer than the delays with the maximum field. When the field was taken at the coil OD (Case 1), the delay was at least 60% longer than with the maximum field. The delays under the low field heater were about 50-150% longer than the shortest delays under the high field heater. Figure 4.16 shows the results in the Cases 2 (B_{max}) and 3 (B_{prof}) of the high field heater. In simulations the delays were 20% longer at 4.5 K than at 1.9 K, but in the experiment the operation temperature did not have a clear effect on the delay.

The simulation of MBHSP02 heaters agreed with the experimental data

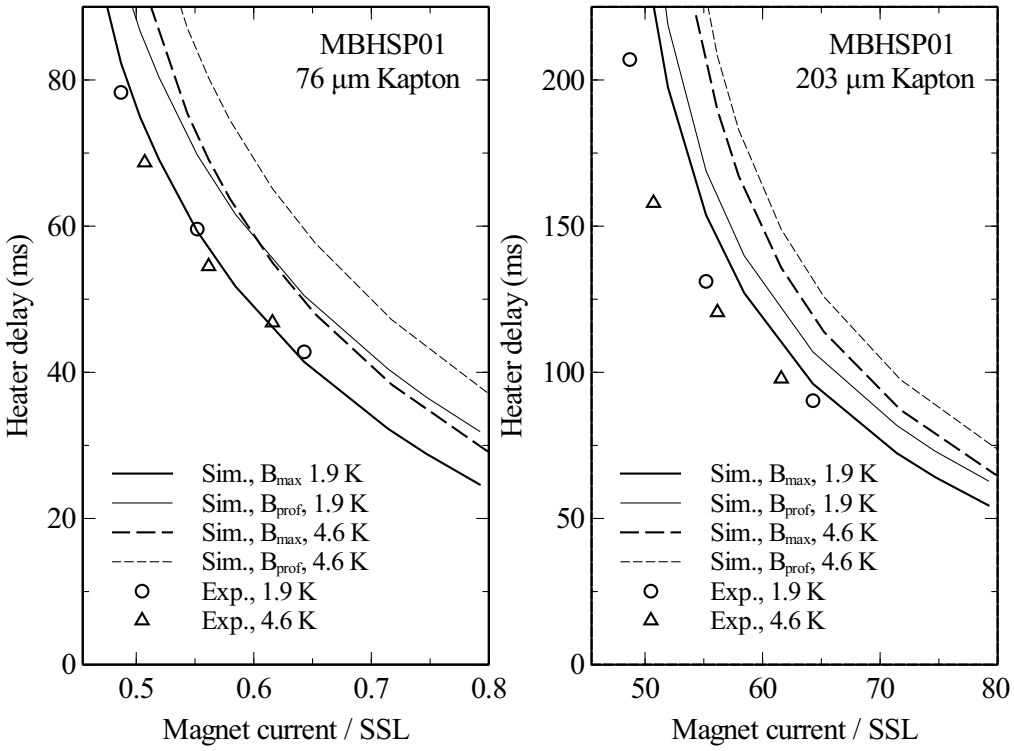

Figure 4.16: Simulation of heater delays in the 11 T dipole MBHSP01 as a function of normalized magnet current at 4.5 or 1.9 K. The simulation used the cable maximum field (B_{max}), or a realistic field profile (B_{prof}).

within 8% (or 2 ms) at 78% of SSL, and within 3% (or 2 ms) at 53% of SSL. At currents below 40% of SSL, the simulated cable temperature did not reach T_{cs}, although in experiment the cable quenched.

One should keep in mind that while tuning the field location may be useful for finding the best expectation for the experimental results, it may give a false sense of accuracy because the cable's anisotropic internal structure is still not modeled.

4.6 Analysis of uncertainties

The uncertainties in the heater delay analysis come from the experimental uncertainty, and from the simulation uncertainty. In this section are summarized the estimated uncertainties related to the various aspects of uncertainty. The analysis is detailed in **Publication 5**.

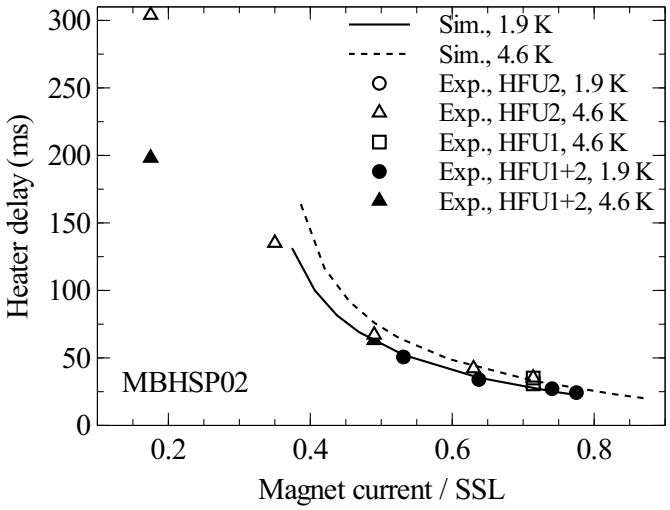

Figure 4.17: Simulation of heater delays in the 11 T dipole MBHSP02 as a function of normalized magnet current at 4.5 or 1.9 K.

4.6.1 Experimental uncertainty

The experimental uncertainty comes from the interpretation of the test voltage signals, and the test representation of reality.

The definition of the quench onset from the coil voltage signals defines the minimum uncertainty. The moment of heater firing is usually clear, but the moment at which the quench initiates at the coil is more ambiguous. Especially at low current the transition is slower, and the impact of the system noise, and the used criteria for quench onset will have a larger impact. Figure 4.18 shows example signals from the heater test at high and low magnet current in the LARP HQ01e magnet.

In the HQ and 11 T dipole tests the uncertainties close to the operation current were about ± 1 ms, increasing at lower currents to about ± 5 ms around 30% of SSL. In HD3 the uncertainties were larger, especially at lower current. Possibly firing the heaters initiated two quenches at symmetric locations which led to the coupling of the coils resistive and inductive voltages, and the used criteria for quench onset was not adequate.

The following guidelines improve the test reliability and improve the signals clarity:

- Heating by AC loss during the ramp is minimized by holding the magnet current constant for several minutes before activating the heater in order

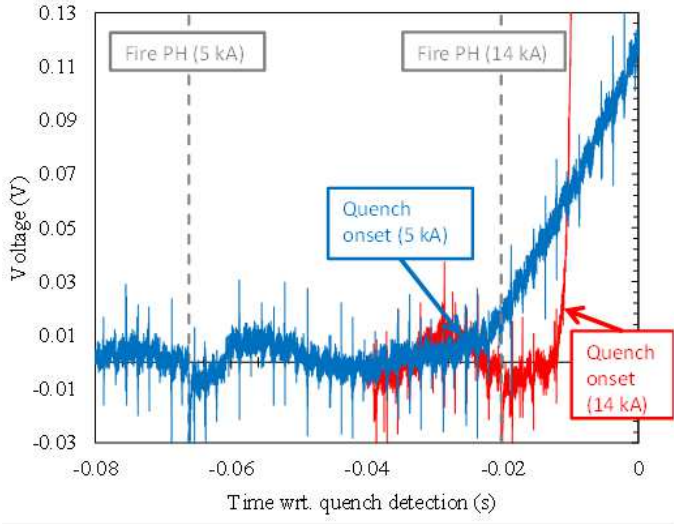

Figure 4.18: Voltage signals from HQ01e heater delay measurement at 5 kA (blue) and 14 kA (red) at 1.9 K. Shown are the voltage tap signals form the segment that quenched first (9B0405). Other signals (such as coil total voltage) may have been used too in the definition of the quench onset time.

to allow the heat generated during the ramp to cool down.

- Probability of conductor degradation is minimized by performing the heater experiments in a coil that does not show premature quenches during the magnet training.
- The voltage signals coupling between the coils is prevented by firing a heater circuit with only one strip to avoid several coils quenching simultaneously and obscure the signals.
- Uncertainties in the heater power is minimized by measuring the heater current.

Although the reproducibility of the delays at high and intermediate current was rather good when repeating the measurement in the same coil in the same conditions during the same test cycle (within 1 ms in the investigated cases), the delay variation between different coils in the same magnet was not negligible. In HQ02 none of the heaters or coils exhibited clear degradation, and all were considered "good" coils. The heater delays were measured at different coils during the two thermal cycles of the HQ02a test. The variation between heater delays in coils #15, #16 and #20 was only a couple of ms at high current although it was up to 20 ms larger at lower current. The

variation may be partially due to small differences in the R&D coils and cables (both design and fabrication). In summary, the interpretation of the signals combined with the experimental variation gives a total uncertainty of about 3 ms at high current and 25 ms at lower current in HQ02.

The measurements have also inherent limitations: Due to the measurement of coil voltage rise associated with the heater induced quench, the measurement will catch only the fastest delay in the coil. In the best case this is the delay at the high field area of the coil. The delay at lower field coil regions is usually not deducible from the measurement. In the worst case, the measured delay was due to a local defect, and the predictions done based on this measurement were overly optimistic if used in designing a quench protection. Therefore, several measurements using different heaters in the same magnet should be used to minimize this risk. After the simulated heater delays are validated for the high-field area, they can be used with more confidence to estimate also the heater delays in the lower field area.

4.6.2 Simulation uncertainty

The simulation uncertainty can be divided to the uncertainty in the input parameters (including the material properties), and to the error which arises from the modeling assumptions and simplifications. These include the homogenization of the cable properties, quench onset criterion, assuming constant field, material properties and constant thickness of all materials. Also, the critical surface at lower fields often has more uncertainty than at higher magnetic fields. The numerical error is also present, but this can be made to less than 1% by a fine spatial discretization.

Input parameters and material properties

The sensitivity of the simulated heater delay to the material properties and input parameters was studied. The impact of each parameter was studied by repeating the simulations by increasing or decreasing its value by 10%, The relative change to the nominal delay is shown in figure 4.19. HQ02 and HD3 were simulated at currents of 80% of SSL (HQ02 at 1.9 K and HD3 at 4.2 K), HQ01 with 73% of SSL at 1.9 K, and 11 T MBPHS02 with 74% of SSL at 1.9 K. The nominal parameters were as presented earlier for the outer layer heater of each magnet. The only change is that the HQ01 heater power was computed based on the measured heater voltage using (3.3). Therefore, the simulation of these three magnets responded differently to the change in stainless steel

properties.

Apart of the heater power and stainless steel, the magnets had similar sensitivity to the material properties and input parameters variation. The most important parameters were the magnetic field, heater power, and the thickness of the heater and cable insulation. In HQ02 the main thermal barrier between heater and coil was polyimide, and it had increased sensitivity to the thermal conductivity of the polyimide with respect to the other magnets. Note, that even if in the 11 T dipole the polyimide thickness was the same than in HQ02, its thermal barrier is also strongly impacted by the thick G10 layer.

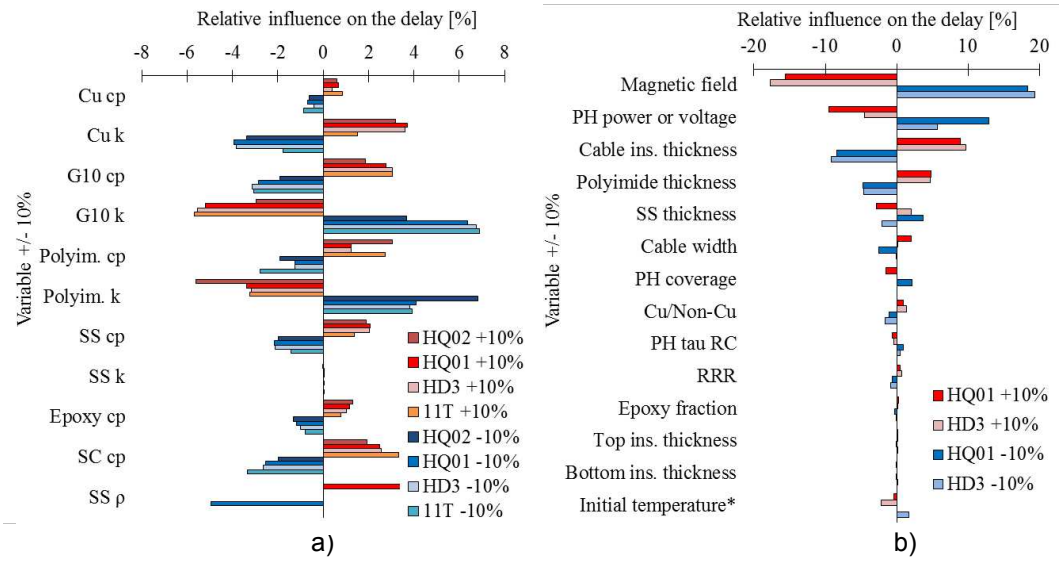

Figure 4.19: Simulated delay sensitivity to ±10% variation of a) material properties and b) input parameters.

Transverse heat diffusion

The assumption of negligible thermal gradients between the coil turns was not justified for a cable at the heater edge, where the adjacent turn was not covered by the heater. Especially in the previous simulations were often simulated the highest field turns which were located near the heater edge. In this study the impact of the transverse heat diffusion was evaluated. The 2-D simulation model was set to represent a fraction of the coil cross-section. It was simulated as a stack of cables, with uniform thickness (cable mid-thickness), and heater on the cable thin side covering only some of the turns. The temperature difference was evaluated between the cable at the center of the heater and the

cable at the heater edge. The heater coverage was assumed very long so that the heat diffusion longitudinally along the cables could be neglected.

The block dimensions roughly approximated the HQ outer layer high field block: Width of the block was 20 mm and the heater strip width was 10 mm. The strip covered 5 turns at the center of the block totally, and below the heater edges about 60% of the turn. The simulated magnetic field was 0.70 of magnet peak field (approximating an average in these turns). The magnet current was 80% of SSL at 1.9 K for HQ01 and HQ02 and at 4.2 K for HD3. The heater power in all simulations was 50 W/cm^2 and the RC circuit time constant was 40 ms. Figure 4.20 a) shows the modeled block with the heater at its center. Due to symmetry it was sufficient to model only half of the block. Figure 4.20 a) shows the simulation domain with the boundary conditions.

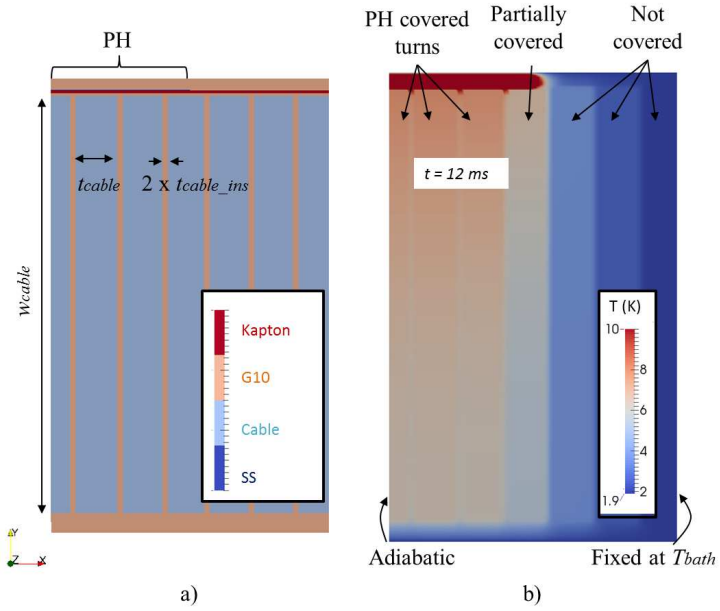

Figure 4.20: Transverse heat diffusion simulation in HQ02: a) domain and materials, b) temperature distribution 15 ms after heater activation. The temperature scale is adjusted to show differences below 12 K. The maximum temperature in the heater at this moment is 90 K.

Figure 4.20 b) shows the temperature distribution 15 ms after the heater activation in HQ02. Figure 4.21 presents the temperatures at that time instant as a function of x-coordinate at the top of the cable and at its center in HQ01, HQ02 and HD3. As expected, at the top of the cable HD3 and HQ01 have very similar temperatures due to similar insulation scheme, but in HQ02 the temperature is lower due to the thicker insulation. Although HQ01 and HD3

have similar temperatures at the top of the cable, the temperatures differ at the center of the cable. It is probably due to the the larger cable in HD3 and the lower cable thermal conductivity due to lower RRR and lower Cu fraction. The stronger temperature gradient across the cable width is consistent with the larger uncertainty margins associated with the HD3 simulations.

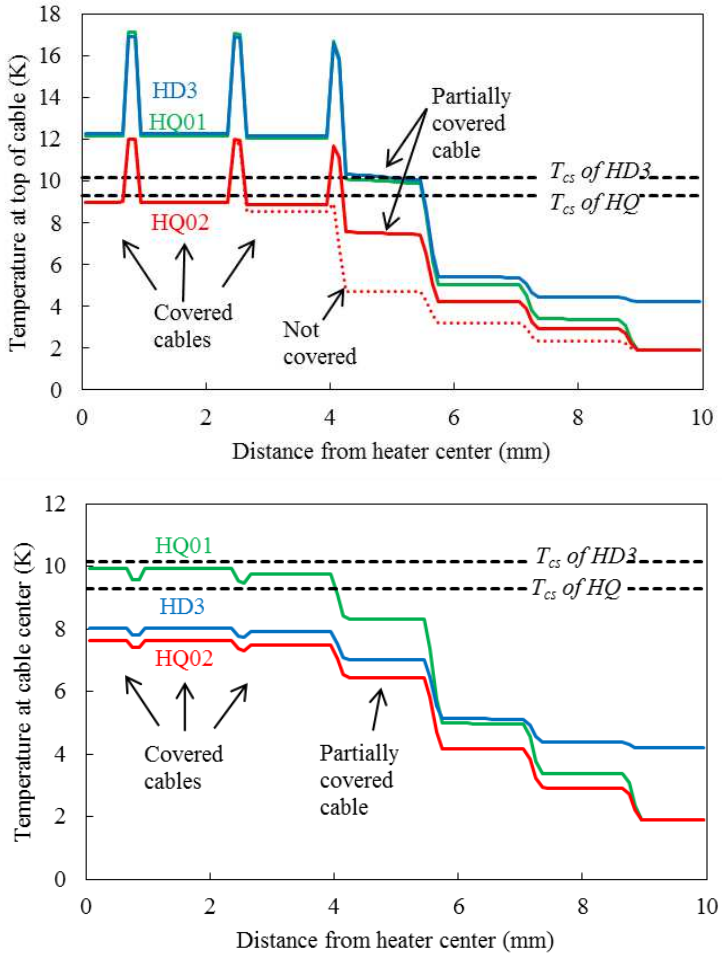

Figure 4.21: Simulated temperature at different turns and insulation in HQ01, HQ02 and HD3 15 ms after heater activation. Top: Temperature at the top of the cable. The dashed line has 8 mm wide heater strip, the solid lines 10 mm. Bottom: Temperature at the center of the cable.

In the simulations lasting 20 or 30 ms, the maximum temperature difference between the partially covered cable and the cable at the heater center was less than 20%. The last fully covered turn at the heater edge had 1-3% lower temperatures than the turn at the heater center. The heater delays in the

fully covered turns were within 1 ms of each other, while the partially covered cable has 5 ms longer delay in HQ01 and in HD3, and 9 ms in HQ02.

For HQ02 was considered also a case with 8 mm long heater. This heater covers exactly 5 turns, but not the cable insulation for the turns below its edge. In this case, the turn at the heater edge had 1-7% lower temperature than the turn at the heater center (at the top of the cable), and it quenched 2 ms later.

Based on this, simulating a fully covered turn, with heater coverage extending even slightly over it, has a tolerable error at the maximum operation current. The error increases with time, therefore with longer delay times – meaning that the temperature margin is high, heater insulation is thick, or heater power is low – the impact of this, as well as other uncertainties, will be larger.

4.7 Concluding remarks

Extensive experimental work has been performed in order to gather heater delay data to be compared with the simulation model, and to understand the unavoidable uncertainty. In this chapter were presented heater delay measurements in several R&D high-field Nb_3Sn accelerator magnets and compared the measured delays with simulations. The impact of operation current and insulation were generally well reproduced around the operation temperature. The results showed that usually the model predicted the delays within 20% near the maximum operation current regime at the coil outer layers, but at lower currents and coil inner layers, the deviation was larger. Fortunately, the low current regime is less critical for the heater design. The uncertainty in the experimental data was also in the 20% range at high currents. At low current the uncertainty was larger, and it depended on the magnet and cable properties as well as on the heater test procedure.

The comparison also aided in the simulation settings definition. First, if the heater design relied on heating stations with length in the centimeter range, the longitudinal heat diffusion along the cable must be taken into account and a 1-D model should not be used. Although no fitting parameters were used in CoHDA, the choice of the field location in the cable and the choice of neglecting the adhesive can be considered such. The right way to add the adhesive is complicated because in reality the insulation thickness between the heater and strands is highly non-uniform.

The sensitivity of the simulation results on an individual parameter was within 20% when the parameter was varied by 10%. The most important

input parameter was the magnetic field. Therefore, modeling the right quench location load line and the critical surface is important.

Chapter 5

Optimization of the heater layout using parametric analysis

In the previous chapter the efficiency of heaters in several existing high-field Nb_3Sn R&D magnets was analyzed. This chapter considers the protection of the future prototype magnets Long HQ (LHQ) and QXF. In these longer magnets the distribution of the heater energy across the coils becomes more critical because the total dissipated energy cannot be increased due to the limitations in the voltage and temperature of the heater. Therefore, the limits of the present heater technology are explored by optimizing the layout design in order to minimize the delay and maximize the coil coverage within the given design constraints.

First, in section 5.1 the required heater delays are estimated. Then, in section 5.2 the most important heater design parameters are identified, and the ranges they are allowed to vary in the heater design are defined. Section 5.3 describes the utilization of series of parametric analyses to define the heater layout which gives the shortest delays. The method is applied to LHQ and QXF in section 5.4. In section 5.5 is presented the test of the new LHQ heater layout in a single coil and a comparison with a traditional heater layout.

The numerical simulations estimating the requirement for the LHQ heater efficiency were published in **Publication 1**. Parametric studies of heater delay were published in **Publication 2** and **Publication 3**. The principle of the heater design, and an all-stainless steel shaped heater design for QXF was described in **Publication 3**.

5.1 Estimations of needed heater efficiency

Both analytical and numerical analysis can be used to estimate the heater delays that are needed for protecting a magnet. One analytical analytical method based on the MIITs curve is the so-called time margin, introduced in [Tod2013a]. The time margin assumes an initial quench, continuing operation at constant current, and then protection heaters quenching the entire magnet uniformly at a certain time instant. Time margin is the time available between the initial quench and the moment the heaters have quenched the entire winding. The aim is to keep the MIITs such that the adiabatic temperature will not exceed a given maximum hotspot temperature. The time margin at 80% of SSL at 1.9 K for a HQ type magnet was 25 ms to stay below 300 K [Tod2013a]. The limit to stay below 350 K is about 27 ms for HQ and 33 ms for QXF [Tod2013b]. With 17 ms delay for detection, validation and switches, the heater delays to quench *all* the cables should be 10 ms in HQ, and about 16 ms in QXF. For comparison, the time margin of the LHC dipole was about 100 ms considering a quench initiating on the outer layer, and 200 ms for a quench in the inner layer [Tod2013a].

5.1.1 Numerical simulation

Numerical approaches are more versatile, because they allow limiting the quench by heaters only to a part of the coil, and then compute quench propagation to the superconducting parts of the cable. Unfortunately, the present dedicated quench analysis tools cannot simulate a quench at different time at each coil turn and the propagation between heating stations. Therefore, in the simulations one considers single heater delay per coil, or coil layer. **Publication 1** presents a numerical simulation for LHQ, which was modeled as a 3.6 m long scale-up of HQ. The simulation was done by Helene Felice using QuenchPro. The simulation result was that heater delay of 5 ms in the inner layer and 10 ms in the outer layer was needed to keep the LHQ magnet peak temperature within 320 K when operating at 17.3 kA at 4.5 K (100% of SSL). The simulations assumed a very optimistic detection time of 6 ms and heater coverage of 100% of the coil surface. The quench propagation velocity was assumed 10 m/s in the inner layer, where the quench is assumed to initiate, and 5 m/s in the outer layer. This prediction gives even smaller ”time-margin”, than the analytic concept for HQ. The difference is at least partially due to the different operation point and the material properties used in the computations. The magnet length should not impact the needed delays because no dump was considered.

5.1.2 Comparison with existing technology

Even if in the HQ01 series the first heater delays were in the order of 6-7 ms there are several reasons why this result cannot be scaled to the longer magnet. First, due to the frequent electrical issues the heater insulation needs to be increased from the used 25 μm. The HQM01 had 50 μm thick heater insulation and had delays of about 5-10 ms. Second, the same heater pattern is not expandable to the longer magnet because the strip length must be increased for longer coils (to avoid taking wires out from the middle of the magnet) but the heater voltage has the same maximum limit in short and long coils. Therefore, long magnets need discrete heating stations that have longer spacing as the coil length increases. This will increase the quench propagation time between the heating stations. Third, the inner layer heaters have not proved to be reliable, thus the coverage needs to be decreased from the approximately 65% in HQ01 and HQM01. And finally, the measurement results showed only the delay of the cable which quenched first. All the heated cables quenched at a later time instant. Consequently, it is impossible to determine the delay to quench the whole block from the experimental setup. An additional concern is brought by the requirement of the redundancy, which was not considered here.

In conclusion, the existing designs as such were not sufficient. Improvements in the technology were needed. To reach the goal, the detailed CoHDA modeling tool was utilized to optimize the design while taking into account all the design parameters such as the heating station length. In addition, the analysis was redefined and the difference between the coil turns operation points was considered. The aim was to remove the overly conservative assumptions that the analytical approaches and QuenchPro consider, where possible.

5.2 Design variables

The aim was to optimize first the present technology that has been proved to be reliable in the Nb_3Sn magnets, and to see its prospects. This technology consists of only stainless steel with shaped heating stations (like LARP LQ) on only coil outer layer, using sufficient insulation. Then, developments such as copper plating and inner layer heaters were considered.

The most important heater parameters are the heater power, the thickness of the heater insulation, and the heater geometry (heating station length and their spacing). In **Publication 2** and **Publication 3** were presented computational and experimental parametric analyses on heater delays in HQ01,

HQ02 and LQ in different operation conditions. It was found that the heater peak power and the heating segment length must be sufficient in order to avoid lengthening the delays, while the heater period did not impact the delay in the considered range. On the other hand, the insulation thickness has more than a linear impact on the delay because it acts as a thermal barrier between the heater and the coil. The important impact of insulation thickness is consistent with earlier studies reported by Imbasciati et al. in [Imb2001] for Nb_3Sn magnets, and Rodriguez-Mateos et al. in [Rod2000, Rod2001] for the LHC Nb-Ti magnets. The impact of power was consistent with earlier studies on the LARP magnets [Fel2009a]. The importance of the heating segment length however had not previously been thoroughly analyzed for Nb_3Sn magnets.

The insulation thickness is an important choice. It should be minimized to fasten the heat diffusion from the heater to the cable. On the other hand, if the electrical integrity requirements are not met, the entire heater must be disconnected. Here, the heater insulation thickness was chosen to be 50 μm. This was based on experience with the R&D magnets. Coils with 25 μm Kapton (HQ01, LQ) had electrical problems, but HQM01 with 50 μm and HQ02 with 75 μm did not. Therefore, the designs were done for 50 μm and further tests will provide evidence regarding its adequacy.

Consideration was also paid to the possibility to replace some of the Kapton with G10, which has better heat conduction properties. The thermal conductivity of Kapton is less than 0.2 W/m/K under 100 K and less than 0.03 W/m/K under 10 K, with thermal diffusivity under 0.45 cm^2/s. The thermal diffusivity of G10 is about 2 to 6 time better in that temperature range. However, the Kapton dielectric strength is superior, 300 kV/mm (60 Hz, 25 μm thick DuPont Kapton HN) [DUPONT], compared to approximately 20-30 kV/mm of G10 [FR4, MATWEB]. Therefore, a thinner layer is sufficient forming a smaller overall barrier. Note that the literature values of dielectric strength cannot be used in design to define the needed insulation thickness (otherwise 25 μm would be sufficient by a large margin). Figure 5.1 shows the thermal conductivity and diffusivity of typical insulation materials in Nb_3Sn accelerator magnets.

The heater peak power is defined by its maximum voltage and shape of the strip. In our design for the outer layer heaters, the maximum heater voltage was limited to 400 V due to the available power supply. For the QXF inner layer heaters the limit was updated to 450 V because in LHC the heater power supplies provide 900 V ($\pm$ 450 V, when the ground is connected in the middle of the heater). The time constant of the voltage decay (τ) is defined by capacitor bank capacitance and the resistance of the heater circuit. τ must be limited

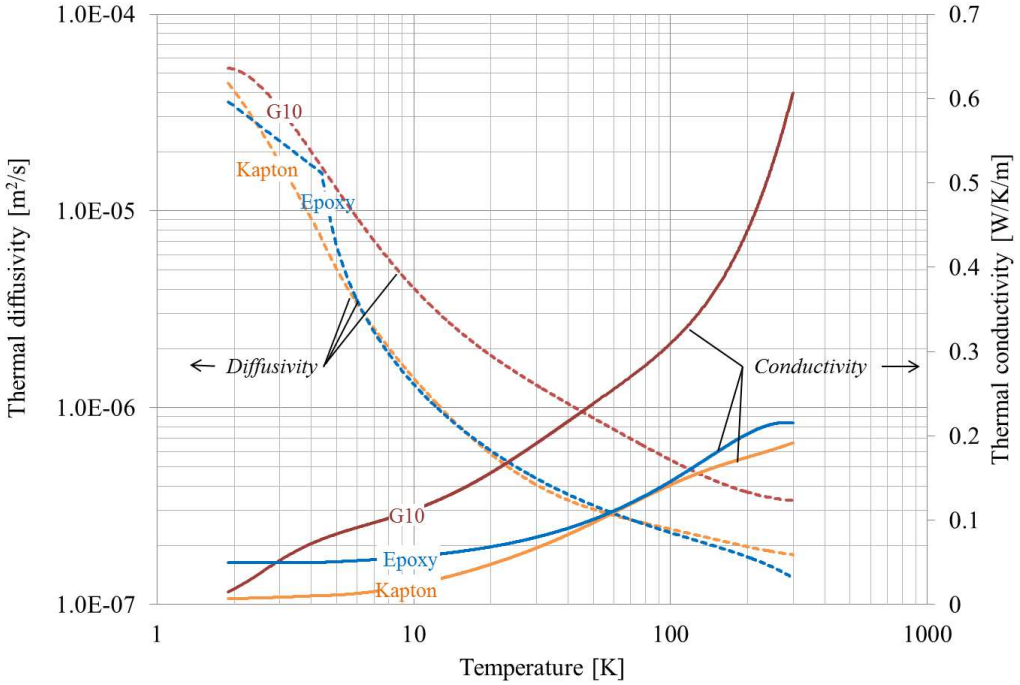

Figure 5.1: Thermal diffusivity and conductivity of typical insulation materials in Nb_3Sn accelerator magnets.

in order to avoid overheating the heater itself. In these analyses the time constant was defined so that the heater maximum temperature remains below 350 K, conservatively, in an adiabatic computation. This is an increase to the 300 K that had be used as a design criterion for the previous model magnets. However, the adiabatic computation also for 350 K is overly conservative in the thin heater because the heat diffuses to the coil as intended to. This result is consistent with the findings from the LHC heater design studies [Son2001c].

With these constraints, the optimization deals with the distribution of the available energy in terms of heating station location, power and geometry. Further constraints to the heater location come from the requirements to leave certain coil turns without a coverage, for example to leave space for the voltage taps on the pole turn, or to leave free space on the inner surface to enhance the cooling. In this analysis was assumed that the heater strip must extend the length of the coil straight section, and low resistance connections bring it to the coil extremities.

5.3 Heater design method

5.3.1 Goal

Different approaches for an optimal heater design could be used. Our goal was to entirely suppress the superconducting state from all the turns covered by the heater as fast as possible. This means that the first heater delay (measured in the previous chapter) was not minimized, but both the heater delay (Δt_{PH}) and the time of quench propagation between the heating stations (Δt_{PH}^{QP}) were considered for each coil turn under the heater. The optimal design was defined so that the time to quench the last turn ($\Delta t_{PH}^{tot,max}$) was minimized. Figure 5.2 shows a diagram of these times in one coil turn after a quench. The delay times vary among the coil turns, because they are exposed to different magnetic fields and consequently non-uniform thermal margin. This design criterion leads to directing more heating to the lower field region than to the higher field. Figure 5.3 shows a schematic of a LQ-style stainless steel heater with a heating station covering both coil high field (HF) and low field (LF) region.

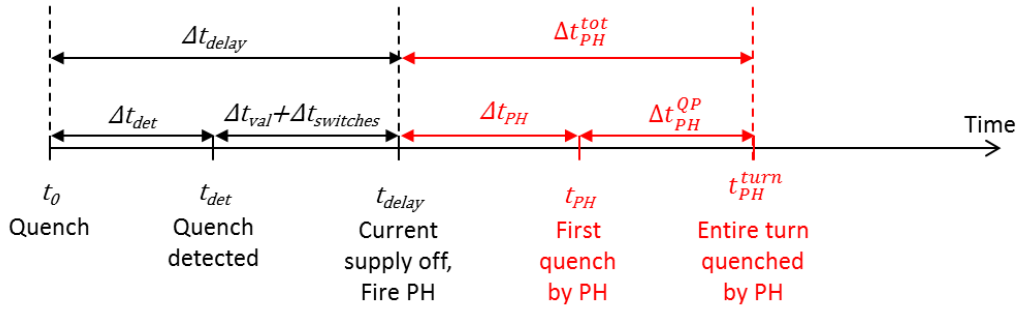

Figure 5.2: Diagram of the times associated with the delays in quench protection. The time instants of t_{PH} and t_{PH}^{turn} are different in different coil turns.

The optimization was done for the highest nominal operation current, typically 80% of the SSL. This is the most critical regime. The protection at 90% of SSL (relevant for the magnet testing phase), and at low current (relevant for the real operation) must be explored separately. However, these investigations are not relevant if the heaters are not able to protect at 80%.

The advantages of this approach is that a large fraction of coil is quenched, presumably leading to a quick current decay and consequently a quench back (discussed in section 2.3.5) for the coil turns that are still superconducting. It also allows the simplest comparison of the time margins to estimate the feasibility of given protection heater design.

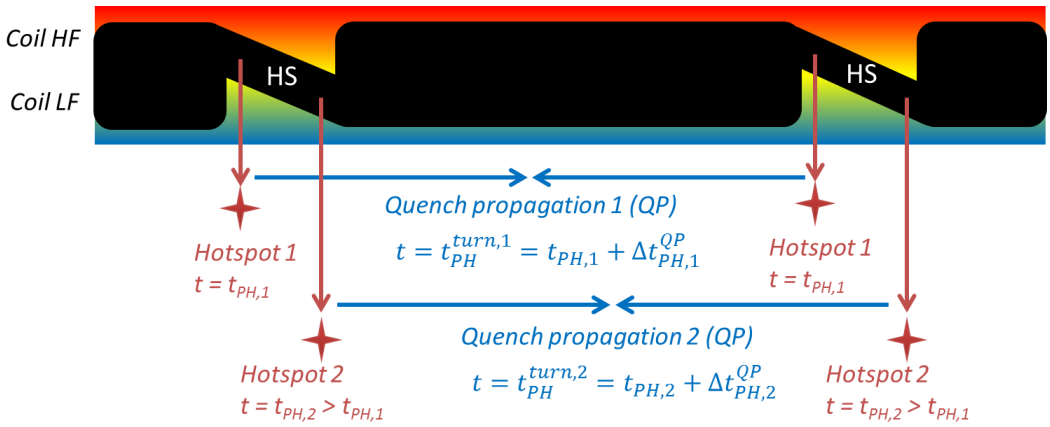

Figure 5.3: LQ-style stainless steel heater, showing the concept of heating stations (HS), and the relation of heater delay and quench propagation time in coil high-field (HF) and low-field (LF) region. The optimization method is to minimize largest t_{PH}^{turn} related to different turns under the heater.

5.3.2 Heater layout concepts

More heating can be provided to the coil lower field region than in high field region by using a higher heater power, or longer heating segments. The higher power can be obtained by using a narrower heating station, however this could lead to local heater hotspots and thus limit the total deposited energy. Therefore, the optimization of heating station lengths was chosen and their width was fixed to be the same at different field regions. Three different heater layouts were considered and they are shown schematically in figure 5.4.

Stair-step

First, an all stainless steel heater was designed for the QXF outer layer. This heater strip had periodically ”stair-steps-shaped” heating station, which consists of three narrow segments, located at different coil field regions. Their widths are 1/3 of the nominal strip width, and their lengths can be varied based on the field regions. The length of the narrow heating segments and their spacing is a result of the optimization study. Based on the heating station shape, here this layout is called the stair-step design.

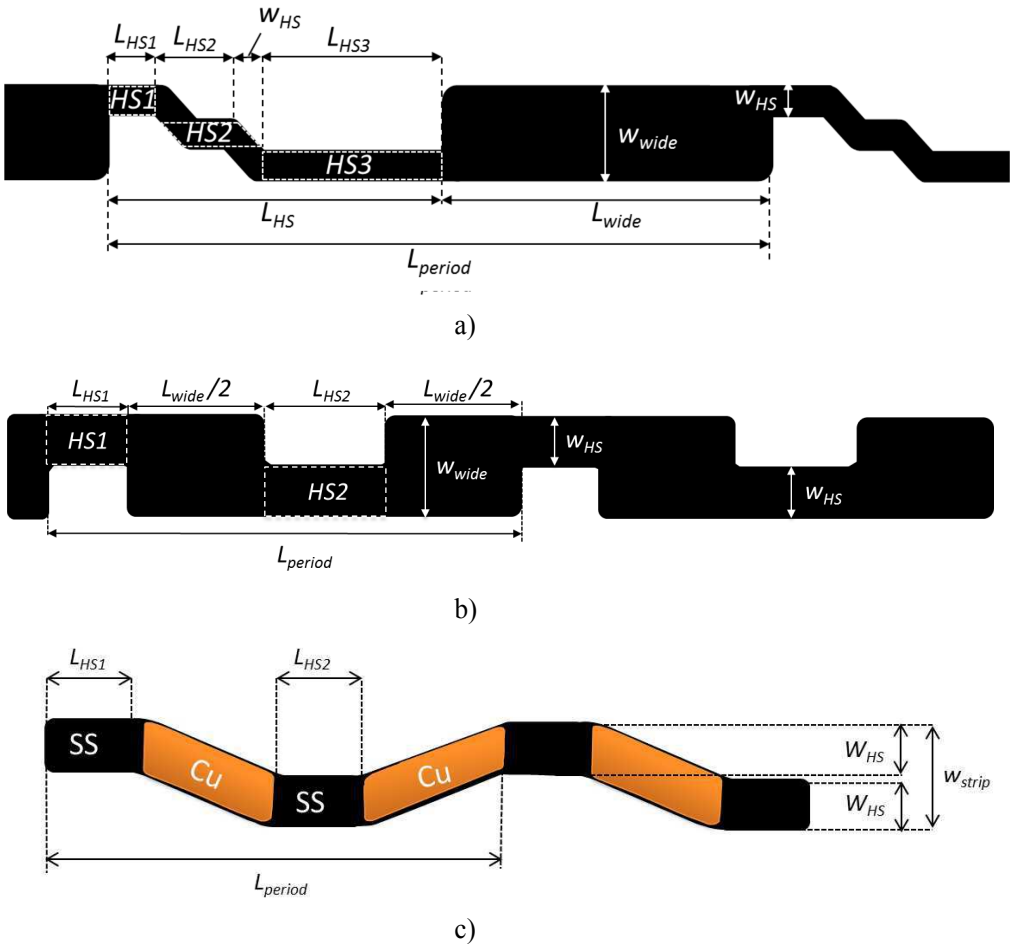

Figure 5.4: Proposed protection heater strip geometry concepts: a) stair-step, b) pulse-wave and c) snake layout.

Pulse-wave

The LHQ outer layer heater design was first based on the stair-step layout. However, then the design evolved to include only two narrow segments per heating station. The transition between the heating stations finally was done by dividing the wide segment into two in order to connect the narrow segments without a special transition area that is used in the stair-step designs. This layout is called the pulse-wave design here, due to the periodical rectangular heating zone ”pulses”.

Snake

The QXF inner layer heater explored the use of copper-plating for the transitions between the heating stations. The layout design started from the pulse-wave design, except that the low-resistance transitions between the heating stations were considered to be copper plated. By M. Marchevsky's suggestion the boxy wide segments between the heating stations were made diagonal and thinner, thus leading to the snake-like layout.

5.3.3 Optimization method

The optimization algorithm was programmed to be used in connection with the CoHDA simulation tool. The routine is based on parametric analysis, which goes through a range of possible combinations of the heating station lengths and powers and consequently determines the allowed periods. The constraints are given by the maximum voltage $V_{PH,max}$ and temperature $T_{PH,max}$, and strip length L_{strip}. Algorithm 1 displays the simulation algorithm that is discussed next.

For each considered power $P_{PH} = P_{PH}(\mathrm{t}{=}0)$ was computed first the decay time constant (heater RC circuit) to ensure that the heater temperature does not exceed the maximum limit that has been calculated adiabatically. This is done by comparing the deposited volumetric energy to the stainless steel enthalpy from operation temperature T_{op} to $T_{PH,max}$, using

$$\tau = 2 \int_{T_{op}}^{T_{PH,max}} \gamma_{ss} C_{p,ss}(T) \mathrm{d}T \frac{d_{ss}}{P_{PH}}, \tag{5.1}$$

where γ_{ss}, $C_{p,ss}$ and d_{ss} are the stainless steel mass density, specific heat and thickness, respectively.

With each considered heater power, the delays are computed for each field region as a function of heating segment length (coverage) using the regular CoHDA simulation. The heater period is assumed to be sufficiently long that it does not impact the result. The heating provided by the wide segment is ignored and the period impacts only on the quench propagation time between the heating stations. Algorithm 1 also describes the optimization criterion to minimize the delay to the time instant when the quench has fully propagated between the heating stations in each of the turns. Here, the term *block* is used to refer to the straight section of the coil turns covered by the heater.

After the heater delays are known for each investigated heater coverage

input : Cable parameters and operation conditions, heater layout type, $L_{strip}, w_{wide}, w_{HS}, d_{ss}, T_{PH,max}, V_{PH,max}$, B for each HS, NZPV between each HS, range of L_{HS} and P_{PH}
output: The layout (HS lengths, period and power) and its $\Delta t_{PH}^{tot,max}$ corresponding to the optimization criterion

foreach *Heater power* P_{PH} **do**
  $\tau \leftarrow$ `ComputeTau(`$P_{PH}, T_{PH,max}, d_{ss}$`);`
  `// The delay dependence on HS lengths for each HS location`
  foreach *HS field* B_{HS} **do**
    foreach *HS length* L_{HS} **do**
      $\Delta t_{PH} \leftarrow$ `ComputeDelay(`$B_{HS}, P_{PH}, \tau, L_{HS}$, *cable and op. cond.*`);`
    end
  end
  `// All combinations of HS lengths that are possible to form one heater period`
  foreach *Combination of HS lengths* $L_{HS,vect}$ **do**
    $L_{period} \leftarrow$ `ComputePeriod(`$P_{PH}, L_{HS,vect}, HeaterType, d_{ss}$`);`
    `// The total delay times including the quench propagation`
    foreach *HS field* B_{HS} **do**
      $\Delta t_{PH}^{QP} \leftarrow (L_{period} - L_{HS})/2/NZPV$;
      $\Delta t_{PH}^{tot} \leftarrow \Delta t_{PH} + \Delta t_{PH}^{QP}$;
    end
    $\Delta t_{PH}^{tot,max} \leftarrow$ The largest Δt_{PH}^{tot} among the HS
  end
  `// The result layout for this` P_{PH}
  Choose the layout ($L_{HS,vect}$ and L_{period}) which gives the smallest $\Delta t_{PH}^{tot,max}$
end
`// The result layout from this routine`
Choose the layout which gives the smallest $\Delta t_{PH}^{tot,max}$ among all P_{PH}

Algorithm 1: Algorithm for heater design.

and power, the total delays are computed for different combinations of HS lengths. For each combination of heater power and heating station lengths, the algorithm computes the maximum number of periods in the strip so that its resistance does not exceed the limitation given by the fixed $V_{PH,max}$ and

the I_{PH} defined by the power. Clearly, the resistance calculation of one period (including the wide part and the heating stations) is different for each of the three heater types considered. In general, the resistances of HS (R_{HS}) and wide part (R_{wide}) are computed analytical as

$$R_{HS} = \frac{\rho_{ss} L_{HS,path}}{w_{HS} d_{ss},} \tag{5.2}$$

and

$$R_{wide} = \frac{\rho_{ss} L_{wide}}{w_{wide} d_{ss},} \tag{5.3}$$

where ρ_{ss} is the stainless steel resistivity at 4.5 K, and $L_{HS,path}$ is the total length of the narrow heating stations in one period, taking into account also the diagonal transitions between the narrow segments in the stair-step-design. The widths of the wide and narrow parts are respectively w_{wide} and w_{HS}. For copper plated heaters, R_{wide} is computed considering the resistivity and the thickness of the plating, assuming a perfect contact between the copper and the stainless steel

In case of only stainless steel heating stations, with L_{HS} being the sum of their lengths in one period (along the coil axis), the smallest period becomes:

$$L_{period} = \frac{R_{HS} L_{strip} - L_{HS} R_{strip}}{R_{strip} - \frac{\rho_{ss} L_{strip}}{d_{ss} w_{wide}}}. \tag{5.4}$$

5.4 New heater designs

The heater design algorithm was applied to the LHQ and QXF magnets. The magnet parameters for heater simulation are listed in the table A.9 in Appendix A. This section describes the results of the heater designs.

5.4.1 LHQ

The LHQ heater design was performed for coil outer layer, using only stainless steel. The final design was the "pulse-shape" layout. Two strips for each coil half were used. This provides redundancy in case one strip could not be used.

Strip dimensions and simulation parameters

The coil length is 3.3 m (updated design since the QuenchPro simulations of section 5.1.1), and the strip was designed to be 3.0 m to cover the coil straight

section. Low-resistance (0.3 Ω) connectors were assumed to extend it to coil ends.

The dimensions of the strips were based on coil outer surface dimensions. Figure 5.5 shows a cross-section of a half-coil with the magnetic field map. The heaters for the two coil blocks were designed separately. The block with higher field (HF block) has an arc-length of about 24.4 mm. In order to leave the pole-turn and the copper-wedge uncovered, the heater strip width was 21.0 mm. The two heating stations were designed to be half of that, i.e., 10.5 mm wide. On the lower field block (LF block), the arc-length was about 20.8 mm. To leave one turn uncovered near the mid-plane, the heater strip width was 18 mm, having two 9 mm wide heating stations. Heater maximum voltage was 400 V and temperature 350 K.

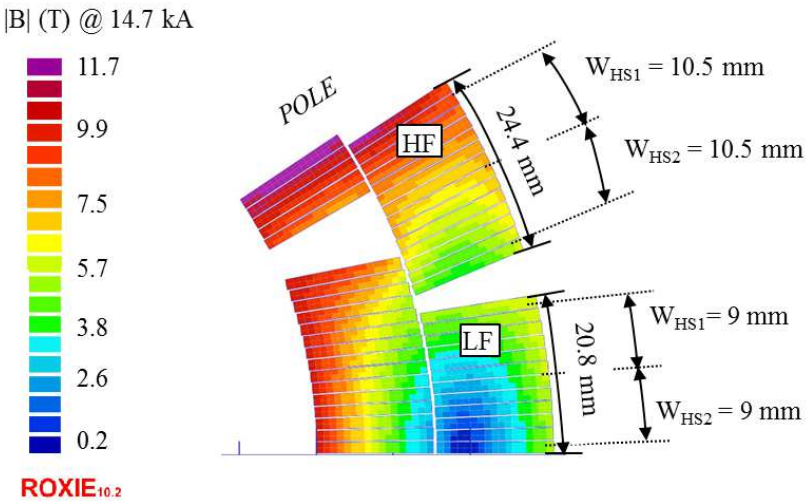

Figure 5.5: Locations of the two heaters and their heating stations on the LHQ coil outer layer HF- and LF blocks.

The optimization was done for magnet current of 15.4 kA, which is 80% of SSL. The field on the coil outer surface was calculated using ROXIE, and the lowest field value under each heating station was used to determine the T_{cs} and consequently the heater delay. On the HF block the fields for HS1 and HS2 were 8.1 T and 5.8 T, respectively, with current sharing temperatures of 9.2 K and 11.0 K. On the LF block the fields were 5.6 T and 5.2 T, and current sharing temperatures 11.2 K and 11.4 K for HS1 and HS2, respectively. The normal zone propagation velocity (NZPV) was assumed to be 12 m/s in the high field block and 7 m/s in the low field block.

Simulated delays

The heater delays were evaluated for heater peak powers from 50 to 300 W/cm^2, with step size of 25 W/cm^2 in HF heater and 28 W/cm^2 in LF heater. Consequently, with strip thickness of 25 μm, the time constant varied from 73 ms (with 50 W/cm^2) to 12 ms (with 300 W/cm^2). Figure 5.6 a) shows an example of the HF heater delay's dependence on the heater longitudinal coverage (HS length) with 50, 134, and 300 W/cm^2. One can see that for HS1 the impact of heating station length starts to saturate at 25 mm if power is 300 or 134 W/cm^2 and at 30 mm if power is 50 W/cm^2. The saturation was defined so that the delay is within 10% of the delay with 50 mm long heating segments. For HS2 the corresponding values are 30 and 35 mm.

The HF heater period length according to (5.4) for different HS length combinations is shown in figure 5.6 b). With 300 W/cm^2 the periods are always larger than 0.5 m, and even larger than 1 m if the sum of heating station lengths is larger than 50 mm. This, combined with only 2-3 ms improvement in the delay compared to the case when the heater power is 134 W/cm^2, suggests that this power is too high for the heater. For the powers 134 and 50 W/cm^2 the periods are between 60 and 170 mm, which is in the range of practical interest. The periods are similar with both powers up to a total HS length of about 60 mm. This is probably because there is a need for minimum wide segment length (42 mm) between the transitions of HS1 and HS2 to make it at least a square.

Figure 5.7 shows the total delays to quench the coil fully between the heating stations with heater powers of 50 and 134 W/cm^2 for the HF heater. The corresponding heating station length, i.e., the heater delay, impacts the delay the most, and the impact of period variation due to the length of the other heating station is smaller. This is expected because the maximum variation of the period was about 110 mm. With 12 m/s quench propagation velocity the impact of this is less than 5 ms. The arrows indicate the HS combinations leading to the smallest delay to quench the entire block. This highlights how the optimum is not the shortest delay obtainable for the higher field location (HS1), but it minimizes the maximum delay.

Tables 5.1 and 5.2 list the HS length combinations for the optimum layouts at each considered power for the HF and LF strip, and the resulting delays. Note, that the voltage needed to obtain the considered power may also be lower than 400 V. This is because the geometry was required to have an integer number of heating stations, and because the wide segment length between the heating stations had the minimum requirement as discussed earlier.

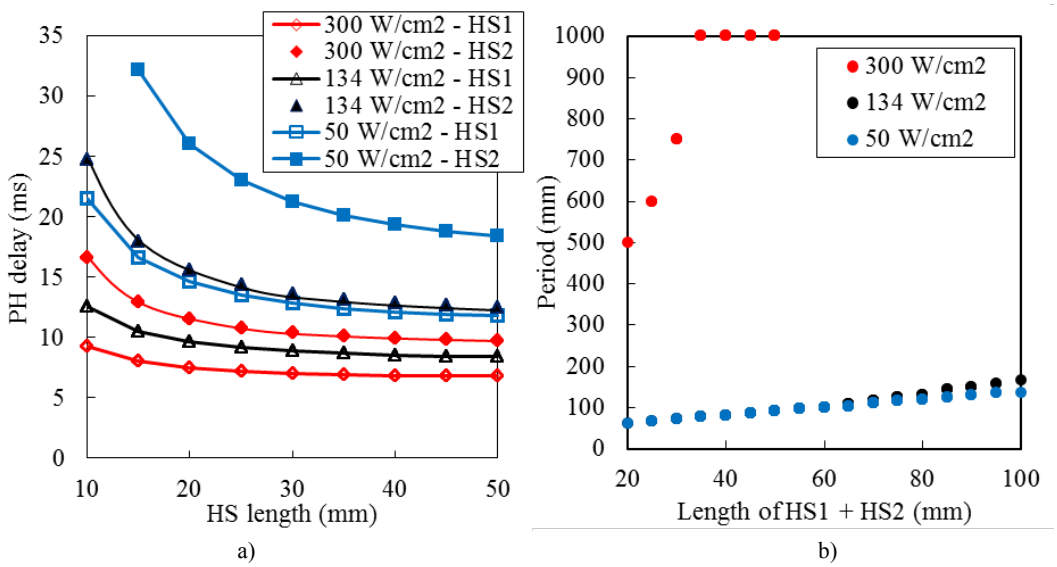

Figure 5.6: a) LHQ HF heater delay as a function of HS length with peak powers of 50, 134, and 300 W/cm^2. b) The minimum period that can be used as a function of the sum of HS lengths.

Table 5.1: Results of the HF heater layout optimization at each power, with delay time for normal zone onset (Δt_{PH}) and transfer to normal state by propagation between the HS (Δt_{PH}^{tot}).

$P_{PH}(0)$ (W/cm^4)	HS length (mm) $HS1 - HS2$	Period (mm)	Δt_{PH} (ms) $HS1 - HS2$	Δt_{PH}^{tot} (ms) $HS1 - HS2$
50	15 – 50	103.45	16.7 – 18.4	20.4 – 20.7
78	15 – 50	103.45	13.3 – 15.2	17.0 – 17.5
106	15 – 50	103.45	11.6 – 13.6	15.3 – 15.8
134	15 – 50	107.14	10.5 – 12.5	14.4 – 14.9
161	10 – 30	90.91	11.6 – 12.7	15.0 – 15.2
189	10 – 30	120.00	10.9 – 12.1	15.5 – 15.8
217	10 – 30	166.67	10.4 – 11.5	16.9 – 17.2
245	10 – 20	187.50	9.9 – 12.3	17.3 – 19.3
273	10 – 20	300.00	9.6 – 11.9	21.7 – 23.6
301	10 – 10	500.00	9.3 – 16.6	29.7 – 37.1

For the HF heater, the optimum layout is the same for powers between 50 and 106 W/cm^2, and the period starts to increase only for the peak power of 134 W/cm^2. This means that with these lower powers the heater resistance

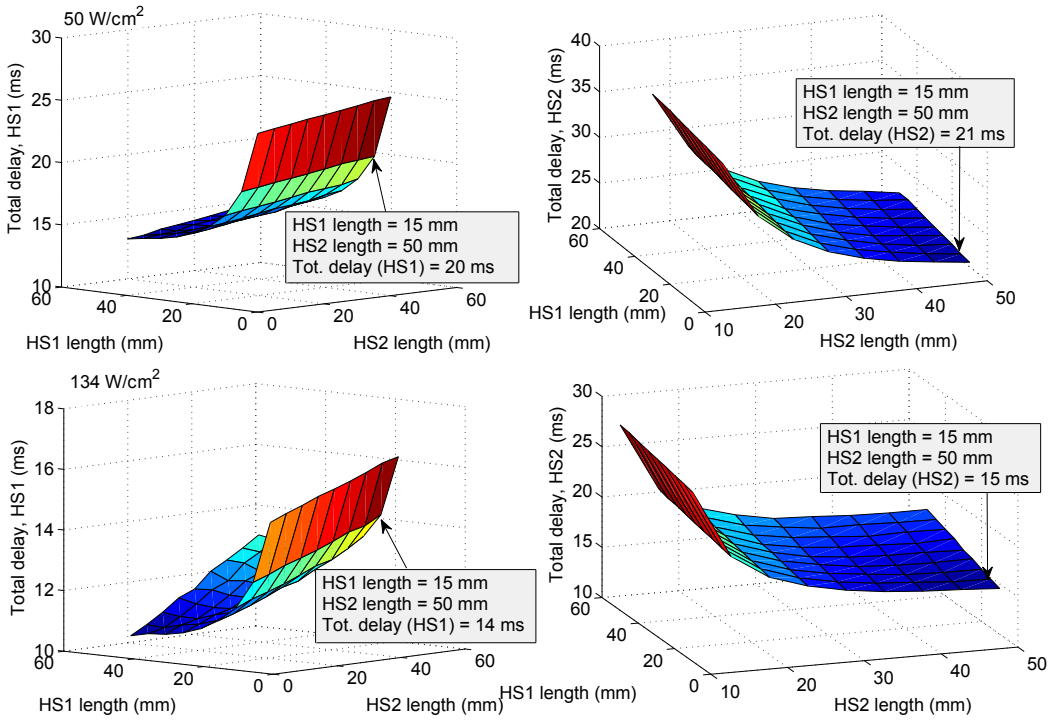

Figure 5.7: The total heater delay under each HS as a function of the HS lengths for peak powers of 50 W/cm^2 (upper row) and 134 W/cm^2 (lower row).

is not the maximum, i.e., the heater can be powered with lower than the maximum 400 V. One could hypothesize that it might be better to have a heater layout with 50-50 mm and larger period in case of 50 W/cm^2, even if this leads to longer quench propagation time, because this could accelerate the quench initiation at the highest field region (by about 4 ms). The tabulated delays show that the proposed layouts had very similar heater delays and total delays for both heating stations. This was obtained by having longer heating stations on the lower field HS than higher field HS. Future developments could be used to change the target function in the optimization, for example to prevent that 1 ms improvement at low field region does not happen at the prize of 5 ms slower quench at high-field region.

Of all optimized layouts, in HF heater the one with 134 W/cm^2 gave the shortest total delay and was chosen as the final design. In this case τ was 27 ms, I_{PH} was 87 A, and R_{strip} was 4.4 Ω, resulting to 28 heating station pairs. The HS1 was 15 mm long, HS2 was 50 mm long, and the period was 107.14 mm. The delay to quench the entire block was modeled to be about

Table 5.2: Results of the LF heater layout optimization at each power, with delay time for normal zone onset (Δt_{PH}) and transfer to normal state by propagation between the HS (Δt_{PH}^{tot}).

$P_{PH}(0)$ (W/cm^4)	HS length (mm) $HS1 - HS2$	Period (mm)	Δt_{PH} (ms) $HS1 - HS2$	Δt_{PH}^{tot} (ms) $HS1 - HS2$
50	40 – 50	125.00	19.9 – 20.3	26.0 – 25.7
75	35 – 40	107.14	17.0 – 17.7	22.1 – 22.4
100	35 – 40	107.14	15.0 – 15.6	20.2 – 20.4
125	30 – 35	100.00	14.2 – 14.7	19.2 – 19.3
150	25 – 30	107.14	13.9 – 14.2	19.8 – 19.7
175	20 – 20	100.00	14.1 – 15.2	19.8 – 20.1
200	15 – 20	115.38	15.0 – 14.4	22.2 – 21.2
225	15 – 15	136.36	14.3 – 15.5	23.0 – 24.2
250	15 – 15	187.50	13.7 – 14.9	26.1 – 27.2
275	10 – 10	200.00	16.6 – 18.5	30.2 – 32.1
301	10 – 10	428.57	16.0 – 17.8	45.9 – 47.7

15 ms. It is good that the optimum layout was very similar at lower powers in case the heater voltage had to be lowered from the 400 V for example due to powering unit limitation, or high-resistance connectors.

In LF heater the optimum layout was found with the power of 125 W/cm^2, having τ of 37 ms, I_{PH} of 73 A, and R_{strip} of 5.3 Ω. With HS1 of 30 mm, HS2 of 35 mm long, and period of 100.0 mm, in total 30 heating station pairs are accommodated. The delay to quench the entire block was 19 ms. It is clear that these delays are above the approximately 10 ms required by the analytical computation of the time margin.

This heater was fabricated and tested in the LHQ coil in a so-called mirror structure. The results are presented in Section 5.5.

5.4.2 QXF

The all stainless steel heater design for the 4 m long coil outer layer was presented in **Publication 3**. The magnet protection studies, using QLASA and ROXIE simulations with delays from the heater layout optimization, were performed by G. Manfreda [Man2014]. They showed that the hotspot temperatures were about 340-400 K, depending on the assumptions related to modeling material properties, quench detection threshold and presence of a dump resis-

tor. Because this was above the target of 350 K, improvement in the modeling, and development for the inner surface heaters were pursued. Confidence for re-considering the copper plating came from the reassuring statements that the copper in LHC dipoles had worked decently, and successful tests of 11 T dipole with copper plated heaters. The protection analysis using the addition of the new inner layer heaters, and considering the losses in the cables during the current decay was performed by V. Marinozzi in [Mar2015]. The simulated hotspot temperatures were below 350 K even in a failure scenario where half of the heaters were dysfunctional, giving confidence of the feasibility of the magnet protection.

In this section is first described the 4-m long outer layer all stainless steel design, and then the 6.8 m long inner layer copper plated design. Although not discussed here, 6.8 m long copper plated heaters were designed also for the coil outer layers. As discussed in Chapter 2.2.2, the QXF magnets will be fabricated in lengths of 4 m long and 6.8 m. This explains the two lengths considered for the heater designs.

Outer layer

The all-stainless steel heater for the 4 m long QXF outer layer was based on the 3-HS "stair-step" layout. Like in LHQ, the proposed heater configuration has 4 heater strips on each coil (2 per side of the metallic pole piece). The strip widths (w_{wide}) were based on the coil block dimensions: 25 mm for the high field heaters, and 32 mm for the low field heaters. Between the strips was foreseen a 3 mm wide gap located on the copper wedge. The heating station widths were 8.3 mm and 10.3 mm, respectively. Heater maximum voltage was 400 V and temperature 350 K. In the analysis 0.2 Ω margin was left for the connectors.

Figure 5.8 shows the cross-section of a coil half, with the magnetic field map and the approximate locations of the heating stations on the coil surface. The ranges of magnetic fields and current sharing temperatures under each narrow segment are detailed in table 5.3. For the design, the lowest field values were used. The normal zone propagation velocity was assumed to be 12 m/s in the high field block and 7 m/s in the low field block. In contrary to Algorithm 1 and the other heater designs, in this calculation the quench propagation time is computed for a point-like quench at the center of the heater covered segment which propagates the entire length of the period.

The optimization routine was run separately for the HF and LF strips, considering powers between 25 and 200 W/cm^2. The resulting delays for the

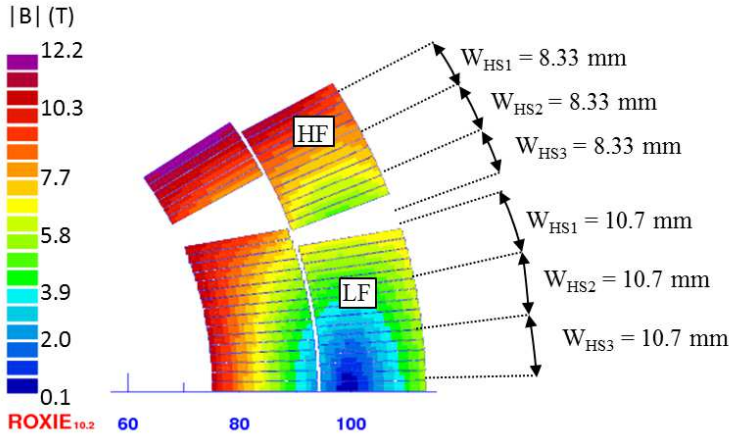

Figure 5.8: The cross-section of QXF coil half with magnetic field distribution at 17.3 kA. The high-field (HF) block and low-field (LF) block will each be covered with a quench heater. The approximate locations of the heating stations (HS) are shown for each block.

Table 5.3: Main parameters of the QXF heating segments: the range of the magnetic field, the associated current sharing temperatures, the heating station length resulting from the optimization, the first heater delay with the optimized heater, and the time delay to transfer normal state the whole turn.

Strip-HS	B (T)	T_{cs} (K)	L_{HS} (mm)	Δt_{PH} (ms)	Δt_{PH}^{tot} (ms)
HF-HS1	9.1-8.6	8.8-9.2	15	16-17	23-24
HF-HS2	8.4-7.6	9.4-9.9	20	16-19	23-26
HF-HS3	7.5-6.5	10.0-10.7	40	16-19	23-26
LF-HS1	7.0-6.4	10.3-10.8	25	22-25	33-36
LF-HS2	6.3-5.9	10.9-11.1	30	24-26	35-37
LF-HS3	5.9-5.7	11.1-11.3	35	25-26	36-37

Table 5.4: QXF heater strip periods and powering conditions.

Strip	L_{period} (mm)	I_{HP} (K)	R_{PH} (Ω)	P_{PH} (W/cm^2)	τ (ms)
HF	167	60	6.7	100	46
LF	160	67	6.0	75	62

optimum layouts at each power are shown in figure 5.9. Each point corresponds to the heater layout, which provided the minimum delay to quench the whole block. A minimum for the high field heater was found at 100 W/cm^2 and for the low field heater at 75 W/cm^2. At lower power the heater delay increased, and at higher power the heating segments needed to be shorter or further

apart, which increased the total delay time. However, within the power range of practical interest (50-150 W/cm^2) delays are impacted by only 1 to 3 ms. Tables 5.3 and 5.4 detail the optimized layouts together with the range of heater delays expected within the covered turns.

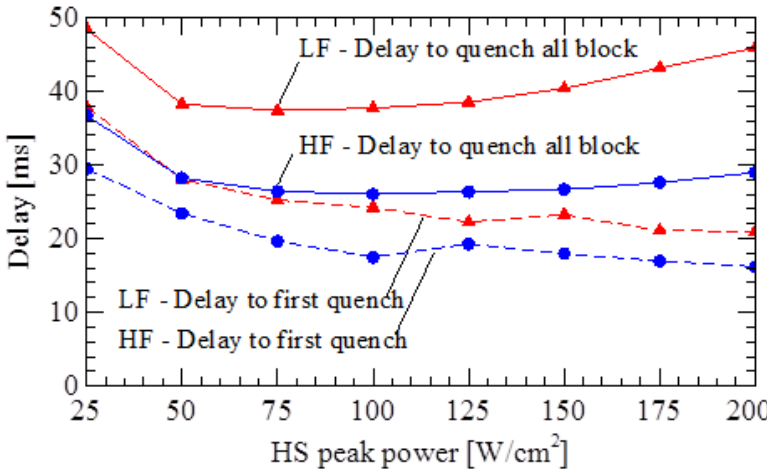

Figure 5.9: The delay in the QXF magnet high field (HF) and low field (LF) blocks, to start a normal zone and propagate the normal zone to the entire block. The peak voltage across the heater is 400 V in all cases. The delay to first quench is given for the optimized layout, corresponding to a given HS peak power, and does not represent the minimum individual delay that could have been achieved.

Inner layer

The QXF inner layer heater design concept was based on the snake design with 10 μm thick copper plating. The heating stations spacing was further adjusted for the cable twist pitch in order to heat different strands at each period. The aim was to interrupt the super-currents in all strands simultaneously thus leading to a faster quench propagation [Amb2015]. However, the impact of this could not be considered with CoHDA.

Strip dimensions and simulation parameters

Only one strip per coil half was used, due to smaller surface area and a requirement to leave at least 50% of the coil inner surface uncovered for cooling purposes. A special perforated polyimide insulation was foreseen to improve the cooling and reduce the formation of the bubbles between the heater and the coil [Amb2015]. The width of the coil inner surface is about 45 mm, therefore

a 22 mm wide heater strip was chosen. For strip resistance computation the resistivity of copper at 4.5 K was assumed to be 0.7 nΩm, and the resistivity of stainless steel was 0.5 $\mu\Omega$m.

The inner layer coil has two blocks with 5 and 17 turns. Between them is a wedge of about 5.6 mm. To leave the free coil surface around the mid-plane, the heater was placed as close as possible to the central pole piece. The pole turn could not be covered to leave space for the voltage taps, so the heater covered 4 turns (7.2 mm) in the inner wedge block. Therefore, on the outer wedge block the heater could cover 9.2 mm, i.e., 5 turns. A heating station width of 10 mm was chosen to focus the heating on the coil turns and not on the wedge. Heater's maximum voltage was 450 V, and in the simulations based on adiabatic computation the heater maximum temperature was allowed to be 350 K.

Figure 5.10 shows the magnetic field on the coil blocks. The field on the coil inner surface, i.e., location closest to the heater, is quite similar in all the turns, about 10-11 T at the nominal operation current. The optimization was performed with the same field under both heating stations, and 9 T, 10 T and 11 T were considered to evaluate the design sensitivity to the used field. The quench propagation velocity was conservatively assumed to be 10 m/s.

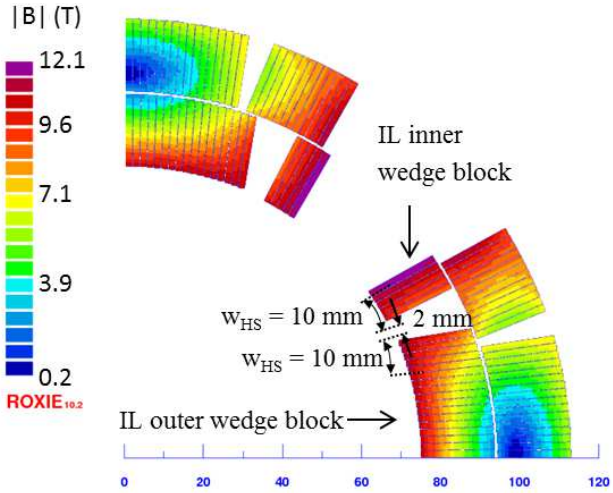

Figure 5.10: Magnetic flux density in the coil cross-section and the heater strip location.

Simulation results and heater layout

The heater delays were evaluated with power varying from 50 to 150 W/cm^2 in 10 W/cm^2 steps, and for coverage from 5 to 50 mm in 4.5 mm steps. As shown in figure 5.11, the delays decreased with increasing coverage, but saturated around 20-30 mm. In all cases, increasing the coverage further than 30 mm improved the delay less than 10%.

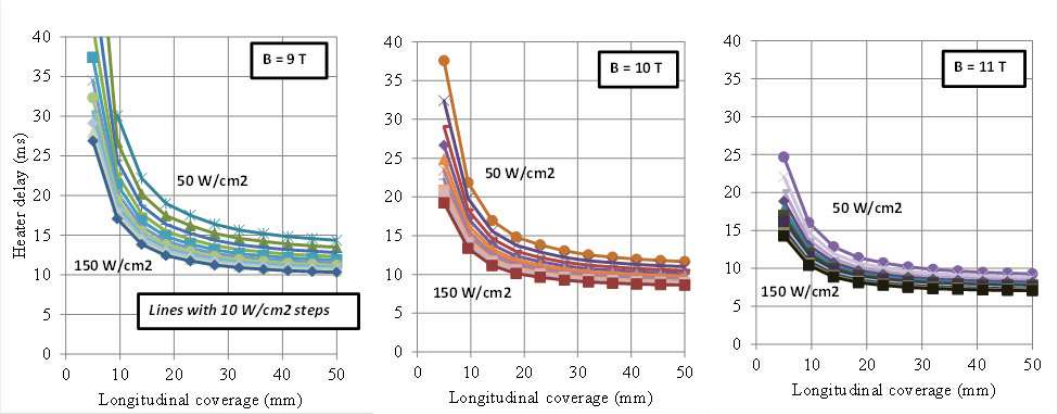

Figure 5.11: Simulated heater delay versus heater coverage at several heater peak powers (from 50 to 150 W/cm^2 in 10 W/cm^2 steps). The magnetic field in the conductor is 9 T (left), 10 T (center), or 11 T (right).

The resulting optimized heater layouts for each field are shown in table 5.5. The optimized layout for 10 and 9 T exhibited heating station lengths of 18.5 mm with a period of 100 mm. Accounting 0.2 Ω margin for the connectors, with 450 V the heater current was 90 A, giving the peak power of 150 W/cm^2. Although the power decay was limited to keep the adiabatic heater temperature below 350 K, the simulated heater temperature did not exceed 150 K.

Since the step of 4.5 mm was quite coarse, the optimization routine was repeated for heater power 150 W/cm^2 for coverages between 11 and 23 mm in less than 2 mm steps. Improvement of more than 0.1 ms in the total delay was not obtained. The design for 10 T was repeated using a 11 mm wide heating stations. The optimized HS lengths and period did not change and even if the heater resistance was lower (4.5 Ω), the optimal power was 150 W/cm^2 also in this case.

The lower field (9 T) was used for the final layout because it based on the most conservative assumption of T_{cs}. First, because the inner layer heater may have a reduced contact with the coil and in shorter heating station this has

Table 5.5: Results of heater geometry optimization. Design 1 (10 T) is the baseline, and Designs 2 (11 T) and 3 (9 T) explore the design sensitivity on the magnetic field choice.

Field for design	10 T	11 T	9 T	9 T (Final)
Heater peak power (W/cm2)	150	150	150	127
RC time constant (ms)	31	31	31	36
Required capacitance (mF)	6.2	6.2	6.2	6.4
Length of HS (mm)	18.5	14.0	18.5	18.32
Period (mm)	100.0	75.6	100.0	91
Heater resistance (Ω)	5.0	5.0	5.0	5.6
Heater current (A)	90	90	90	80
Heater delay (ms)	10.1	8.9	12.4	13
Total delay (ms)	14.2	11.9	16.5	17

more impact. And second, because the modeling of short heating stations has more uncertainty since the delay vs. coverage curve is steeper in this region.

The design was further adjusted to the cable twist pitch (109 mm). The closest patterns of HS length and period combination were: A) 18.2 mm for the station length and 127.2 mm for period, or B) 18.32 mm HS length and 91 mm period. The power with Option A (with the maximum voltage) would exceed the maximum allowed (245 vs 150 W/cm^2), thus option B was chosen. The heater delay with this layout for 9 T was 13 ms, and the quench propagation time between heating stations was 4 ms. This design is going to be tested in a SQXF coil in 2015. Figure 5.12 displays a photo of this heater impregnated on the coil inner surface.

5.5 Test results with new LHQ heater design

The optimized heater layout was tested in an individual LHQ coil in a mirror structure. A description of the mirror structure for HQ coils can be found from [Bos2012]. The outer layer trace had on its other side the new design, and on the other side was a LQ-style design for comparison. The inner layer trace did not have a heater, but only the voltage taps. Figure 5.13 shows a CAD-drawings of the traces, a zoom-in to the heater features, and a photo of the coil surface. Both heater strips of the pulse-wave design were connected together at the coil ends. The reason was that the grooves in the coil end-shoes were already designed for only one connection and the coil fabrication schedule did not allow the re-design of the end-parts. This is not expected to

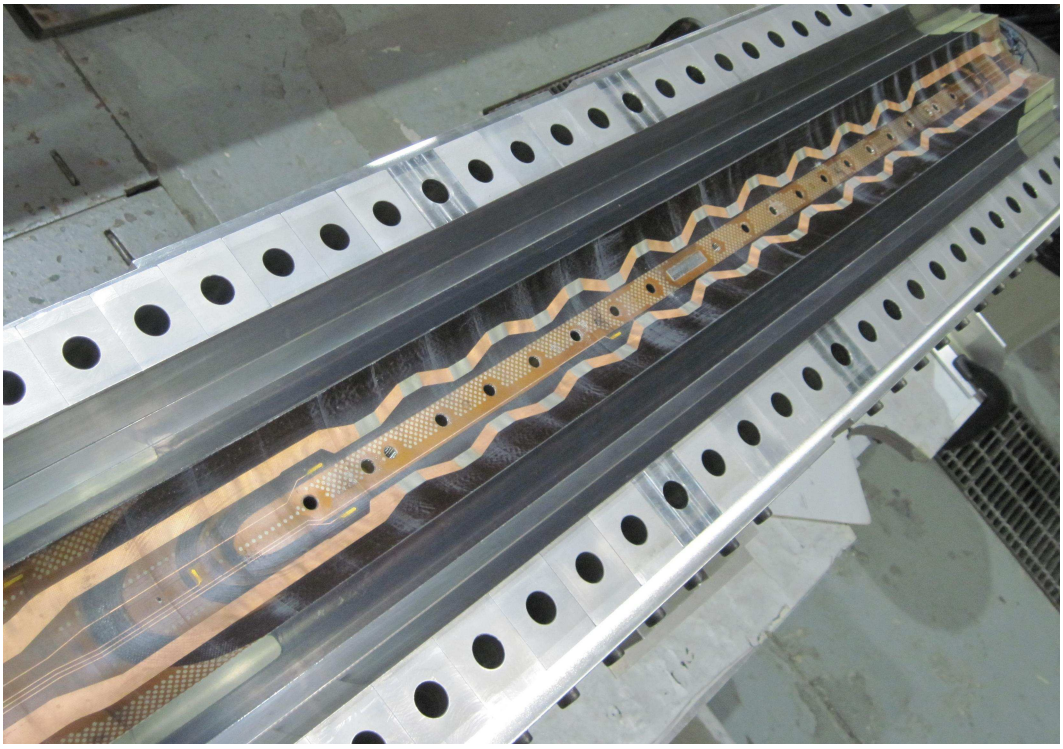

Figure 5.12: Photo of the SQXF coil inner layer with the impregnated snake heater.

impact the heater peak power since the voltage will be the same across both strips, although the optimal time constants (capacitance values) could not be selected. A more significant disadvantage was that this way the strips could not be tested individually, and the advantage of added redundancy was lost.

5.5.1 Comparison of measured and calculated resistances

The heater resistances were measured, and the results were compared with computations. The final implemented heater had 26 HS pairs for the HF strip and 29 for the LF strip. The measured resistance of the parallel connected strips at 4.5 K was 3.124 Ω. Computation assuming a stainless steel resistivity of 0.5 $\mu\Omega$m suggested 2.6 Ω, i.e., 17% less. The resistance of the LQ-style heater was computed to be 3.7 Ω, being within 23% of the measured 4.8 Ω. Partial explanation for the difference are the uncertainty in the literature value of resistivity, a non-uniform thickness of the stainless steel, the connecting wires from the heaters to the outside of the magnet and cryostat, and the resistance

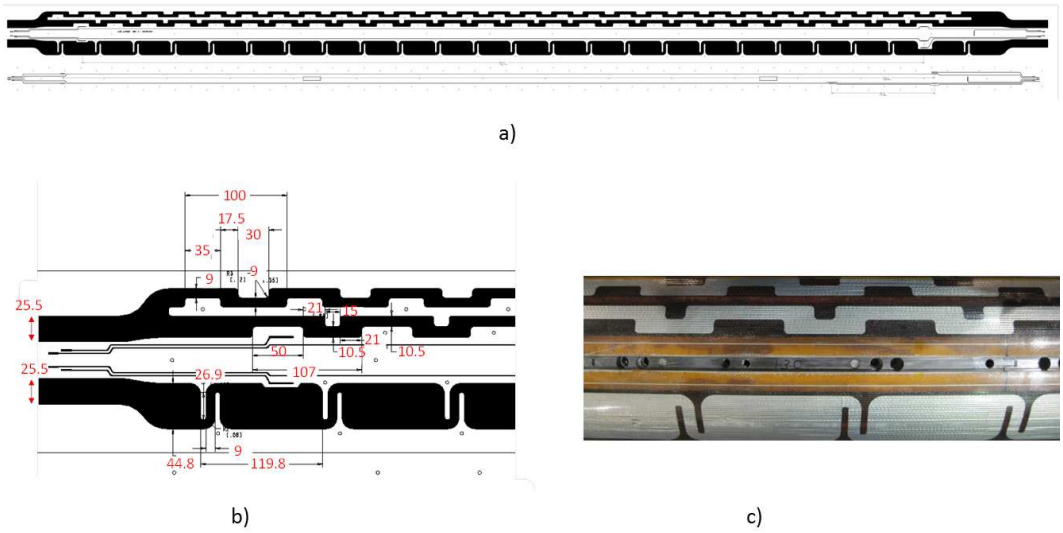

Figure 5.13: a) Trace design for LHQ including two heaters b) zoom-in with the most important dimensions marked (in mm), and c) a photo of the coil surface after impregnation. The heater above is the new design, and the heater below and LQ-style heater.

computation method [1].

To evaluate the error made by the computation method, an FE-model was built with COMSOL Multiphysics to simulate the geometry of one heater period of each heater design. The dimensions were based on the CAD-drawing shown in figure 5.13 b). A potential difference of 1 V was applied across the period (boundaries 1 and 2 in figure 5.14 a)), and all the other boundaries were electrically insulated ($\partial V/\partial n = 0$). The Laplace equation

$$\nabla \frac{1}{\rho_{ss}} \nabla V = 0, \tag{5.5}$$

was solved in the modeling domain. The resistance was computed from the line integral of current density at the boundary 2,

$$R_{period} = \frac{V_0}{d_{ss} \int_{bound2} \frac{1}{\rho_{ss}} \frac{\partial V}{\partial n} \mathrm{d}l}, \tag{5.6}$$

where V_0 is 1 V, ρ_{ss} is 0.5 $\mu\Omega$m, and d_{ss} is 25.4 μm. The line integration is over the boundary 2, n being a unit vector in its normal direction.

For the pulse-wave heater the resulting resistances were 0.18 Ω per period of HF-heater and 0.20 Ω per period of LF-heater. Using these values the

[1] Formula $R = \rho l/A$ was used though l and A were not well defined for these heaters.

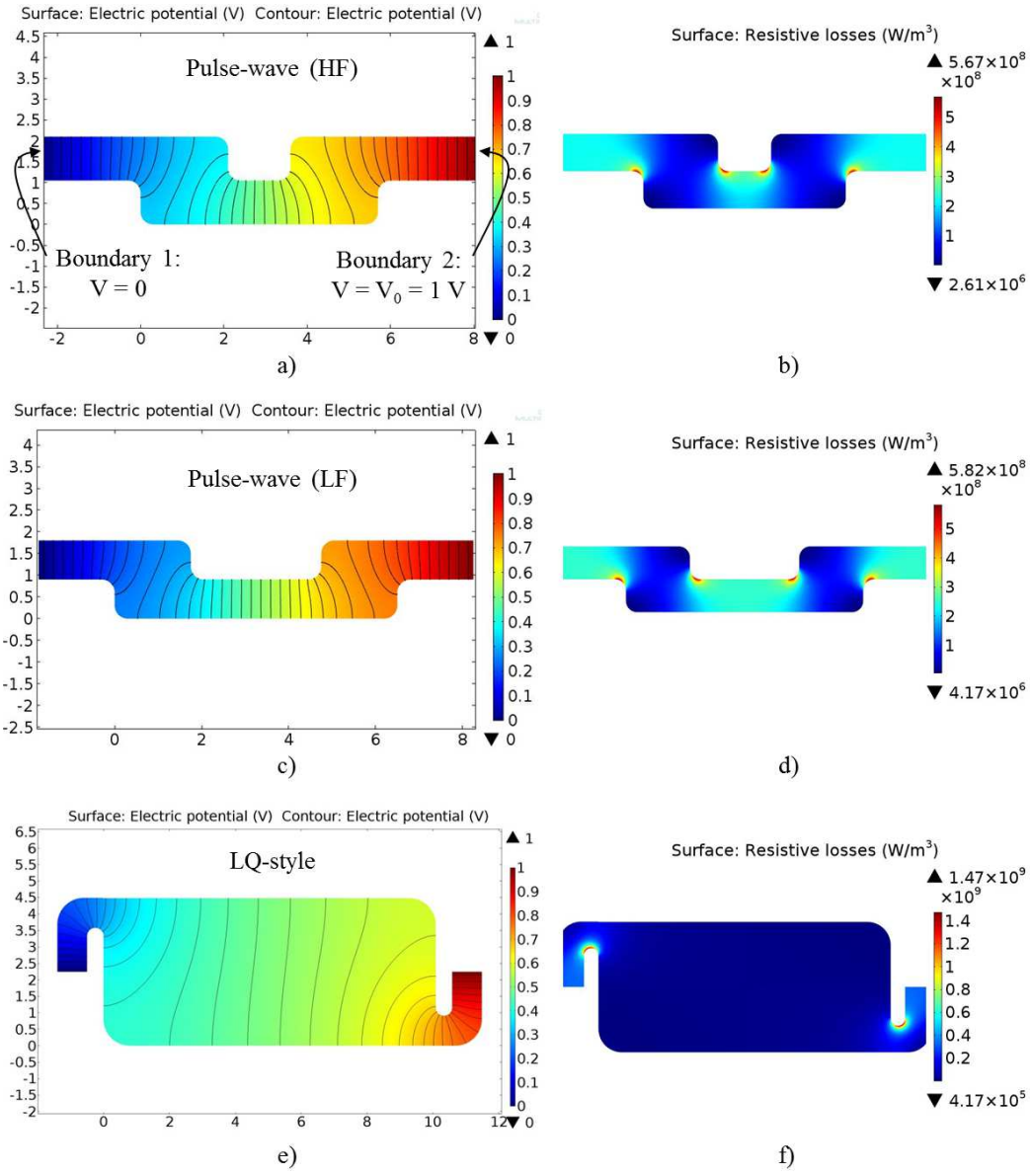

Figure 5.14: COMSOL models of the LHQ heaters. On the left are shown the electric potential build-up when 1 V potential difference was applied across an heater period. On the right are shown the distributions of the corresponding volumetric resistive losses.

computed resistance of the entire heater (with the two strips in parallel + connections) was closer to the measured value, differing only by 10% or 0.3 Ω.

For the LQ-style heater, the resistance per period from COMSOL was

0.17 Ω, leading to total computed resistance of 4.4 Ω, which is within 0.5 Ω or 11% of the measurement. This shows the advantage of using a FEM analysis for an accurate resistance calculation when designing heaters with complex heating station shapes.

Figure 5.14 shows the electric potential for each heater geometry, and also the distribution of resistive losses. It shows that the losses are not uniform in short heating stations, and that hotspots develop near the corners of the heaters. This highlights the importance of using a sufficiently large radius for rounding the corners.

Finally, both heater designs were connected to individual HFUs. The cold resistance measurement of the LQ-style heater circuit (HFU1) was 5.22 Ω and the pulse-wave heater (HFU2) was 3.45 Ω. This measurement included the wires in the HFU circuit. Therefore, with 400 V the computed power for pulse-style heater was 72 W/cm^2 in HF heater and 67 W/cm^2 in LF heater. This is a significant decrease from the designed 134 and 125 W/cm^2. This shows that in addition of the more accurate FEM resistance calculation, more resistance margin must be left in the heater designs in future magnets.

5.5.2 Measured and simulated delays

Figure 5.15 shows the measured delays for both heaters as a function of magnet current. Both heaters were used with the same power (approximately 70 W/cm^2), so the pulse-wave design (B02) was powered with 400 V and the LQ-style (B01) with 280 V. The time constant was 25 ms for the LQ-style and 17 ms for the new style. The delays were similar at currents of 9 kA and higher, but at 6 kA the new design was considerably more effective. The LQ-style did not cause a quench at lower current when powering voltage as 280 V. A measurement was repeated at 5 kA using 101 W/cm^2 in the LQ-style and 50 W/cm^2 for the pulse-wave style. In these conditions both heaters were equally effective.

Simulations of the heaters in these conditions were performed in order to find the first delays for both heater layouts that could be compared with measurements. The results are shown in figure 5.16. The simulated delays for the pulse-wave heater simulation agreed very well with the measurement, except at 14.6 kA, where the measured delay was shorter. Simulation of the LQ-style heater gave systematically longer delays than measured – similarly than the LQ heater simulation in Chapter 4.3. This can be due to the uncertainty in modeling short heating stations, or to a hotter spot in the heating station due to its shape, which was neglected in the simulations due to the assumption

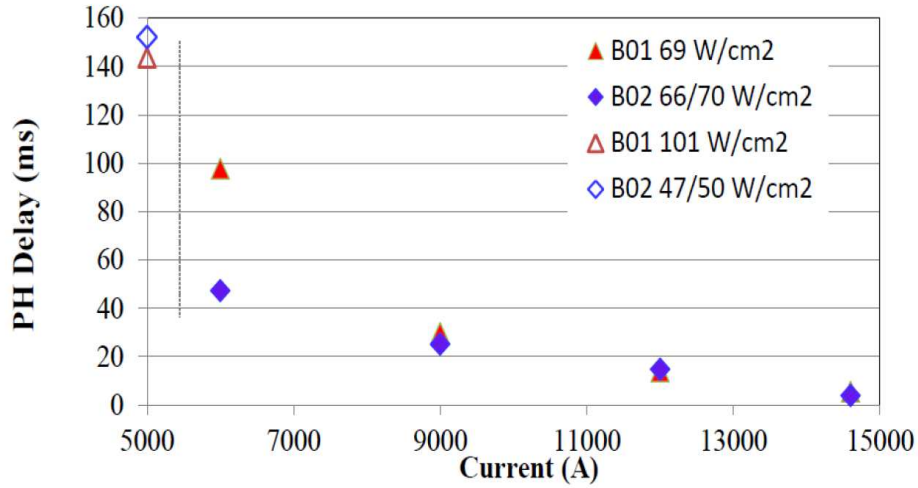

Figure 5.15: LHQ heater delay time dependence on magnet current for the traditional LQ-style heater design (B01) and for the optimized pulse-wave heater design (B02).

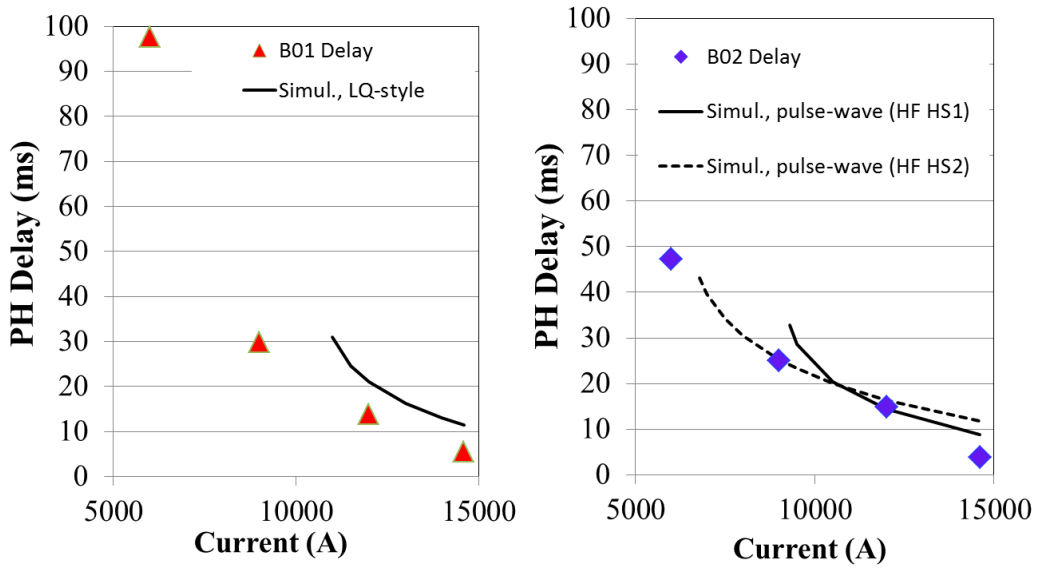

Figure 5.16: Measured heater delays in LHQ compared with simulations for a) LQ-style heater and b) pulse-wave heater design. Both heating stations of the pulse-wave HF heater strip were simulated.

of uniform power density. The impact of the wide part was accounted in the simulations.

5.5.3 Current decay for the different heater geometries

A special test was done in order to measure if the pulse-wave heater, which was designed to minimize the delay to quench the entire coil, led to a faster current decay than the traditional design. The magnet was ramped up to a constant current, the dump resistor was effectively disconnected (by adding 1000 ms delay time to the switch), and one of the heaters was activated manually. The other heater was not used. The goal was to measure the MIITs related to the current decay induced by only one heater. The test was repeated for both heater strips. The amount of MIITs could not be predicted at high current, therefore the target current was first 30% of SSL. The current was increased gradually in order to ensure a controlled quench load increase and avoid damaging the coil.

Figure 5.17 shows the measured MIITs after protection with each heater. When the heater power was about 72 W/cm^2, the pulse-wave heater protection lead to about 1 MIIT lower quench load (approximately 25-30 K) than the traditional design. However, if the LQ-style was powered with its full potential (400 V leading to 154 W/cm^2), the MIITs were similar. Unfortunately the constructed new heater design did not allow its use at full potential due to the larger resistance of the heater circuit than estimated.

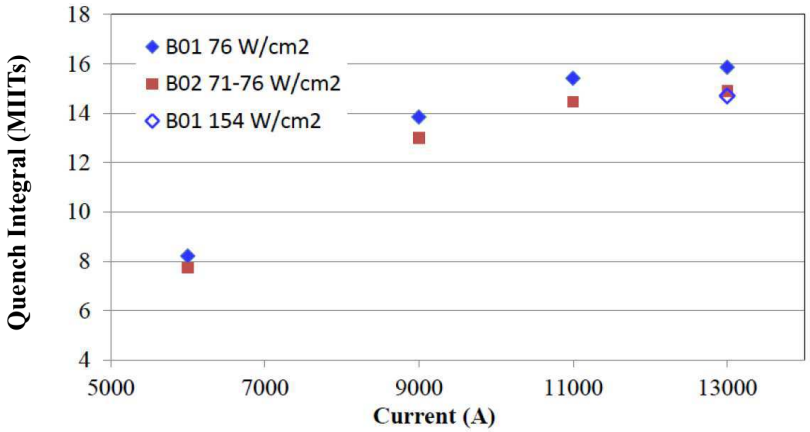

Figure 5.17: LHQ quench load after inducing a current decay with the different heater designs. Square markers refer to the pulse-wave design (B02) and diamonds to the traditional LQ-style design (B01).

5.6 Concluding remarks

In this chapter the needed improvements in the protection heaters efficiency in long high-field magnets LHQ and QXF were discussed. Analytical and numerical analyses suggested that the heater delays should be within 5-20 ms to quench the entire coil, which did not seem to be reachable using the existing heater technology as such. After analyzing the heater design parameter space, the performance optimization came down to the layout design. An algorithm was presented to design layouts that minimize the delay to quench the coils. The idea was to optimize the heating station length depending on coil field region so that the lower field region is heated more. The heater delay versus HS length and power were simulated using CoHDA and the rest was calculated based on the assumptions.

The routine was first applied to optimize the protection using only stainless steel heaters on coil outer layer. At nominal operation current the simulated delay after heater activation to quench the entire outer layer was about 20 ms in LHQ and 37 ms in QXF. The first quenches by heaters were below 11 ms in LHQ and about 16 ms in QXF. Based on simulations this did not provide a reliable enough protection, therefore heaters for the QXF coil inner layer were designed too, using copper plating to reduce the overall resistance.

The LHQ heater was tested in single coil in a mirror structure. This test showed that the heater managed to protect the magnet at least as well as the LQ-style heater that was used for comparison. However, the full potential of the new heater could not be tested, because the final heater resistance was higher than in the analysis. In the future heater design studies therefore the heater resistance should be verified with FEM-calculation in case of complex shape heating stations, and at least 0.5-1 Ω margin must be left for the connections to the power-supply. The test result comparison with simulation gave confidence in modeling longer heating stations, but highlighted the uncertainty in modeling short heating stations with complex shape and non-uniform power dissipation. Future studies should also investigate protection at low current, and add sufficient margin in the design as discussed in previous chapter.

Chapter 6

Simulation of protection heaters in an HTS coil

Chapter 5 discussed the protection of the LTS magnets for the High-Luminosity LHC. In this chapter the focus is shifted to the HTS magnets, which are being considered for the next upgrade, High-Energy LHC [FCC2015]. Their protection is going to be more difficult than LTS magnets due to at least two times larger temperature margin, and ten times slower quench propagation.

Two computational studies were performed to predict how LTS-type protection heaters would work when applied to an YBCO coil. Study 1 examined the general behavior of the delay as a function of the most important parameters, and compared it with the experience from LTS magnets. This was presented in **Publication 6**. Study 2 extended the analysis to compute the quench propagation between heating stations. This study was presented at the WAMHTS-2 workshop in Kyoto 2014 [WAMHTS2014]. The results demonstrate that large heater energies are mandatory. Even though large-energy resistive heaters are not an attractive solution, two new heater concepts are proposed which can potentially provide the required large energies.

6.1 Reference YBCO coil

A race-track type YBCO coil was considered. The parameters were based on the Feather-M2 (FM2) and Feather-M0 (FM0) magnets which are being designed within the EuCARD-2 project work package 10 ”Future magnets” [Ros2015]. The FM2 coil is a so-called aligned block design, in which the cable wide side is oriented almost parallel to the field lines, thus optimizing

the cable's local critical current densities. The magnet can be used as a stand-alone with iron yoke producing a 5 T dipole field in the bore. It can be also used as an insert in 13 T background field inside the CERN Fresca 2 [Fer2013] dipole. In this case it provides 16.9 T in the bore (at 70% of SSL). FM0 is a smaller version, which is used to study the coil assembly procedure and quench protection. Figure 6.1 shows the magnetic field lines alignment with the coil blocks, and 3-D schematics of FM2 and FM0. [Kir2014, Van2015]

The cable that was considered for the heater simulations is slightly different in the two studies because the cable design proceeded after Study 1 was done. Parameters for both cables are summarized in table 6.1.

In Study 1, the cable was simpler. It consisted of four 12 mm wide YBCO tapes stacked together and insulated with 30 μm Kapton, see figure 6.2 for a 3-D representation.

In Study 2 was considered the Roebel cable designed for the FM0 magnet [Kir2014]. The cable geometry was modeled in 2-D as a stacked tape cable conserving the cable area and material fractions, see figure 6.3.

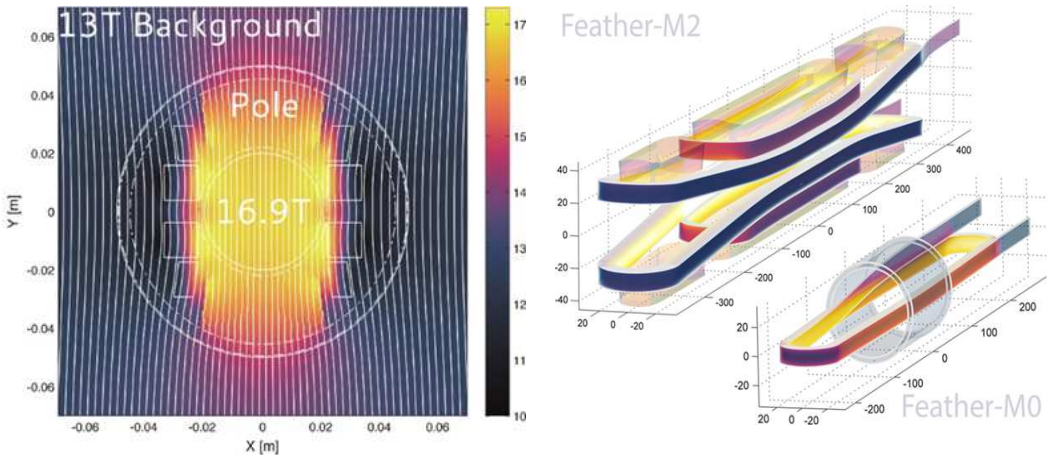

Figure 6.1: a) Magnetic field in Feather-M2 in a 13 T external field of FRESCA 2. b) Feather-M2 and sub-scale Feather-M0.[Kir2014]

6.2 Developments in the simulation model

The CoHDA simulation tool was improved to adapt it to simulations of heaters in HTS coils. The improvements included the quench onset criterion for the

Table 6.1: Cable parameters. In Study 2 the fifteen 5.5 mm wide tapes of the Roebel cable were modeled as if 7.5 tapes with 11.4 mm width were stacked together. The cable insulation at top and bottom were considered separately. In Study 1 the cable insulation on the sides was neglected. In Study 2, they were embedded in the cable properties.

Parameter (unit)	Study 1	Study 2
Cable width (bare) (mm)	12.00	11.39
Number of tapes	4	7.5
Cable thickness (bare) (mm)	0.376	0.75
Insulation thickness (mm)	0.030	0.03
Cable area (mm^2)	4.51	12.04
Cu-%	50	32
Cable Hastelloy-%	50	39
Inter-layer insulation (mm)	0.1 (Kapton)	0.3 (G10)
Ground insulation (mm)	0.04 (Kapton)	0.3 (G10)

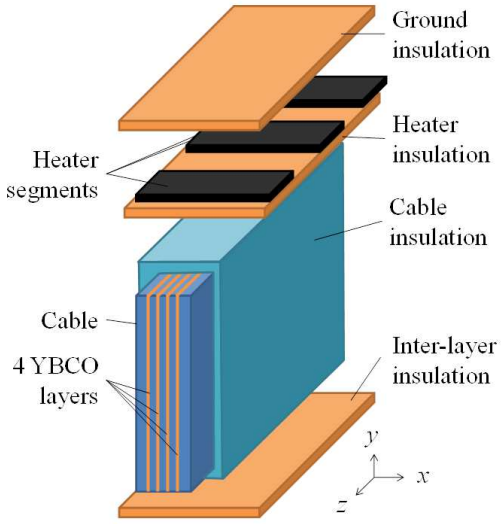

Figure 6.2: Schematic view of the YBCO cable and the heater with periodic heating segments (not in scale).

heater delay, and quench propagation computation. Hastelloy properties were added to the CoHDA material property library, based on [Lu2008].

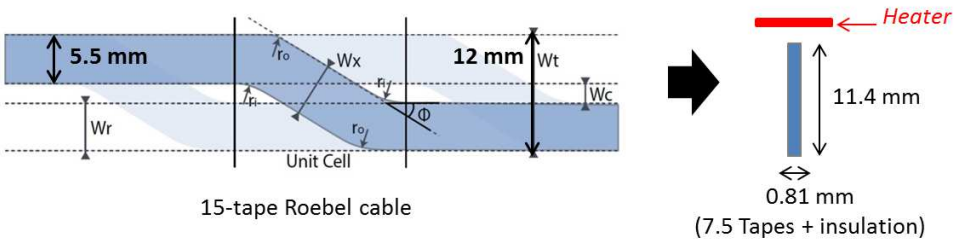

Figure 6.3: Roebel cable modeled as a stacked tape cable. Cable image from [Kir2014].

6.2.1 Heater delay definition

In the LTS magnets the heater induced quench onset was defined as the moment when the cable maximum temperature reached T_{cs}. This criterion was improved by accounting the current redistribution within the non-uniformly heated HTS tape. This means that when the warmer parts of the cable (closer to the heater) reach T_{cs}, these parts will continue carrying the J_c related to its temperature, and the excess current diffuses into the cooler parts of the cable. The heater delay was computed to the moment when J_c was reached at each location. It was assumed that after this part of the current diffuses into the copper stabilizer and a resistive signal can be measured. In **Publication 5** a similar criterion was applied to Nb_3Sn magnets, and it managed to give an upper limit enclosing over 90% of the measured data.

6.2.2 Quench propagation

As I_c is reached in the cable cross-section, the difference between I_{mag} and I_c diffuses into the copper and generates a resistive loss. Until I_c is zero, losses are generated also in the superconductor. This is the so-called current sharing regime. Typically, the current sharing regime, defined also by the difference between T_{cs} and T_c, is larger in HTS materials than in LTS.

The volumetric average heat generation during both phases is computed using

$$f_{gen}(T,B) = \frac{I_{mag}E_z}{A_{cable}} = \frac{I_{mag}I_{Cu}\rho_{Cu}(B,T)\lambda_{Cu}}{A_{Cu}^2}, \tag{6.1}$$

where I_{mag} is the magnet current, E_z is the local electric field in the direction of current flow and I_{Cu} is the current flowing in copper. A_{cable} and A_{Cu} are the areas of the cable and copper cross-section, respectively. This heat generation is used in the heat balance equation (3.1) the same way than the heat generation in the heater. The computation is done at each time-step for cable cross-section

at the N_z discrete locations on the z direction as described in Chapter 3.1.3. In our analysis I_{mag} was constant during the entire analysis, but it could be considered to be also time dependent to simulate the magnet current decay during the quench process.

6.3 Study 1: Parametric studies of heater delay

The aim of this analysis was to get the first idea of the heater delays that could be expected in an YBCO coil, if it was protected with the existing state-of-the-art protection heaters used in the protection of high-field Nb_3Sn magnets.

6.3.1 Parameters

The reference parameters were based on the high-field location of the coil, and the typical heater parameters in LTS coils. The impact of operation point and the most important heater design parameters were studied through a parametric analysis, where each parameter was varied individually as the others were kept constant at their reference values. Table 6.2 lists the reference values and the ranges of variation.

Table 6.2: Parameters' reference values and their range of variation in the parametric analysis of heater delays. The current sharing temperature is based on the magnetic field.

Parameter (unit)	Reference	Variation range
Magnetic field (T)	20	6.5 - 50
Current sharing temperature (K)	16.5	4.9 - 26.6
Heater peak power (W/cm^2)	50	20 - 200
Heater time constant (ms)	50	N/A
Heater insulation (mm)	0.05	0.001 - 0.15
Heater coverage (mm)	100%	10-100 (period 120)
Heater thickness (mm)	0.025	0.025 or 0.050

The reference operation point was 4.5 K, 5 kA and parallel field of 20 T. The impact of the operation point was studied by varying the magnetic field from 6.5 to 50 T, which allowed exploring T_{cs} range from 4.9 to 26.6 K. The same variation could have been obtained by changing also the operation current or the field angle. The used source of copper thermal properties [CRYOCOMP] had data only up to 30 T. Therefore, in the simulations with higher field the thermal properties are computed using 30 T.

The new criterion to quench onset is called delay to current sharing (cs). For comparison is presented also the delay that would be obtained by using the "default criterion" that was used for LTS magnets, i.e., delay to current redistribution (cr).

6.3.2 Delay time dependence on current sharing temperature

Figure 6.4 shows the simulated delay as a function of the current sharing temperature. Two regimes can be distinguished: A nearly linear increase of delay as T_{cs} increases from about 6 K to 15 K, and an exponential increase of delays for higher T_{cs}. After about 100 ms simulation time, when the cable temperature was about 21.5 K, the cable started to cool down. Simulations for T_{cs} higher than 21.5 K therefore never led to a quench. This limit corresponds to B = 12 T. In our reference case (T_{cs} = 16.5 K) the delay was 25 ms to current redistribution and 34 ms to the current sharing. The duration of the current redistribution phase was 5-20 ms (15-65%) in all cases with T_{cs} above 10 K.

The limit of heater efficiency at high T_{cs} was analyzed by comparing the energy provided by the protection heater and the cable energy margin to quench. To perform the analysis per coil's surface area, the energy margin of the cable was scaled with the tape width:

$$E_{margin} = w_{tape} \int_{T_{op}}^{T_{cs}} \gamma c_p \mathrm{d}T, \tag{6.2}$$

where w_{tape} is the non-insulated tape width, c_p its the specific heat capacity, and γ the mass density. The energy of the protection heater per area was computed using:

$$E_{PH} = \int_0^{\infty} P_{PH}(t)\mathrm{d}t = P_{PH}(0) \times \frac{\tau_{RC}}{2}. \tag{6.3}$$

In this case E_{PH} was 12500 J/m^2, equal to E_{margin} when T_{cs} was 25.9 K. To confirm this limit, the simulation was repeated with adiabatic boundary conditions also at top and bottom of the simulation domain (see Chapter 3.1.2). When the heat flow away from the system was prevented, the delay time was proportional to the energy margin, and cable quenched for T_{cs} = 25 K, but not for T_{cs} = 26 K (right side in figure 6.4). At T_{cs} 16.5 K, or lower, the difference between adiabatic and non-adiabatic simulations was less than 2 ms.

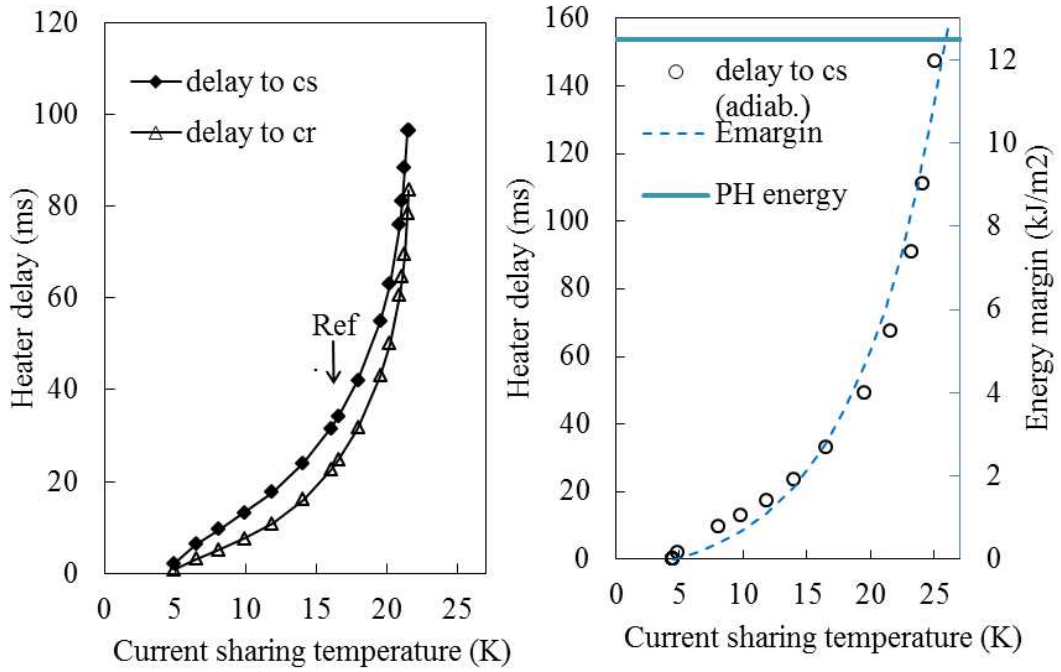

Figure 6.4: Simulated heater delay vs. current sharing temperature. The magnet operates at 4.5 K and 5 kA and the magnetic field is varied from 50 T (T_{cs} = 4.9 K) to 6.5 T (T_{cs} = 26.6 K). The left side figure shows the simulation with regular boundary conditions. The right side shows the simulation with adiabatic boundary conditions at all boundaries and cable the energy margin (on the right axis) as well as the total energy provided by the heater.

To protect coils operating with higher T_{cs} and larger E_{margin}, the heater energy must be increased. This can be obtained either by increasing the peak power or the time constant, or by increasing the heater volume by using a thicker stainless steel (and at the same time the total energy to be dissipated in the heaters). Note, that the T_{cs} limits cited here are specific to operation at 4.5 K. At higher operation temperatures smaller temperature margins may lead to larger energy margins because of the increase in the volumetric specific heat of the cable.

6.3.3 Delay time dependence on heater power

The heater delay dependence on heater peak power is shown in figure 6.5. Consistently with LTS magnets, the delays increased strongly when the heater power was reduced below 50 W/cm^2 [Fel2009a]. The delay decreased by 50%

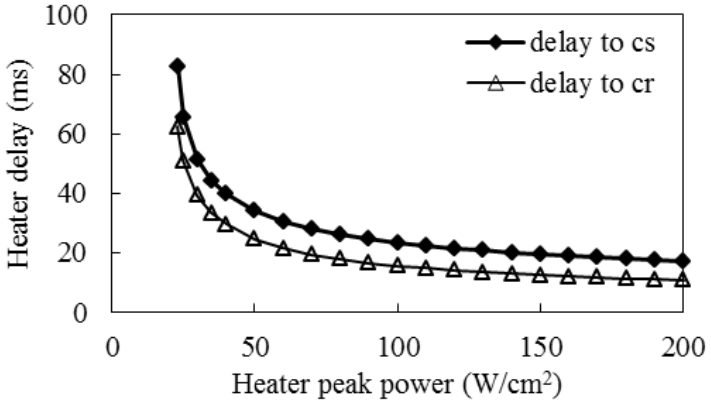

Figure 6.5: Simulated heater delay vs. heater peak power. The heater was powered with a voltage pulse decaying exponentially with τ = 50 ms.

when the heater power was increased to 200 W/cm^2.

For the 200 W/cm^2 peak power, with τ of 50 ms, E_{PH} corresponded to E_{margin} for T_{cs} of 37 K. However, the temperature of the heater becomes a concern with such a high power. The heater temperature, computed adiabatically from stainless steel heat capacity, predicts temperatures above 350 K. However, this limit may be overly conservative for thin heaters because the simulated heater temperature was below 200 K. This suggests that a large fraction of the heater energy is diffused away from the heater.

6.3.4 Delay time dependence on heater thickness

One way to increase the heater temperature as well as energy would be to use a thicker stainless steel strip, with the same volumetric energy. The advantage of a thicker strip compared to simply increasing the peak power is that the energy increase is obtained by increasing the heater current and not the voltage which is limited by the insulation threshold. However, a larger capacitance is needed for the powering.

To study a thicker heater, the simulation with 100 W/cm^2 was repeated with two times thicker stainless steel heater (50.8 μm). The volumetric power density was the same than in the reference case with 50 W/cm^2 (19.7 W/mm^3). The simulated delays were about 20% shorter with the thicker stainless steel (20 ms to current redistribution and 28 ms to current sharing). The heater temperature was 30% larger (130 K). Similar result was obtained when applying adiabatic boundary condition directly on top of the heater component.

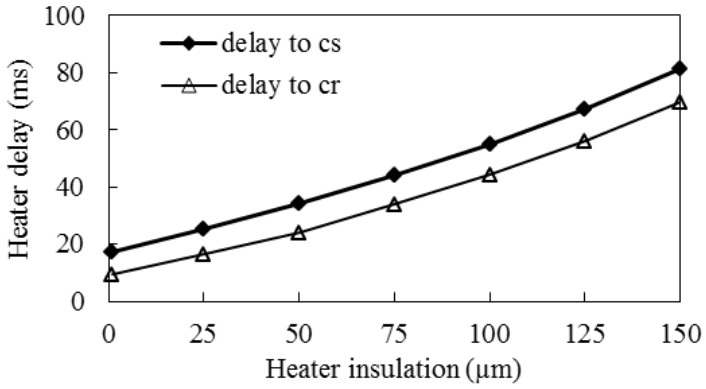

Figure 6.6: Simulated heater delay vs. heater insulation.

6.3.5 Delay time dependence on heater insulation thickness

Figure 6.6 presents the heater delay as a function of heater Kapton insulation thickness. Consistently with the studies of Nb_3Sn magnets (see **Publication 2**), the delay increased faster than linearly when increasing the insulation thickness. In this case each additional 25.0 μm Kapton layer on top of the nominal 50.0 μm thick insulation increased the delay by about 10 to 15 ms (20-40%). The increase was larger with larger total insulation thickness.

6.3.6 Delay time dependence on heater geometry

The simulated delay as a function of heater longitudinal coverage is shown in figure 6.7. The results suggested that the coverage should be at least 40 or 50 mm to be within 10% from the reference 1-D cases. This is in the same range than the low field regions in Nb_3Sn magnets (see Chapter 5 and **Publication 3**).

6.4 Study 2: Quench propagation between heating stations

The Study 1 suggested that the energy of the heaters must be increased in the HTS magnets to be able to quench the cables also in the regions of lower field and at lower operation current. Therefore, in the Study 2 was considered a heater with four times more energy than typical LTS heaters have.

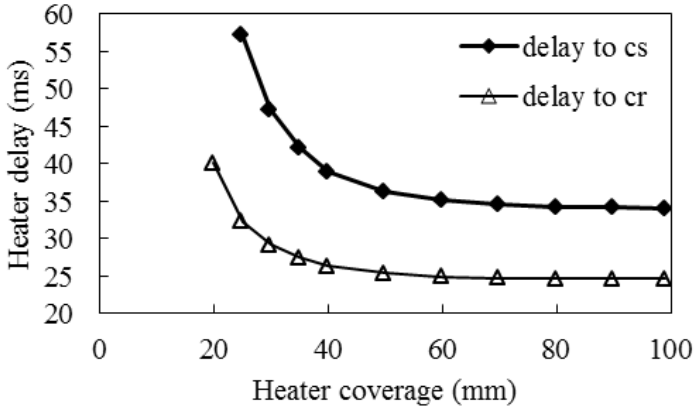

Figure 6.7: Simulated heater delay vs. heater coverage. The period is 120 mm.

In this study the heater thickness was 50 μm, and peak power 200 W/cm^2 (40 W/mm^3). With a time constant of 50 ms, the heater energy was 50 kJ/m^2.

Four operation points were considered. They are listed in table 6.3. Note the strong increase of energy margin between cases B and C. Even if the temperature margin was the smallest in case D, it had the highest energy margin because of the higher operation temperature. It was clear that the heater will not cause a quench, so it was not included into the further analysis. The heater delay criterion was the delay to current sharing, which was the more conservative one used in Study 1.

Table 6.3: Parameters reference values and their range of variation in the parametric analysis of heater delays.

Case	A	B	C	D
Operation temperature (K)	4.5	4.5	4.5	35
Magnet current (kA)	6	10	6	6
Magnetic field (T)	15	10	10	1.5
Field angle to tape width (°)	5	5	5	5
Current sharing temperature (K)	22.3	22.7	28.8	52.5
Temperature margin (K)	17.8	18.2	24.3	17.5
Energy margin (kJ/m^2)	8.1	8.6	18.6	92.4

6.4.1 Needed heater coverage

Figure 6.8 shows the heater delay to quench versus the longitudinal heater coverage. The needed coverages in cases A, B and C were respectively 50, 60,

and 80 mm in order to get delays within 10% when compared to the 1-D case. The delays were about 54 ms in cases A and B, and 113 ms in case C. Note, that the needed coverages and delays are slightly higher than in the previous analysis because of the larger energy margins.

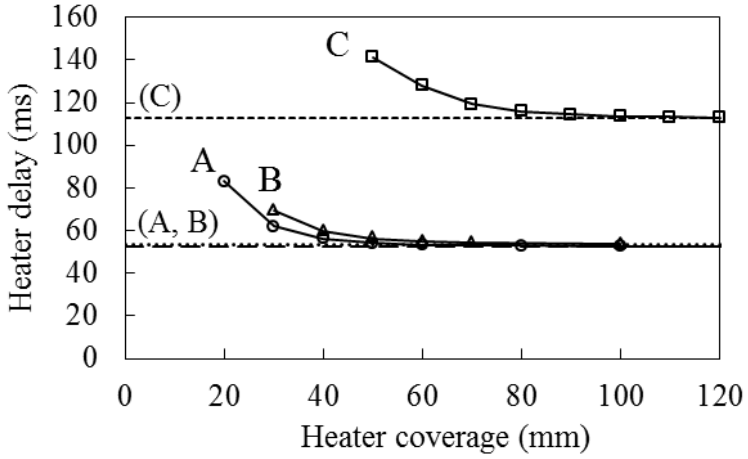

Figure 6.8: Simulated heater delay vs. heater coverage at three operation points. The straight, dashed lines represent the 1-D simulations.

6.4.2 Time to quench between heating stations

The normal zone propagation was computed in each of the cases. The propagation velocity (NZPV) was the highest in case B, 0.8 m/s, probably because of the highest current. In case A it was 0.5 m/s, and in case C 0.3 m/s. These values are of the same order of magnitude than the results from other studies about quench velocity measurements and simulations [Här2015]. With the simulated velocities, it would take about 10-30 ms for a quench would to propagate 1 cm. In these simulations the heater period was so long that it did not impact the result.

Simulations were performed using the coverages of 50, 60, and 80 mm in cases A, B and C respectively, as found in the study presented in section 6.4.1, and by varying the heater period. The times to quench the entire cable, including space between the heating stations, are shown in figure 6.9.

One could have hypothesized that the pre-heating by the heater, and the approaching warm front from the neighboring heating segments might accelerate the quench propagation between the heating stations compared to the quench propagation velocity in a cold cable. However, this was not seen in the

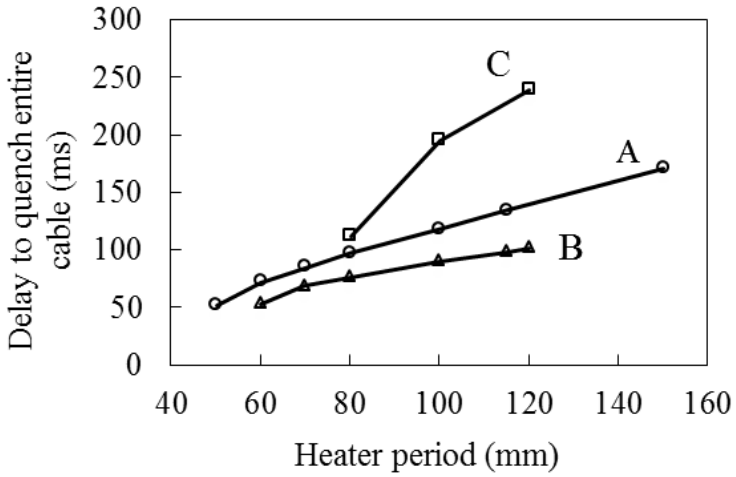

Figure 6.9: Delay time to quench the entire cable vs. heater period at three operation points.

simulations. See for example the case A with coverage of 50 mm and period of 60 mm, i.e., only 10 mm between the heating stations. The delay to quench is about 50 ms in the 1-D case, but 75 ms in the 2-D case (to quench the entire period).

If the period was longer than 120 mm (cases B and C) or 150 mm (case A), the temperature under the heater reached 300 K before the entire length between the heating stations was quenched. Based on this study, the coverage should be at least 30-70% of the period. The advantages of using heating stations in HTS coils seem few, because a large fraction must be covered, and the time to quench between the heating stations is long. If heaters are used, it may be more efficient to focus the effort on developing heater technologies that can cover the entire cable surface rather than on the heating station geometry optimization. Note, that this analysis was not complete because the current and field decay during a quench were neglected.

6.5 Ideas for alternative heaters

In this section are proposed two ideas for alternative heater technology, which could provide the required large heater energies for future HTS magnets

6.5.1 Co-wound heater

One option is an insulated strand-shaped heater strip, which is co-wound in the Roebel cable, see figure 6.10. The advantage is that it provides almost continuous connection to the wide side of the strands adjacent to it. When heating the wide side, a larger fraction of the cable perimeter is covered, and the heat is distributed more uniformly over the cable.

The disadvantage is that the resistance of the strip may become too high to allow powering with a tolerable voltage, and that the inductance of the heater strip may become large. Although likely to require additional "take-outs" from the cable due to the voltage limitations, this type of development could be investigated in the future.

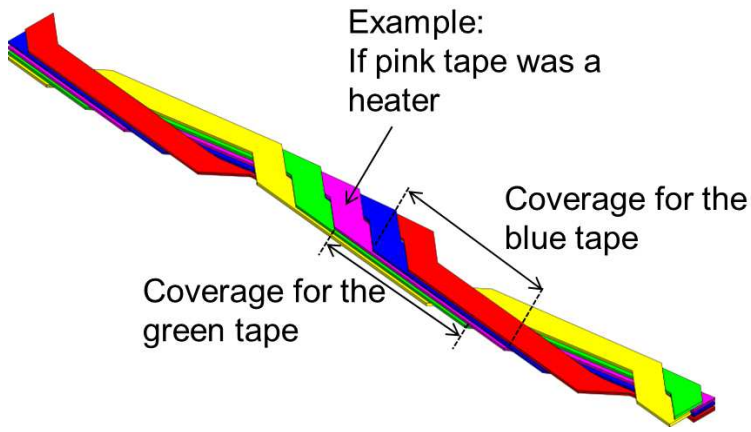

Figure 6.10: A heater co-wound as one of the strands. If the pink strand was a heater, if would provide a continuous connection to the strands above and below (blue and green). Cable image from [Bar2012].

6.5.2 Layered heater

One of the most limiting requirements for the heater design has been the requirement to get heater current leads out only from the coil ends, as discussed in Chapter 5. This has led to designs of heater strips that extend the entire coil length, and therefore to the insufficiency of heater energy as the heater voltage and current have upper limitations. One way to surpass this limitation could be a layered heater design. The idea is to have several short strips one after another. Low-resistance copper current leads to each strip would be on top of a Kapton insulation that separates the heaters from the current leads, see

figure 6.11. The advantage is that now the strip voltage is not a restriction. The disadvantage is the need of several power supplies, and the increasing number of wires coming out from the magnet.

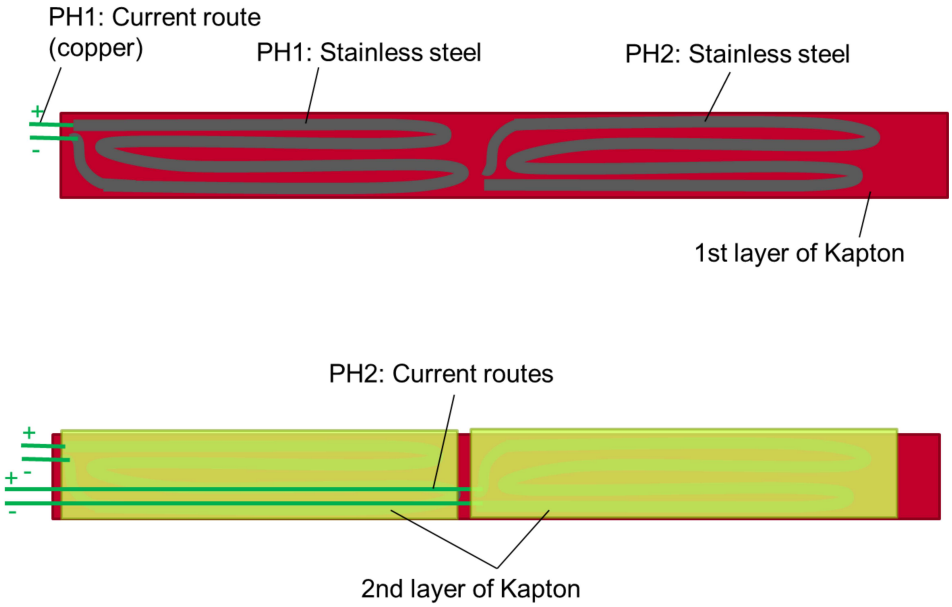

Figure 6.11: A layered heater design consisting of several short heaters.

6.6 Concluding remarks

In this chapter the CoHDA simulation tool was applied to an HTS coil operating at 4.5 K, and the efficiency of heater based protection was investigated. As expected, the simulated delays were longer than in LTS coils. Due to slow quench propagation it also took a significantly longer time to quench between heating stations.

For cables with T_{cs} above 20 K the power per heater surface must be increased from typical values in LTS coils. The analysis suggested that the needed heater energy can be estimated from the cable's energy margin to quench. In the study 50 kJ/m^2 heater energy was considered for T_{cs} up to 29 K. Two new approaches were discussed which could provide the large heater energies, still having low heater voltage. However, there is no way around the fact that to supply large energies, several large heater power supplies (and additional wires into the cryostat) are needed. Therefore, also alternative quench protection methods must be explored, such as those discussed in Chapter 2.3.5.

Chapter 7

Conclusions

The research included in this thesis studied the protection of high-field accelerator magnets using quench protection heaters. The research was launched because the used adiabatic models suggested that the magnets under development for the LHC upgrades could not be reliably protected using the existing protection heater technology as such. The central research questions were:

- How to computationally simulate the efficiency of the state-of-the-art heater technology in Nb_3Sn based accelerator magnets and benchmark the results experimentally?
- How to optimize the heater design for the future magnets using the existing technology?
- Can the HTS-based magnets be protected using heaters? What are the limits that are faced in the heater based quench protection?

The efficiency of protection heaters is characterized by their ability to induce widespread quenches in the superconducting coils. This increases the resistance of the coils and consequently rapidly drives down the magnet current. The performed heater design analysis focused on the heater delay modeling, taking into account the different coil field regions that the heater covers. A numerical simulation tool was developed to compute the heat conduction from the heater to the cable trough the various insulation materials. The solution is based on the thermal network method in a 2-D modeling domain. The modeling domain includes one individual coil turn, thus neglecting the transverse heat diffusion between the turns. The problem is simplified also by assuming uniformly thick material layers and homogenized structure of the bare cable. This approach allows to use sufficiently fine spatial and temporal

discretization and still deliver the results for a given study in minutes. The delay to quench onset is taken as the time instant when the cable maximum temperature reaches the current sharing temperature, T_{cs}. This is assumed to be comparable with the first occurrence of resistive voltage in a heater delay measurement. The correct implementation of the tool was verified using comparisons with analytical solution and a commercial FEM software.

The simulated heater delays had an acceptable agreement with the delays measured in several Nb_3Sn R&D magnets, without using any fitting variables. Even if the delays varied several-fold between the different magnets (6-25 ms at high current), usually the simulated heater delays on coil outer layer were within 2-3 ms of measured values near the maximum operation current (80% of short-sample limit, SSL). The uncertainty increased at lower currents, however usually being within 20% of measurement for magnet currents above 50% of SSL. The uncertainties were comparable with the experimental uncertainties. The exception was the LARP LQ magnet, which had very short heating stations: The simulations predicted 5 ms (32%) shorter delays at 60% of SSL. In all magnets, the simulated delays for inner layer heaters tended to give too optimistic delays and the deviation was larger, especially at lower current. This discrepancy was associated with the degradation of the heater contact on the coil inner surfaces.

The present protection heater technology was optimized for the LARP LHQ and QXF using the simulations. Within the constraints that were defined for the heater strip (length, voltage, temperature and materials), the optimization came down to defining the heating station lengths and peak power in an optimum way. New heater layouts were proposed where the lengths of the heating stations were optimized for different coil field regions. A routine consisting of a series of parametric studies was written to explore the available options, and propose designs which minimize the delay to quench all the coil turns under the heater, including the quench propagation between the heating stations. The optimizations were performed at 80% of SSL since this is the most critical region for the protection.

The optimized heaters had peak powers varying from 75 to 150 W/cm^2 and heating stations between 15 and 50 mm. The LHQ outer surface heater was tested and compared with a traditional heater design. It was found that the 0.3 Ω margin that was left in the design for the connections to the power supply was not sufficient. The larger than expected total resistance led to powering with a lower voltage and almost half of the designed peak power. Nevertheless, it managed to protect the magnet at least as well as the traditional layout.

To get an idea of the heaters' suitability for HTS coils, the model was applied to a YBCO based coil which was designed in an R&D program related to the LHC energy upgrade. In this simulation the current redistribution in the non-uniformly heated tape was accounted because the T_c and T_{cs} differed considerably more than in LTS. It became obvious that there is a hard limit in the heaters ability to quench the cables. It could be evidenced by the comparison of the cable's enthalpy margin to quench with the energy provided by the heater. On the other hand, the HTS cables were quenched too when sufficient energy was provided. I also modeled the quench propagation between the heating stations by considering the current diffusion to the stabilizing copper and the generated losses. Due to the slow propagation velocities, there does not seem to be a significant advantage of using heating stations in HTS. Improvements on the technology, such as increasing the stainless steel thickness, and using "layered heaters" were proposed which could allow increasing the heater energy without increasing its voltage. These concepts are applicable to LTS too, and the limitations of the heater based protection can be related to the number of heater power supplies that can be used per magnet.

This research showed that there are still several concepts that can be explored in the design of heaters for future magnets. As research on alternative protection methods must remain active, there is no need to consider the heaters as a protection mechanism belonging only to the history, even for HTS.

Six peer-reviewed publications are included in this thesis. Here is a summary of the content of each of them:

Publication 1 presented measurements of the heater delays and the resulting current decays when using the state-of-the-art heaters in the LARP HQ01, HQM01 and LQ R&D magnets. Numerical simulations were used to estimate the required heater delays in the LHQ magnet. The reasons why the required delays cannot be obtained with the present technology were indicated.

Publication 2 described for the first time how the heater delays can be reliably simulated in Nb_3Sn magnets. The simulation and experimental data were compared using HQ01 and the first model of the 11 T dipole.

Publication 3 presented parametric studies demonstrating the heater delays' dependence on various design parameters. The analysis considered the HQ01, HQ02 and LQ magnets, and the simulation results were validated using comparison with experimental data. This publication also described the optimization based approach to heater design, and presented the new QXF outer layer heater.

Publication 4 described the simulation tool that was developed for the analyses, its numerical implementation, and validation. This publication also discussed the difficulties in modeling the heater delays at low magnet currents, and suggested procedures that can reduce the experimental uncertainty. The sensitivity of the simulation results, i.e. the computed heater delays, to the input parameters and material properties was analyzed.

Publication 5 presented a summary of simulated and measured delays in HQ01, HQ02, LQ, HD3 and the two models of the 11 T dipoles. First time the simulations for inner layer heater were included. The uncertainties in the experimental data and in the simulation were analyzed in detail, considering also the impact of neglecting the transverse heat diffusion. A safety margin to be applied in simulation based heater design was proposed, either by adding a percentage to the nominal simulation results, or by using an a simulation criterion which accounts for the current redistribution in the non-uniformly heated cable before the quench starts to propagate. The importance of careful definition of the simulation input parameters was highlighted.

Publication 6 applied the heater delay modeling to an HTS coil. It proposed, that the first estimation of the heaters suitability in HTS can be found by comparing their deposited energy per coil surface with the cable volumetric energy margin scaled with the cable width. Parametric analysis of the delay showed similar dependencies than found when LTS magnets were studied.

Appendix A

Coil and heater parameters

A.1 HQ01 and HQ02

The Nb_3Sn critical surface was calculated using Godeke fit [Arb2009, God2006] with parameters from extracted strand measurements in coils 9 and 20 [God2013].

A.2 LQ

LQ critical surface parameters based on Godeke fit, using $C_{a1} = 41.24$ T, $C_{a2} = 42642.16$ T, $\epsilon_{0a} = 0.0025$, $B_{c2}(0,0) = 27.69$ T, $T_c(0,0) = 16.7$ K, $C_I = 1976.94$ A, $p = 0.5$, $q = 2.0$, ϵ = -0.002.

A.3 HD3

The critical surfaces are based on the Godeke fit using $C_{a1} = 43$ T, $C_{a2} = 44462$ T, $\epsilon_{0a} = 0.0014$, $B_{c2}(0,0) = 31.18$ T, $T_c(0,0) = 16.7$ K, $C_I = 2216.23$ A, $p = 0.5$, $q = 2.0$, ϵ = -0.002 for coil 3. For coil 1 we replaced $B_{c2}(0,0) = 30.23$ T and $C_I = 2666.22$ A.

A.4 11 T

The critical surfaces are based on the Summers fit [Sum1991]. The fit parameters for MBHSP01: $B_{c20} = 24.8$ T, $T_{c0} = 16.5$ K, $C = 9080$. The fit parameters

for MBHSP02: B_{c20} = 26.81 T, T_{c0} = 17.22 K, and C = 8490 [Bar2013].

A.5 LHQ and QXF

During the heater design, the critical surface for the LHQ cable was based on HQ coil 15 [God2013]. In the simulations of the constructed heater, the critical surface was based on measurements of the tested LHQ03 coil, using B_{c2}(0,0) = 28.43 T, and C = 1879.51 TA.

The QXF critical surfaces are based on the Godeke fit. The fit parameters for outer layer are B_{c2}(0,0) = 28.46 T, and C = 2105 TA. The parameters for the inner layer are B_{c2}(0,0) = 30.88 T, and C = 1519 TA. They are different, because cable design proceeded between these two heater design studies.

Table A.1: HQ magnet parameters.

Magnet (coil)	HQ01e (#9)	HQ02a (#20)
Magnet length [m]	1	1
Aperture [mm]	120	120
Short sample limit (SSL) @1.9 K [kA]	19.3	18.3
Short sample limit (SSL) @4.4 K [kA]	17.5	16.6
B_{peak} at SSL [T] (1.9 K)	15	14.3
$B_{peak}(I)$ [T]	$0.001271I^{0.950511}$	
Strand	RRP 54/61	RRP 108/127
# strands	35	35
Strand diameter (mm)	0.800	0.790
Copper RRR	190	155
Strand Cu/SC	1.05	1.20
Voids fraction (bare cable)	0.12	0.15
Core	No	ss 25 μm
Cable mid-thickness [mm]	1.44	1.38
Cable width [mm]	15.0	1.49
Cable ins. (G10) [mm]	0.09	0.09
Inter-layer ins. (G10) [mm]	0.71	0.70
Heater-collar ins. (G10) (OL) [mm]	0.300	0.4
Heater-bore ins. (G10) (IL) [mm]	0.250	0.250
Stainless steel [mm]	0.0254	0.0254
Heater width (L1/L2) [mm]	10.0/11.0	10.0/11.0
Heater ins. polyimide [mm]	0.0254	0.0762

Table A.2: Parameters in protection heater delay simulations in HQ.

Parameter	HQ01e	HQ02a
Heater initial voltage (V)	230	270
Heater initial current (A) (L1, L2)	50, 53	51,58
Heater peak power (W/cm^2) (IL, OL)	49, 46	55
Heater circuit time constant (ms) (IL, OL)	40, 40	50, 45
Op. temperature (K)	1.9, 4.4	1.9, 4.4
Heaters fired to provoke a quench	1	1
Ramp rate to quench current (A/s)	10-90	50
Holding time at plateau (min)	3-5	3

Table A.3: LQ magnet parameters.

Magnet (coil)	LQ (#7]
Coil length [m]	3.3
Aperture [mm]	90
Short sample limit (SSL) @1.9 K [kA]	15.2
Short sample limit (SSL) @4.4 K [kA]	13.8
B_{peak} at SSL [T] (1.9 K)	13
$B_{\text{peak}}(I)$ [T]	$0.00197I^{0.92}$
Strand	RRP 54/61
# strands	27
Strand diameter (mm)	0.7
Copper RRR	250
Strand Cu/SC	0.85
Voids fraction (bare cable)	0.15
Core	No
Cable width [mm]	10.1
Cable ins. (G10) [mm]	0.090
Inter-layer ins. (G10) [mm]	0.3
Heater-collar ins. (polyim.) (OL) [mm]	1.4
Stainless steel [mm]	0.0254
Heater width (HS/WS) (OL) [mm]	9/20
Heater ins. polyimide [mm]	0.0254

Table A.4: Parameters in protection heater delay simulation in LQ.

Magnet	LQ
Heater initial voltage (V)	250
Heater initial current (A) (OL)	40
Heater peak power (W/cm^2) (OL)	40
HFU capacitance (mF)	19.2
Heater circuit time constant (ms)	35
Op. temperature (K)	4.5
Heaters fired to provoke a quench	10
Ramp rate to quench current (A/s)	20-200
Holding time at plateau (min)	up to 5

Table A.5: HD3 magnet parameters.

Magnet (coil)	HD3b (#3,#1)
Magnet length [m]	1
Aperture [mm]	43
Short sample limit (SSL) @1.9 K [kA]	20.7 (#3)
Short sample limit (SSL) @4.4 K [kA]	18.7, 18.9
B_{peak} at SSL [T] (1.9 K)	16.3 (4.4 K)
$B_{\mathrm{peak}}(I)$ [T]	$0.002025I^{0.91417}$
Strand	RRP 54/61, 60/61
# strands	51
Strand diameter (mm)	0.813
Copper RRR	150, 100
Strand Cu/SC	0.83, 0.65
Voids fraction (bare cable)	0.12
Core	No
Cable mid-thickness [mm]	1.4
Cable width [mm]	22.00
Cable ins. (G10) [mm]	0.100
Inter-layer ins. (G10) [mm]	1.10
Heater-collar ins. (G10) (L2) [mm]	0.635
Heater-bore ins. (G10) (L1) [mm]	0.635
Stainless steel [mm]	0.0254
Heater width (L1/L2) [mm]	11.5/13.4
Heater ins. polyimide [mm]	0.0254

Table A.6: Parameters in protection heater delay measurements in HD3.

Parameter	HD3b
Heater initial voltage (V)	260
Heater initial current (A) (L1, L2)	53, 63
Heater peak power (W/cm^2) (L1, L2)	55, 56
Heater circuit time constant (ms) (L1, L2)	48, 42
Op. temperature (K)	4.2
Heaters fired to provoke a quench	2
Ramp rate to quench current (A/s)	20-50
Holding time at plateau (min)	< 1

Table A.7: 11 T Magnet parameters.

Magnet (model)	11 T (MBHSP01)	11 T (MBHSP02)
Magnet length [m]	2	1
Aperture [mm]	60	60
Short sample limit (SSL) @1.9 K [kA]	15.1	16.0
Short sample limit (SSL) @4.6 K [kA]	13.1	14.3
B_{peak} at SSL [T] (1.9 K	14.1	14.8
$B_{\text{peak}}(I)$ [T]	$0.0023I^{0.9062}$	
Strand	RRP 108/127	RRP 150/169
# strands	40	40
Strand diameter (mm)	0.700	0.700
Copper RRR	100	100
Strand Cu/SC	1.227	1.02
Voids fraction (bare cable)	0.13	0.12
Core	No	ss25 μm
Cable mid-thickness [mm]	1.31	1.25
Cable width [mm]	15	15
Cable ins. (G10) [mm]	0.1	0.1
Inter-layer ins. (G10) [mm]	0.7	0.7
Heater-collar ins. (Kapton) [mm]	0.64	0.64
Stainless steel [mm]	0.0254	0.0254
Heater width (OL) [mm]	26	26
Heater ins. polyimide [mm]	0.0762 or 0.203	0.0762

Table A.8: Parameters in protection heater delay measurements in 11 T.

Parameter	11 T (MBHSP01)	11 T (MBHSP02)
Heater initial voltage (V)	400	350
Heater initial current (A)	77	107
Heater peak power (W/cm^2)	18.5	40
Heater circuit time constant (ms)	25	16
Op. temperature (K)	1.9, 4.6	1.9, 4.6
Heaters fired to provoke a quench	2	2 or 4
Ramp rate to quench current (A/s)	20-50	20-50
Holding time at plateau (min)	1	1

Table A.9: Coil parameters used in the LHQ and QXF heater optimization. The QXF outer layer parameters are based on an earlier design version [Bor2012] than the parameters used for the inner layer [Bor2014, Amb2015].

Heater location	LHQ	QXF OL	QXF IL
Design ref.	(HQC15)	v0	v2b
Coil (strip) length (m)	3.3	4.0	6.8
SSL@1.9 K (kA)	19.3	21.7	21.3
Operation current (kA)	15.4	17.3	17.5
B max at I op (T)	12.1	12.2	12.1
# strands	35	40	40
Strand diam. (mm)	0.79	0.85	0.85
RRR	90	150	150
Strand Cu/non-Cu ratio	1.20	1.13	1.22
Epoxy fraction	0.18	0.15	0.15
Cable width (mm)	15.0	18.3	18.5
Cable ins. G10 (mm)	0.1	0.15	0.15
Inter-layer ins. G10 (mm)	0.5	0.5	0.5
Ground ins. (mm) (polyim.)	0.38 (G10)	0.5	0.4
Stainless steel (mm)	0.025	0.025	0.025
Heater ins polyim. (mm)	0.050	0.050	0.050
G10 between IL heater and bore (mm)	N/A	N/A	0.150

Bibliography

[TIARA2015] Accelerators for Society project. Website sponsored by the TIARA project: `http://www.accelerators-for-society.org/` (Accessed Mar 17 2015)

[ALICE2008] The ALICE Collaboration, et al. 2008 *Journal of Instrumentation* **3** S08002 "The ALICE experiment at the CERN LHC" doi:10.1088/1748-0221/3/08/S08002

[Amb2001] Ambrosio G, Andreev N, Barzi E, Bauer P, Chichili D, Ewald K, Feher S, Imbasciati L, Kashikhin V V, Kim S W, Limon P, Novitski I, Rey J-M, Yadav S, and Yamada R, Zlobin A V and Scanlan R 2001 *Proceedings of PAC 2001* **5** 3409 "Design and development of Nb_3Sn single-layer common coil dipole magnet for VLHC" doi:10.1109/PAC.2001.988127

[Amb2007] Ambrosio G, Andreev N, Anerella M, Barzi E, Bossert R, Dietderich D, Feher S, Ferracin P, Ghosh A, Gourlay S, Kashikhin V V, Lietzke A, McInturff A, Muratore J, Nobrega F, Sabbi G.L, Schmalzle J, Wanderer P and Zlobin A V 2007 *IEEE Trans. Appl. Supercond.* **17** 1035 "Design of Nb_3Sn coils for LARP long magnets" doi:10.1109/TASC.2007.897289

[Amb2008] Ambrosio G, Andreev N, Anerella M, Barzi E, Bossert R, Caspi S, Chlachidize G, Dietderich D, Feher S, Felice H, Ferracin P, Ghosh A, Hafalia R, Hannaford R, Kashikhin V V, Kerby J, Lamm M, Lietzke A, McInturff A, Muratore J, Nobrega F, Novitsky I, Sabbi G.L, Schmalzle J, Tartaglia M, Turrioni D, Wanderer P, Whitson G and Zlobin A V 2008 *IEEE Trans. Appl. Supercond.* **18** 268 "LARP long Nb_3Sn quadrupole design" doi:10.1109/TASC.2008.922277

[Amb2011] Ambrosio G, Andreev N, Anerella M, Barzi E, Bingham B, Bocian D, Bossert R, Caspi S, Chlachidize G, Dietderich D, Escallier J, Felice

H, Ferracin P, Ghosh A, Hafalia R, Hannaford R, G. Jochen, Kashikhin V V, Kim M J, Kovach P, Lamm M, McInturff A, Muratore J, Nobrega F, Novitsky I, Orris D, Prebys E, Prestemon S, Sabbi G.L, Schmalzle J, Sylvester C, Tartaglia M, Turrioni D, Velev G, Wanderer P, Whitson G and Zlobin A V 2011 *IEEE Trans. Appl. Supercond.* **21** 1858 "Test results of the first 3.7 m long Nb_3Sn quadrupole by LARP and future plans"
doi:10.1109/TASC.2010.2089586

[Amb2015] Ambrosio G, Anerella M, Borgnolutti F, Bossert R, Cheng D, Chlachidize G, Dietderich D, Felice H, Ferracin P, Ghosh A, Godeke A, Hafalia R, Izquierdo Bermudez S, Kashikhin V V, Krave S, Marchevsky M, Muratore J, Nobrega F, Novitski I, Prestemon S, Sabbi G L, Schmalzle J, Wanderer P, Yu M and Zlobin A V *LARP_note Feb. 20, 2015 Version DRAFT_4* "SQXF1 design report" (To be published)

[Apo2014] Apollinari G 2014 *DOE Review of LARP, Feb 17-18, 2014 (slides)* "LARP status and prospects" Available online: `https://indico.fnal.gov/conferenceDisplay.py?confId=7951` (Accessed Mar 17 2015)

[Arb2009] Arbelaez D, Godeke A, and Prestemon S.O. 2009 *Supercond. Sci. Technol.* **22** "An improved model for the strain dependence of the superconducting properties of Nb_3Sn"
doi:10.1088/0953-2048/22/2/025005

[ASC2015] ASC website: `http://fs.magnet.fsu.edu/~lee/image/hts/index.htm` (Assessed Jan 4 2015)

[Baj2013] Bajas H, Ambrosio G, Anerella M, Bajko M, Bossert R, Caspi S, Chiuchiolo A, Chlachidze G, Dietderich D, Dunkel O, Felice H, Ferracin P, Feuvrier J, Fiscarelli L, Ghosh A, Giloux C, Godeke A, Hafalia A R, Marchevsky M, Russenschuck S, Sabbi G L, Salmi T, Schmalzle J, Todesco E, Wanderer P, Wang X and Yu M 2013 *IEEE Trans. Appl. Supercond.* **23** 4002606 "Cold test results of the LARP HQ Nb_3Sn quadrupole magnet at 1.9 K"
doi:10.1109/TASC.2013.2245281

[Baj2015] Bajas H, Ambrosio G, Anerella M, Bajko M, Bossert R, Bottura L, Caspi S, Cheng D, Chiuchiolo A, Chlachidze G, Dietderich D, Felice H, Ferracin P, Feuvrier J, Ghosh A, Giloux C, Godeke A, Hafalia A R, Marchevsky M, Ravaioli E, Sabbi G L, Salmi T, Schmalzle J, Todesco E, Wanderer P, Wang X and Yu M 2015 *IEEE Trans. Appl. Supercond.*

25 4003306 "Test Results of the LARP HQ02b Magnet at 1.9 K" doi:10.1109/TASC.2014.2378375

[Bar1957] Bardeen J, Cooper L N and Schrieffer J R 1957 *Phys. Rev.* **108** 1175 "Theory on superconductivity" doi:10.1103/PhysRev.108.1175

[Bar2012] Barth C 2012 *Wikimedia commons* "Schematical drawing of a Roebel cable assembled out of REBCO high temperature superconductor tape tapes." `http://commons.wikimedia.org/wiki/File:Roebel_assembled_coated_conductor_cable_(RACC).svg` (Accessed Jan 4 2015)

[Bar2015] Barth C, Takayasu M, Bagrets N, Bayer C M, Weiss K-P and Lange C 2015 *Supercond. Sci. Technol.* **28** "Temperature and field dependent characterization of a twisted stacked-tape cable" doi:10.1088/0953-2048/28/4/045015

[Bar2013] Barzi E and Turrioni D 2013 *FERMILAB-TM-2552-TD* "Short sample limit calculation for 1 m long dipole MBHSP02 made of 150/169 RRP strand and cored cable"

[Bau2000] Bauer P, Zlobin A, Lamm M, Sabbi G and Ogitsu T 2000 *Fermilab TD report TD-00-027* "Concept for a QUENCH-CALCULATION PROGRAM for the analysis of quench protection systems for superconducting high field magnets"

[Bau2001a] Bauer P, Imbasciati L, Ambrosio G, Kashikin V, Lamm M and Zlobin A V 2001 *Fermilab TD report TD-01-003* "Quench protection calculations for Fermilab's Nb_3Sn high-field magnets for VLHC- Part1"

[Bau2001b] Bauer P, Imbasciati L, Ambrosio G, Kashikin V, Lamm M and Zlobin A V 2001 *Fermilab TD report TD-01-004* "Quench protection calculations for Fermilab's Nb_3Sn high-field magnets for VLHC- Part2"

[Bau2001c] Bauer P, Bossert R, Chiesa L, DiMarco J, Feher S, Lamm M J, Mcinturff A D, Nobrega A, Orris D, Tartaglia M, Tompkins J C and Zlobin A V 2001 *IEEE Trans. Appl. Supercond.* **11** 1617 "Quench protection of the LHC inner triplet quadrupoles built at Fermilab" doi:10.1109/77.920089

[Bed1986] Bednorz J G and Müller K A 1986 *Z. Phys. B – Condensed Matter* **64** 189 "Possible highTc superconductivity in the Ba-La-Cu-O system" doi:10.1007/BF01303701

[Blo1996] Blomberg T 1996 *PhD dissertation* Lund University, Lund, Sweden "Heat conduction in two and three dimensions: Computer modelling of building physics applications"

[Boc2008] Bocian D, Dehning B and Siemko A 2008 *IEEE Trans. Appl. Supercond.* **18** 112 "Modeling of quench limit for steady state heat deposits in LHC magnets"
doi:10.1109/TASC.2008.921338

[Boc2009] Bocian D, Dehning B, and Siemko A 2009 *IEEE Trans. Appl. Supercond.* **19** 2446 "Quench limit model and measurements for steady state heat deposits in LHC magnets"
doi:10.1109/TASC.2009.2019060

[Boc2012] Bocian D, Ambrosio G, Barzi E, Bossert R, Caspi S, Chlachidze G, Dietderich D, Feher S, Felice H, Ferracin P, Hafalia R, Kashikhin V V, Lamm M, Sabbi G L, Turrioni D, Wanderer P and Zlobin A V 2012 *IEEE Trans. Appl. Supercond.* **22** 4003704 "Steady state heat deposits modeling in the Nb_3Sn quadrupole magnets for the upgrade of the LHC inner triplet"
doi:10.1109/TASC.2011.2174591

[Bor2012] Borgnolutti F 2012 *2nd HiLumi-Larp meeting, Frascati, Italy, Nov. 2012* "Coil cross-section, end design and parts, and winding test" (slides) Available online: `https://indico.cern.ch/contributionDisplay.py?contribId=94&sessionId=16&confId=183635` (Accessed Mar 17 2015)

[Bor2014] Borgnolutti F, Ambrosio G, Izquierdo Bermudez S, Cheng D, Dietderich D R, Felice H, Ferracin P, Sabbi G.L., Todesco E and Yu M 2014 *IEEE Trans. Appl. Supercond.* **24** 4000405 "Magnetic design optimization of a 150 mm aperture Nb_3Sn low-beta quadrupole for the HiLumi LHC"
doi:10.1109/TASC.2013.2279905

[Bos2002] Bossert R, Carcagno R, Chiesa L, Feher S, Kerby J, Lamm M J, Nobrega A, Orris D, Schlabach P, Tartaglia M, Tompkins J C and Zlobin A V 2002 *IEEE Trans. Appl. Supercond.* **12** 133 "Quench protection of the fermilab-built LHC inner triplet quadrupole MQXB"
doi:1051-8223(02)03445-0

[Bos2003] Bossert R, Kerby J, Nobrega F, Lamm M J, Rife J, Feher S, Robotham W, Schlabach P, Yadav S and Zlobin A V 2002 *IEEE*

Trans. Appl. Supercond. **13** 1297 "Construction experience with MQXB quadrupole magnets built at Fermilab for the LHC interaction regions" doi:10.1109/TASC.2003.812653

[Bos2012] Bossert R, Ambrosio G, Andreev N, Anerella M, Barzi E, Caspi S, Cheng D, Chlachidze G, Dietderich D, Felice H, Ferracin P, Ghosh A, Hafalia A R, Kashikhin V V, Lamm M, Nobrega A, Novitski I, Sabbi G L, Schmalzle J, Wanderer P and Zlobin A V 2012 *IEEE Trans. Appl. Supercond.* **13** 1297 "Optimization and test of 120 mm LARP Nb_3Sn quadrupole coils using magnetic mirror structure" doi:10.1109/TASC.2011.2177235

[Bot1998] Bottura L 1998 *Physica C* **310** 316. "Modelling stability in superconducting cables" doi:10.1016/S0921-4534(98)00482-1

[Bot2000a] Bottura L, Rosso C and Breschi M 2000 *Cryogenics* **40** 617 "A general model for thermal, hydraulic, and electric analysis of superconducting cables" doi:10.1016/S0011-2275(01)00019-4

[Bot2000b] Bottura L 2000 *IEEE Trans. Appl. Supercond.* **10** 1054 "A practical fit for the critical surface of NbTi" doi:10.1109/77.828413

[Brü2004] Brüning O S, Collier P, Lebrun P, Myers S, Ostojic R, Poole J and Proudlock P (editors) 2004 *CERN-2004-003* "LHC design report vol. 1: The LHC main ring" doi:10.5170/CERN-2004-003-V-1

[Brü2007] Brüning O and Collier P 2007 *Nature* **19** 285 "Building a behemoth" doi:10.1038/nature06077

[Bur2001] Burkhardt E E, Yamamoto A, Nakamoto T, Ogitsu T, Shintomi T and Tsuchiya K 2001 *IEEE Trans. Appl. Supercond.* **11** 1621 "Quench protection heater studies of the 3rd 1-m model magnet for the KEK-LHC low-β quadrupoles" doi:10.1109/77.920090

[Car2003] Cardwell D A and Ginley D S (editors) 2003 *IOP Publishing Ltd* "Handbook of superconducting materials, Volume I"

[Car1959] Carslaw H S and Jaeger J C 1959 *Oxford press, London* 113 "Conduction of heat in solids, 2nd ed"

[Cas2003] Caspi S, Chiesa L, Ferracin P, Gourlay S A, Hafalia R, Hinkins R, Lietzke A F and Prestemon S 2003 *IEEE Trans. Appl. Supercond.* **13** 1714 "Calculating quench propagation with ANSYS " doi:10.1109/TASC.2003.812867

[Cas2005] Caspi S and Ferracin P 2005 *Proceedings of PAC 2005* 107 "Limits of Nb_3Sn accelerator magnets" doi:10.1109/PAC.2005.1590372

[Cas2014] Caspi S, Borgnolutti F, Brouwer L, Cheng D, Dietderich D R, Felice H, Godeke A, Hafalia R, Marchevsky M, Prestemon S, Rochepault E, Swenson C and Wang X 2013 *IEEE Trans. Appl. Supercond.* **24** 4001804 "Canted-Cosine-Theta Magnet (CCT) – A concept for high field accelerator magnets" doi:10.1109/TASC.2013.2284722

[Cen2003] Cengel Y 2003 *McGraw-Hill Education* "Heat transfer a practical approach"

[CERN2015a] CERN website: `http://home.web.cern.ch/about/engineering/radiofrequency-cavities` (Accessed Mar 17 2015)

[CERN2015b] CERN website: `http://home.web.cern.ch/about/experiments` (Accessed Mar 17 2015)

[CERN2015c] CERN website: `http://home.web.cern.ch/topics/higgs-boson` (Accessed Mar 17 2015)

[CERN2009] CERN website: `http://press.web.cern.ch/press-releases/2009/11/two-circulating-beams-bring-first-collisions-lhc` (Accessed Mar 17 2015)

[Che2013] Cheng D W, Caspi S, Dietderich D R, Felice H, Ferracin P, Hafalia A R, Marchevsky M, Prestemon S and Sabbi G 2013 "Design and fabrication experience with Nb_3Sn block-type coils for high field accelerator dipoles" *IEEE Trans. Appl. Supercond.* **23** 4002504 doi:10.1109/TASC.2013.2246811

[Chl2008] Chlachidze G 2008 *Fermilab, December 30-31, 2008* "LQ Protection heater test at ln temperature" (slides) Available online: `https://indico.fnal.gov/getFile.py/access?resId=2&materialId=slides&confId=2045` (Accessed Mar 17 2015)

[Chl2009] Chlachidze G, Ambrosio G, Felice H, Lewis F, Nobrega F and Orris D 2009 *Fermilab TD report TD-09-007* "LQ protection heater test at liquid nitrogen temperature"

[Chl2011] Chlachidze G, Ambrosio G, Andreev N, Barzi E, Carcagno R, Caspi S, Dietderich D, Felice H, Ferracin P, Ghosh A, Kashikhin V V, Kim M J, Lamm M J, Lewis F, Nobrega F, Novitski I, Orris D, Sabbi G L, Schmalzle J, Sylvester C, Tartaglia M, Tompkins J C, Velev G, Wanderer P and Zlobin A V 2010 *Fermilab TD report TD-10-001* "LARP LQS01 magnet test summary"

[Chl2013] Chlachidze G, Andreev N, Apollinari G, Auchmann B, Barzi E, Bossert R, Karppinen M, Nobrega F, Novitski I, Rossi L, Smekens D, Tartaglia M, Yamada R and Zlobin A V 2013 *IEEE Trans. Appl. Supercond.* **23** 4001205 "Quench protection study of single-aperture Nb_3Sn demonstrator dipole for LHC upgrades"
doi:10.1109/TASC.2013.2237871

[Chl2014] Chlachidze G, Ambrosio G, Anerella M, Borgnolutti F, Bossert R, Caspi S, Cheng D W, Dietderich D, Felice H, Ferracin P, Ghosh A, Godeke A, Hafalia A R, Marchevsky M, Orris D, Roy P K, Sabbi G, Salmi T, Schmalzle J, Sylvester C, Tartaglia M, Tompkins J, Wanderer P, Wang X R and Zlobin A V 2014 *IEEE Trans. Appl. Supercond.* **24** 4003805 "Performance of HQ02, an optimized version of the 120 mm Nb_3Sn LARP quadrupole"
doi:10.1109/TASC.2013.2285885

[COMSOL2013] COMSOL Multiphysics, version 4.4, 2013, website: `http://www.comsol.com/comsol-multiphysics`

[CRYOCOMP] CRYOCOMP - a material property library for materials commonly used in cryogenic temperatures (Copyright Eckels Engineering Inc.)

[Dai1995] Dai P, Chakoumakos B C, Sun G F, Wong K W, Xin Y and Lu D F 1995 *Physica C: Superconductivity* **243** 201 "Synthesis and neutron powder diffraction study of the superconductor $HgBa_2Ca_2Cu_3O_{8+\delta}$ by Tl substitution"
doi:10.1016/0921-4534(94)02461-8

[Dah2001] Dahlerup-Petersen K, Rodriguez-Mateos F, Schmidt R and Sonnemann E 2001 *Proceedings of PAC 2001.* **5** 3448 "Energy extraction for

the LHC superconducting circuits"
doi:10.1109/PAC.2001.988140

[Dav2011] Davies A 2011 "Material properties data for heat transfer modeling in Nb_3Sn magnets" Available online: `http://www.illinoisacceleratorinstitute.org/2011%20Program/student_papers/Andrew_Davies.pdf` (Accessed Mar 17 2015)

[Dav2013] Davis J C Seamus and Lee D-H 2013 *Proceedings of the National Academy of Sciences* **110** 17623 "Concepts relating magnetic interactions, intertwined electronic orders, and strongly correlated superconductivity"
doi:10.1073/pnas.1316512110

[Den2011] Denz R and Rodriguez-Mateos F 2001 *Proceedings of Particle Accelerator Conference, 2001. PAC 2001.* **5** 3445 "Detection of resistive transitions in LHC superconducting components"
doi:10.1109/PAC.2001.988139

[Den2006] Denz R 2001 *IEEE Trans. Appl. Supercond.* **16** 1725 "Electronic systems for the protection of superconducting elements in the LHC"
doi:10.1109/TASC.2005.864258

[Dev2004] Devred A 2004 *CERN-2004-006* "Practical low-temperature superconductors for electromagnets"

[DUPONT] DuPont Kapton HN polyimide film Technical data sheet Available online: `www.dupont.com/products-and-services/membranes-films/polyimide-films/brands/kapton-polyimide-film/products/kapton-hn.html` (Accessed Mar 02 2015)

[Eva2009] Evans L (editor) 2009 *CERN and EPFL press* "The Large Hadron Collider: A marvel of technology"

[Eys1995] Eyssa Y and Markiewicz D 1995 *IEEE Trans. Appl. Supercond.* **5** 487 "Quench simulation and thermal diffusion in epoxy-impregnated magnet system"
doi:10.1109/77.402572

[FCC2015] FCC website: `https://espace2013.cern.ch/fcc/Pages/default.aspx` (Accessed Mar 17 2015)

[Feh1998] Feher S, Bossert R, DiMarco J, Mitchell D, Lamm M J, Limon P J, Mazur P, Nobrega F, Orris D, Ozelis J P, Strait J B, Tompkins J C and Zlobin A V 1998 *Proc. PAC, 1997.* **3** 3389 "Quench protection of SC quadrupole magnets"
doi:10.1109/PAC.1997.753218

[Fel2009a] Felice H, Ambrosio G, Chlachidze G, Ferracin P, Hafalia R, Hannaford R C, Joseph J M, Lietzke A F, McInturff A D, Muratore J F, Prestemon S, Sabbi GL, Schmalzle J, Wanderer P and Wang X R 2009 *IEEE Trans. Appl. Supercond.* **19** 2458 "Instrumentation and quench protection for LARP Nb_3Sn magnets"
doi:10.1109/TASC.2009.2019062

[Fel2009b] Felice H, Ambrosio G, Bajko M, Barzi E, Bordini B, Bossert r, Caspi S, Dietderich D, Ferracin P, Feuvrier J, Ghosh A, Godeke A, Lizarazo J, Rossi L, Sabbi G, Wanderer P, Wang X and Zlobin AV 2009 *JoP Proc. EUCAS 09* **234** "Test results of TQS03: a LARP shell-based Nb_3Sn quadrupole using 108/127 conductor"
doi:doi:10.1088/1742-6596/234/3/032010

[Fel2013] Felice H and Todesco 2013 *in Proceedings of WAMSDO 2013, edited by E. Todesco* 17 "Quench protection analysis in accelerator magnets, a review of the tools"
doi:10.5170/CERN-2013-006.17

[Fer2004] Ferracin P, Caspi S, Chiesa L, Gourlay S A, Hafalia R R , Imbasciati L, Lietzke A F, Sabbi G and Scanlan R M 2004 *IEEE Trans. Appl. Supercond.* **14** 361 "Thermal, electrical and mechanical response in Nb_3Sn superconducting coils"
doi:10.1109/TASC.2004.829130

[Fer2013] Ferracin P, Devaux M, Durante M, Fazilleau P, Fessia P, Manil P, Milanese A, Munoz Garcia J E, Oberli L, Perez J C, RifiňĆet J M , de Rijk G, Rondeaux F and Todesco E 2013 *IEEE Trans. Appl. Supercond.* **23** 4002005 "Development of the EuCARD Nb_3Sn dipole magnet FRESCA2"
doi:10.1109/TASC.2013.2243799

[Fer2014] Ferracin P 2014 *HL-LHC/LARP International review of the inner triplet quadrupoles (MQXF) design 10-12 December 2014* "MQXF Overall design" (slides) Available online: `https://indico.cern.ch/event/355818/timetable/#20141210.detailed` (Accessed Mar 17 2015)

[Flo1979] Flora R H, and Tool G S 1979 *IEEE Transactions on Nuclear Science* **26** 3451 "Doubler-tevatron p quench protection system" doi:10.1109/TNS.1979.4330066

[FR4] Fr4 CRYOGENIC G10 SPECIFICATIONS Available online: `http://www.g10fr4.com/g10\_fr4\_technical\_data\_specifications.html` (Accessed Mar 02 2015)

[God2005] Godeke A 2005 *PhD dissertation* University of Twente, Enschede, The Netherlands "Performance boundaries in Nb_3Sn superconductors"

[God2006] Godeke A, ten Haken B, ten kate H H J and Larbalestier D C 2006 *Supercond. Sci. Technol.* **19** R100 "A general scaling relation for the critical current density in Nb_3Sn wires" doi:10.1088/0953-2048/19/10/R02

[God2013] Godeke A, Chlachidze G, Dietderich D R , Ghosh A K, Marchevsky M, Mentink M G T and Sabbi GL 2013 *Supercond. Sci. Technol.* **26** 095015 "A review of conductor performance for the LARP high-gradient quadrupole magnets" doi:10.1088/0953-2048/26/9/095015

[Gre1984] Green M A 1984 *Cryogenics* **24** 3 "Quench back in thin superconducting solenoid magnets" doi:10.1016/0011-2275(84)90049-3

[Gre1992] Greene A F 1992 *Proceedings of ICFA 1992, KEK proceedings 92-14* 100 "Recent status of superconductors for accelerator magnets"

[Gur2011] Gurevich A 2011 *Nature materials* **10** 255 "To use or not to use cool superconductors?" doi:10.1038/nmat2991

[Hag1992] Hagedorn D and Rodriguez-Mateos F 1992 *IEEE Trans. on Magn.* **28** 366 "Modelling of the quenching process in complex superconducting magnet systems" doi:10.1109/20.119887

[Här2015] Häro E, Järvelä J and Stenvall A 2015 *J Supercond. Nov. Magn.* "Variation of quench propagation velocities in YBCO cables" doi:10.1007/s10948-015-2976-y

[Imb2001] Imbasciati L, Bauer P, Ambrosio G, Kashikin V, L amm M and Zlobin AV 2001 *Proceedings PAC 2001* **5** 3454 "Quench protection of

high field Nb_3Sn magnets for VLHC"
doi:10.1109/PAC.2001.988142

[Imb2003] Imbasciati L, 2003 *PhD dissertation* Vienna University of Technology, Wien, Austria "Studies of quench protection in Nb_3Sn superconducting magnets for future particle accelerators"

[Kir2014] Kirby G A and Durante M 2014 *EuCARD2 Milestone report: EuCARD2-Mil-MS64-Final* "YBCO magnet design completion"

[Koe1979] Koepke K, Kalbfleisch G, Hanson W, Tollestrup A, O'Meara J and Saarivirta J 1979 *IEEE Trans. on Magn.* **15** 658 "Fermilab doubler magnet design and fabrication techniques"
doi:10.1109/TMAG.1979.1060074

[Lam2004] Lamm M J 2004 *Fermilab TD report TD-04-057* "Status of LQXB06 Quench Protection Heaters"

[Lam2006] Lamm M J, Bossert R, DiMarco J, Feher S, Hocker J A, Kerby J, Nobrega F, Novitski I, Rabehl R, Schlabach P, Strait J, Sylvester C, Tartaglia M, Tompkins J, Velev G and Zlobin A V 2004 *Proceedings of EPAC 2006* 2637 "Test results of Fermilab-built quadrupoles for the LHC interaction regions"

[Lau1998] Laukien D D and Tschopp W H 1998 "Nuclear magnetic resonance spectroscopy for chemical applications" in Seeber B (Editor) 1998 *Bristol: Institute of Physics Publishing)* "Handbook of Applied Superconductivity, vol 2"

[LARP2015] LARP website: `www.uslarp.org` (Accessed Mar 17 2015)

[Lee2014] Lee P J 2014 "Master Jc Plots and Nb_3Sn Scaling Spreadsheet Apr 16 2014" ASC maintained pages for The Applied Superconductivity Center: `http://fs.magnet.fsu.edu/~lee/plot/plot.htm` (Accessed Mar 17 2015)

[Lie1997] Lietzke A, McInturff A D and Scanlan R M 1997 *IEEE Trans. Appl. Supercond.* **7** 606 "Superfluid performance of tevatron IR quad heaters"
doi:10.1109/77.614577

[Lon2010] Long N J, Badcock R A, Hamilton K, Wright A, Jiang Z and Lakshmi L S 2010 *J. Appl. Phys.* **234** 022021 "Development of YBCO Roebel cables for high current transport and low AC loss applications"
doi:10.1088/1742-6596/234/2/022021

[Lu2008] Lu J, Choi E S, and Zhou H D 2008 *Journal of applied physics* **103** 064908 "Physical properties of Hastelloy C-276 at cryogenic temperatures"
doi:10.1063/1.2899058

[LUVATA2015] Luvata website: `http://www.luvata.com/en/News-Room/News/Luvata-joins-forces-to-develop-superconductor-technology/` (Accessed Jan 4 2015)

[Lyl2013] Lyly M, Zermeno V, Stenvall A, Lahtinen V and Mikkonen R 2013 *IEEE Trans. Appl. Supercond.* **23** 6000105 "Finite element simulations of twisted NbTi conductors"
doi:10.1109/TASC.2012.2228532

[Man2011] Manfreda G 2011 *CERN internal note 2011-24* "Review of ROXIE's material database for quench simulations"

[Man2014] Manfreda G, Ambrosio G, Felice H, Marinozzi V, Salmi T, Sorbi M, Todesco E and Volpini G 2014 *IEEE Trans. Appl. Supercond.* **24** 4700405 "Quench protection study of the Nb_3Sn Low-β quadrupole for the LHC luminosity upgrade"
doi:10.1109/TASC.2013.2285099

[Mar2014] Marchevsky M, Caspi S, Cheng D W, Dietderich D R, DiMarco J, Felice H, Ferracin P, Godeke A, Hafalia A R, Joseph J, Lizarazo J, Roy P K, Sabbi G, Salmi T, Turqueti M, Wang X and Prestemon S 2014 *IEEE Trans. Appl. Supercond.* **24** 4002106 "Test of the high-field dipole magnet HD3b"
doi:10.1109/TASC.2013.2285881

[Mar2013] Marinozzi V 2013 *Fermilab TD report TD-13-008* "Guidelines for the quench analysis of Nb_3Sn accelerator magnets using QLASA"

[Mar2015] Marinozzi V, Ambrosio G, Bellomo G, Chlachidze G, Felice H, Marchevsky M, Salmi T, Sorbi M and Todesco E 2015 *IEEE Trans. Appl. Supercond.* **25** 4002905 "Study of quench protection for the Nb_3Sn Low-β quadrupole for the LHC luminosity upgrade (HiLumi-LHC)"
doi:10.1109/TASC.2014.2383435

[Mar2000] Marquardt E D, Le J P, and Radebaugh R 2000 *Proc. 11th Int. Cryocooler Conf., Keystone* "Cryogenic material properties database" Available online `http://cryogenics.nist.gov/MPropsMAY/material%20properties.htm` (Accessed Mar 17 2015)

[Mat2002] Mattafirri S 2002 *Laurea thesis Pisa university, also Fermilab TD report TD-02-21* "Kinetics of phase growth during the Cu-Sn diffusion process and the Nb_3Sn formation. Optimization of superconducting properties."

[Mat1954] Matthias B T, Geballe T H, Geller S and Corenzwit E 1954 *Phys. Rev.* **95** 1435 "Superconductivity of Nb_3Sn" doi:10.1103/PhysRev.95.1435

[MATWEB] MatWeb material property data for G10. Available online: `http://www.matweb.com/search/datasheet.aspx?matguid=8337b2d050d44da1b8a9a5e61b0d5f85&ckck=1` (Accessed Mar 02 2015)

[Meß1998] Meß K H 1998 "Quench propagation and magnet protection" in Seeber B (Editor) 1998 *Handbook of Applied Superconductivity, vol 1* (Bristol: Institute of Physics Publishing)

[Mia2005] Miao H, Marken K R, Meinesz M., Czabaj B and Hong S 2005 *IEEE Trans. Appl. Supercond.* **15** 2254 "Development of round multifilament Bi-2212/Ag wires for high field magnet applications" doi:10.1109/TASC.2005.847648

[Mia2012] Miao H, Huang Y, Meinesz M, Hong S and Parrell J 2012 *Advances in Cryogenics Engineering* **58** 315 "Development of Bi-2212 round wires for high field magnet applications" doi:10.1063/1.4712111

[Nak2002] Nakamoto T, Burkhardt E, Ogitsu T, Yamamoto A, Shintomi T and Tsuchiya K 2002 *IEEE Trans. Appl. Supercond.* **12** 170 "Quench protection study of a prototype for the LHC low-beta quadrupole magnets" doi:10.1109/TASC.2002.1018376

[NOBEL2013] Nobel Prize website: `http://www.nobelprize.org/nobel_prizes/physics/laureates/2013/` (Accessed Mar 17 2015)

[Nob2013] Nobrega F (Fermilab) 2013, private communication.

[OPERA2015] OPERA website: `http://www.cobham.com/about-cobham/communications-and-connectivity/about-us/antenna-systems/specialist-technical-services-and-software/products-and-services/design-simulation-software/opera/opera-2d.aspx` (Accessed Mar 17 2015)

[OST2015] OST website: `http://www.oxford-instruments.com/products/superconducting-magnets-and-wire/superconducting-wire/nb3sn-iter-lowloss` (Accessed Jan 4 2015)

[PATENT2013] Patent: "AC-Current induced quench protection system",EU Appl. no. EP13174323.9, Jun. 28, 2013

[Per1996] Perin R 1996 *CERN-AT/96-60 (MA)* "Field, forces and mechanics of superconducting magnets"

[Pre2011] Prestemon S (LBNL) 2011, private communication.

[Rav2014] Ravaioli E, Datskov V I, Giloux C, Kirby G, ten Kate H H J and Verweij A P 2015 *IEEE Trans. Appl. Supercond.* **24** 0500905 "New, coupling loss induced, quench protection system for superconducting accelerator magnets"
doi:10.1109/TASC.2013.2281223

[Rav2015] Ravaioli E, Bajas H, Datskov V I, Desbiolles V, Feuvrier J, Kirby G, Maciejewski M, Sabbi G, ten Kate H H J and Verweij A P 2015 *IEEE Trans. Appl. Supercond.* **25** 4001305 "Protecting a full-scale Nb_3Sn magnet with CLIQ, the new coupling-loss-induced quench system"
doi:10.1109/TASC.2014.2364892

[Rod2000] Rodriguez-Mateos F, Pugnat P, Sanfilippo S, Schmidt S, Siemko A and Sonnemann F 2000 *Proceedings of EPAC 2000* 2154 "Quench heater experiments on the LHC main superconducting magnets"

[Rod2001] Rodriguez-Mateos F and Sonnemann F 2001 *Proceedings of PAC 2001* **5** 3451 "Quench heater studies for the LHC magnets"
doi:10.1109/PAC.2001.988141

[Ros2004] Rossi L and Sorbi M 2004 *INFN/TC-04/13* "A computer code for quench simulation in adiabatic multicoil superconducting windings"

[Ros2005] Rossi L and Sorbi M 2005 *CARENote-05-018-HHH* "MATPRO: a computer library of material property at cryogenic temperature"

[Ros2006] Rossi L and Todesco E 2006 *Phys. Rev. STAB* **9** 102401 "Electromagnetic design of superconducting quadrupoles"
doi:10.1103/PhysRevSTAB.9.102401

[Ros2007] Rossi L and Todesco E 2007 *Phys. Rev. STAB* **10** 112401 "Electromagnetic design of superconducting dipoles based on sector coils"
doi:10.1103/PhysRevSTAB.10.112401

[Ros2012] Rossi L 2012 *Fermilab TD report TD-12-11* "Study of superconducting-to-resistive transition for the US-LARP large high field quadrupoles for the LHC upgrade"

[Ros2015] Rossi L, Badel A, Bajko M, Ballarino A, Bottura L, Dhalle M M J, Durante M, Fazilleau P, Fleiter, Goldacker W, Haro E, Kario A, Kirby G, Lorin C, van Nugteren J, de Rijk G, Salmi T, Senatore C, Stenvall A, Tixador P, Usoskin A, Volpini G, Yang Y and Zangenberg N 2015 *IEEE Trans. Appl. Supercond.* **25** 4001007 "The EuCARD-2 future magnets european collaboration for accelerator-quality HTS magnets" doi:10.1109/TASC.2014.2364215

[Rus2006] Russenchuck S 2006 "Electromagnetic design of accelerator magnets" in Brandt D (editor) 2006 *CERN-2206-002* 411 "Proceedings of CERN Accelerator school, DESY, Zeuthen, Germany, 15-26 September 2003" doi:10.1109/TASC.2014.2365471

[Rus2010] Russenschuck S 2010 *New York: Wiley* "Field Computation for Accelerator Magnets: Analytical and Numerical Methods for Electromagnetic Design and Optimization"

[Sab2015] Sabbi G, Bottura L, Cheng D W, Dietderich D R, Ferracin P, Godeke A, Gourlay S A, Marchevsky M, Todesco E and Wang X 2015 *IEEE Trans. Appl. Supercond.* **25** 4001407 "Performance Characteristics of Nb_3Sn Block-Coil Dipoles for a 100 TeV Hadron Collider" doi:10.1109/TASC.2014.2365471

[SABER] Saber software by SYNOPSYS. Website: `http://www.synopsys.com/Systems/Saber/Pages/default.aspx`

[Sch2008] Schwerg N, Auchmann B and Russenschuck S 2008 *IEEE Trans. on Magn.* **44** 934 "Quench simulation in an integrated design environment for superconducting magnets" doi:10.1109/TMAG.2007.916304

[Sch2009] Schwerg N, Auchmann B, Mess K H and Russenschuck S 2009 *IEEE Trans. Appl. Supercond.* **19** 2428 doi:10.1109/TASC.2009.2018790

[Sie2013] *CERN COURIER* Aug.19, 2013 "Safeguarding the superconducting magnets" Availble online: `http://cerncourier.com/cws/article/cern/54383`

[Son2001a] Sonnemann F 2001 *LHC-PROJECT-NOTE-265* "Quench simulation studies: Program documentation of SPQR"

[Son2001b] Sonnemann F and Schmidt R 2001 *Cryogenics* **40** 519 "Quench simulations for superconducting elements in the LHC accelerator" doi:10.1016/S0011-2275(01)00008-X

[Son2001c] Sonnemann F 2001 *CERN-THESIS-2001-004* "Resistive transition and protection of LHC superconducting cables and magnets"

[Sti1979] Stiening R, Flora R, Lauckner R and Tool G 1979 *IEEE Trans. on Magn.* **15** 670 "A superconducting synchrotron power supply and quench protection scheme" doi:10.1109/TMAG.1979.1060065

[Sum1991] Summers L T, Guinan M W, Miller J R and Hahn P A 1991 *IEEE Trans. on Magn.* **27** 2041 "A model for the prediction of Nb_3Sn critical current as a function of field, temperature, strain and radiation damage" doi:10.1109/20.133608

[SUPERPOWER2015] SuperPower website: `http://www.superpower-inc.com/content/2g-hts-wire` (Accessed Jan 4 2015)

[The1993] Theilacker J C, Norris B L and Soyars W M 1993 *Advances in Cryogenic Engineering* **39** 469 "Tevatron quench pressure measurement"

[tim2007] Timmerhaus K D and Reed R P (editors) 2007 *Cryogenic Engineering, International Cryogenics Monograph Series* 285 "Understanding Properties and Fabrication Processes of Superconducting Nb_3Sn Wires" doi:10.1007/0-387-46896-X_12

[Tod2011] Todesco E and Zimmermann F 2011 *CERN Yellow Report 2011-3* "The high energy LHC"

[Tod2013a] Todesco E 2013 *in Proceedings of WAMSDO:Workshop on accelerator magnet superconductors, design and optimization, edited by E. Todesco, CERN-2013-006* 10 "Quench limits in the next generation of magnets" doi:10.5170/CERN-2013-006.10

[Tod2013b] Todesco E 2013 *QXF protection WG.3 #30 meeting on 28 Oct 2013* "Extrapolation of preliminary HQ test results to QXF" (slides) Available online: `https://indico.cern.ch/event/338446/`

[Tol2008] Tollestrup A and Todesco E 2008 *Rev. Sci. Accel. Tech.* **1** 185 "The development of superconducting magnets for use in particle accelerators: from Tevatron to the LHC"
doi:10.1142/S1793626808000101

[Tur2013] Turrioni D (Fermilab) 2013, Private communication.

[Van2009] van der Laan D C 2009 *Supercond. Sci. Technol.* **22** 065013 "$YBa_2Cu_3O_{7-\delta}$ coated conductor cabling for low ac-loss and high-field magnet applications"
doi:10.1088/0953-2048/22/6/065013

[Van2013] van der Laan D C, Noyes P D, Miller G E, Weijers H W and Willering G P 2013 *Supercond. Sci. Technol.* **26** 045005 "Characterization of a high-temperature superconducting conductor on round core cables in magnetic fields up to 20 T"
doi:10.1088/0953-2048/26/4/045005

[Van2015] van Nugteren J, Kirby G A, de Rijk G, Rossi L, ten Kate H H J and Dhalle M M J 2015 *IEEE Trans. Appl. Supercond.* **25** 4000705 "Study of a 5 T research dipole insert-magnet using an anisotropic ReBCO Roebel cable"
doi:10.1109/TASC.2014.2361797

[Ver1995] Verweij A P 1995 *PhD dissertation* University of Twente, Enschede, the Netherlands "Electrodynamics of Superconducting Cables in Accelerator Magnets"

[Ver2006] Verweij A P 2006 *Cryogenics* **46** 619 "CUDI: A model for calculation of electrodynamic and thermal behaviour of superconducting Rutherford cables"
doi:10.1016/j.cryogenics.2006.01.009

[Ver2008] Verweij A et al. 2006 *Proceedings of EPAC08* "Performance of the main dipole magnet circuits of the LHC during commissioning"

[WAMHTS2014] WAMHTS-2: The 2014 Kyoto Workshop on HTS Magnet Technology for High Energy Physics –The 2nd Workshop on Accelerator Magnet in HTS Website: `https://indico.cern.ch/event/319762/` (Accessed Mar 17 2015)

[Wie2007] Wiedemann H 2007 *Springer Berlin Heidelberg New York* "Particle accelerator physics" 3rd ed.

[Wil2009] Willering G 2009 *PhD dissertation* University of Twente, Enschede, the Netherlands "Stability of superconducting rutherford cables"

[Wil1983] Wilson M N 1983 *Oxford University Press, New York* "Superconducting magnets"

[Yam2003] Yamada et al. 2003 *IEEE Trans. Appl. Supercond.* **13** 1696 "2D/3D Quench Simulation Using ANSYS for Epoxy impregnated Nb_3Sn High Field Magnets"
doi:10.1109/TASC.2003.812870

[Yam2005] Yamamoto A, Nakamoto T, Ogitsu T, Ohuchi N, Ajima Y, Higashi N, Iida M, Kimura N, Ohhata K, Shintomi T, Sugawara S, Sugita K, Tanaka K, Terashima A, Tsuchiya K, Fujii T, Hashiguchi E, Kanahara T, Murai S, Odajima W and Orikasa T 2005 *IEEE Trans. Appl. Supercond.* **15** 1084 "Production and measurement of the MQXA series of LHC low-β insertion quadrupoles"
doi:10.1109/TASC.2005.849501

[Zlo2005] Zlobin A V 2005 *Workshop on beam generated heat deposition and quench levels for LHC magnets, CERN 3-4 March 2005* "Thermal analysis and its experimental verification for the present and future IR triplets" (slides)

[Zlo2012] Zlobin A V, Andreev N, Apollinari G, Auchmann B, Barzi E, Bossert R, Karppinen M, Nobrega F, Novitski I, Rossi L, Smekens D, Turrioni D, Yamada R 2012 *IEEE Trans. Appl. Supercond.* **22** "Design and fabrication of a single-aperture 11 T Nb_3Sn dipole model for LHC upgrades"
doi:10.1109/TASC.2011.2177619

[Zlo2013] Zlobin A V, Andreev N, Apollinari G, Auchmann B, Barzi E, Bossert R, Chlachidze G, Karppinen M, Nobrega F, Novitski I, Rossi L, Smekens D, Turrioni D and Yamada R 2013 *IEEE Trans. Appl. Supercond.* **23** 4000904 "Development and test of a single aperture 11 T Nb_3Sn demonstrator dipole for LHC upgrades"
doi:10.1109/TASC.2012.2236138

[Zlo2014] Zlobin A V, Andreev N, Apollinari G, Auchmann B, Bajas H, Barzi E, Bossert R, Chlachidze G, Karppinen M, Nobrega F, Novitski I, Rossi L, Smekens D and Turrioni D 2014 *IEEE Trans. Appl. Supercond.* **24** 4000305 "Quench Performance of a 1 m Long Single-Aperture 11 T Nb_3Sn Dipole Model for LHC Upgrades"
doi:10.1109/TASC.2013.2281782

Tampereen teknillinen yliopisto
PL 527
33101 Tampere

Tampere University of Technology
P.O.B. 527
FI-33101 Tampere, Finland

ISBN 978-952-15-3554-3
ISSN 1459-2045